

Danmarks Tekniske Universitet



# **Characterization and parametric study of the flow properties of cohesive powders at temperatures up to 850 °C**

---

Master Thesis

February 2012 – July 2012

Arnau Mestres Rosàs

Supervisors: Kim Dam-Johansen, Anker Degn Jensen,  
Peter Szabo, Claus Maarup Rasmussen

Department of Chemical and Biochemical Engineering,  
Technical University of Denmark, DTU



## Title sheet

**Project title:**

Characterization and parametric study of the flow properties of cohesive powders at temperatures up to 850 °C

**Project type:**

Master Thesis, 30 ECTS Credits

**Supervisors:**

Kim Dam-Johansen  
Anker Degn Jensen  
Peter Szabo  
Claus Maarup Rasmussen

**Department:**

Department of Chemical and Biochemical Engineering

**Author:**

Arnau Mestres Rosàs

**Delivery date:**

11 July 2012

**Date and signature:**

---

Arnau Mestres Rosàs

## Acknowledgements

Writing this Master Thesis would not have been possible without the support of several mentors.

Foremost I would like to thank Technical University of Denmark for giving me the opportunity to carry out all the experiments and write this thesis at the Department of Chemical and Biochemical Engineering. Special thanks go to my supervisors Anker Degn Jensen and Peter Szabo for their great support and guidance and to the PhD student Claus Maarup Rasmussen for his patience and all the time he has dedicated to me. I could not forget to greatly thank the people from the workshop for building me the metal test cells I have been using these last months to perform the experiments.

I would also thank all the friends that I have made during this unforgettable Erasmus exchange. Special thanks go to Veaceslav Ghilas, Sergi Rotger, Irene Gallo Stampino, Wee Kian, Hailemariam Ayalew, Wee Kiat, Gebeyehu Manie, Katharina Ka, Helge Simon and Simone Boscolo, amongst others for standing and supporting me, as well as for the experiences that we have shared in Copenhagen.

Also a thank to my friends from Spain for their remarkable support throughout these past five years of my degree, these include Myriam Fichter, Rubén Rodríguez, Joan Fons, Cristina Campillo, Ainoa Tajada, Erika Bocos, Nadia Casasayas, Marta Casasayas, Joan Galceran, David Gracia, Daniel García, Eduard Laguarda, Martín Méndez, Marc Dalmau and Sílvia Neira, amongst others.

At last but not least, I would like to express my sincerely and deep gratitude to my parents Jaume and M<sup>a</sup> Asunción for giving me the opportunity to study, as well as my brothers Jordi and Oscar and my sister Alba for their unconditional support during my student's career.



## Abstract

In connection with the design of a new preheater for the application in the cement manufacturing plant which does not use a cyclone tower, particle beds may be formed inside the equipment when raw meal is heated up to approximately 850 °C. Experiences and equipment design from the industry show that congested particles that cause blockages are often occurring, especially at temperatures above 600 °C – 700 °C. For this reason, the study of the flow properties of the raw meal, so that the design of the new preheater can ensure a correct operation, is highly important.

Therefore, the aim of this thesis was to study which parameters affect the flow properties of the bulk solids and, more specifically, to experimentally determine the dependence of the raw meal flow properties with the temperature using different testing methods carried out at temperatures up to 850 °C, which needed to be previously designed and developed.

The methods used for the flowability characterization were the uniaxial shear test, the rheological shear test and the poured angle of repose measurement. Precisely, the rheological shear test was an innovation on this thesis, since until the date a rheometer had not been used with this purpose.

The results obtained with the flowability testing methods concluded that the raw meal flow behavior is kept nearly constant until a temperature around 700 °C, and from that temperature onwards an increase of the cohesion is achieved, decreasing is flowability. This results matched with another results obtained with coal fly ash found in the literature. Besides, in terms of the effectiveness and reliability of the methods, the uniaxial shear test and the rheological shear test seemed to be fairly adequate for the particle characterization at high temperatures.



# List of contents

1. Introduction.....	9
1.1 Cement .....	10
1.1.1 Cement chemistry.....	10
1.2 Cement production .....	12
1.2.1 Preheating facility .....	13
1.2.2 Problems with bulk solids .....	14
2. Flowability .....	17
2.1 Principles.....	17
2.1.1 Adhesive forces .....	17
2.1.2 Particle size .....	18
2.1.3 Forces and stresses exerted.....	19
2.1.4 Bulk density.....	21
2.2 Flow properties.....	21
2.2.1 Flow function and time flow function .....	21
2.2.2 Numerical classification of flow behavior .....	23
2.2.3 Yield limit .....	24
2.2.4 Yield locus and time yield locus (shear tests) .....	25
2.2.5 Wall friction .....	27
2.3 Testing methods .....	28
2.3.1 Uniaxial compression test .....	28
2.3.2 Jenike shear test.....	28
2.3.3 Uniaxial shear test .....	29
2.3.4 Angle of repose measurement .....	30
2.3.5 Cohesion tests.....	32
2.3.6 Torsional shear test.....	33
3. Previous research .....	35
3.1 Classification of powders .....	35
3.2 Flowability research .....	36
4. Material and methods.....	43
4.1 Raw meal.....	43
4.2 Uniaxial shear test .....	45
4.2.1 Experimental setup .....	45
4.2.2 Experimental procedure .....	48
4.2.3 Experiments.....	49
4.2.4 Calculation and statistical analysis.....	50
4.3 Rheological shear test.....	53
4.3.1 Experimental setup .....	54
4.3.2 Experimental procedure .....	55
4.3.3 Experiments.....	57
4.3.4 Calculation and statistical analysis.....	57

4.4	Angle of repose measurement .....	58
4.4.1	Experimental setup .....	58
4.4.2	Experimental procedure .....	59
4.4.3	Experiments.....	59
4.4.4	Calculation and statistical analysis.....	60
5.	Results.....	63
5.1	Uniaxial shear test .....	63
5.1.1	Bulk density.....	63
5.1.2	System behavior .....	65
5.1.3	Raw meal flow functions.....	66
5.1.4	Other evidences .....	72
5.2	Rheological shear test.....	77
5.3	Angle of repose measurement .....	82
5.3.1	Analysis A .....	82
5.3.2	Analysis B .....	83
6.	Statistical analysis.....	85
6.1	Uniaxial shear test .....	85
6.1.1	System behavior .....	85
6.1.2	Raw meal flow functions.....	86
6.2	Rheological shear test.....	89
6.3	Angle of repose measurement .....	91
7.	Discussion .....	93
8.	Conclusions.....	97
9.	References.....	99
Apendix A.	Tables with the data.....	101
Apendix B.	Chemical Risk Assessment (APV) for the uniaxial shear test.....	113



# 1. Introduction

In the traditional preheating process in a cement manufacturing plant, the cold raw meal is heated up from room temperature to approximately 850 °C in a cyclone-base preheating tower before it enters to the rotary kiln. The heating is performed using the exhaust gases from the calcination (in the calciner) and combustion processes (in the kiln).

However, in connection with the design of a new preheater for the application in the cement plant which does not use cyclones, particle beds may be formed inside the equipment. Experiences and equipment design from the industry show that congested particles that cause blockages are often occurring, especially at temperatures above 600 °C – 700 °C. Therefore, it is important to study the flow properties of the raw meal in order to design the new preheater in order to ensure a correct operation of the new preheater.

There are several methods to evaluate particle flow properties at room temperature, but measuring the relevant flow related properties for particles at high temperature has not been an object of interest, partly due to lack of experimental methods at high temperature and also because the interpretation of the results is difficult. Characterizing particle flow related properties may provide a qualitative knowledge of what parameters are of importance in the particles flowability, which can be used to predict operation stability by means of a correct design of the geometry of the devices to ensure a steady particle flow.

Therefore, the parameters affecting the flow properties of the particles (e.g. temperature, particle size distribution, particle types and pre-measurement treatment, amongst others) are investigated. Thus, according to these parameters, a study of the raw meal flow properties and behavior is done using the following experimental methods (carried out at temperatures up to 850 °C), which design, assembly and start-up of the devices used to be correctly performed needed to be developed:

- Uniaxial shear test.
- Rheological shear test.
- Poured angle of repose measurement.

Varying the system temperature of the experimental methods provided information about the internal and flowability changes occurring in the raw meal when increasing the temperature.

Finally, the obtained results are analyzed and compared with high temperature results from literature. Moreover, the effectiveness of the three different used methods is evaluated and discussed in terms of the reliability and accuracy of the results.

## 1.1 Cement

An introduction to the cement manufacturing process as well as the importance of the determination of bulk solids flowability is also given in the introduction section.

Cement is a widely known building material made basically from a mixture of limestone and clay. It is reported that it has been used as a hydraulic binder since several thousands of years ago [1].

By mixing cement with water and sand one can obtain a malleable paste which gradually hardens due to hydrolysis and hydration reactions of the constituents, yielding to a hard hydrated product which is mechanically resistant. This paste can be used as a binder in construction or used as an ingredient in the production of mortar or concrete.

Although there is a large number of cement types depending of their operational conditions or applications (e.g. aggressive environments, sea water, sulfated soils, acid environments), the most used is the Portland cement [2].

The mixture of raw materials (called raw meal) for the production of cement clinker consists mainly of calcareous components (limestone) and argillaceous components (aluminosilicates like clay or marl) in the appropriate proportions in order to satisfy the stoichiometric needs.

However, when it is impossible to reach the suitable stoichiometric needs, it is necessary to use corrective materials such as bauxite, laterite, iron ore or blue dust, sand or sandstone, amongst others [2].

Therefore, the raw meal is mainly formed of  $\text{CaCO}_3$ ,  $\text{Al}_2\text{O}_3$  and  $\text{Fe}_2\text{O}_3$  (contained in limestone), and  $\text{SiO}_2$  (found in clays or other argillaceous substances). Otherwise, there are other minority components such as  $\text{MgO}$ ,  $\text{Na}_2\text{O}$ ,  $\text{K}_2\text{O}$ ,  $\text{SO}_3$  and  $\text{Cl}$  which are essentials for the properties of the clinker produced [3].

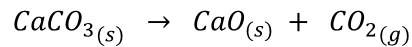
As a rule of thumb, the raw meal can be assumed to consist of approximately 75% of limestone and 25% of clay.

### 1.1.1 Cement chemistry

First of all it is needed to be said that the raw meal composition and its mineralogical composition, together with the residence time and temperature profile in the rotary kiln are important factors that affect to the clinker composition and mineralogy.

The chemical transformation of the raw meal begins with the evaporation of the free water at 100 °C and the absorbed water in the clay minerals between 100 - 300 °C. After, the chemically bound water is removed at temperatures between 450 - 900 °C [1].

The raw meal contains a huge quantity of  $\text{CaCO}_3$ , and at temperatures in the range of 700 - 850 °C a calcination takes place, releasing  $\text{CO}_2$  to form  $\text{CaO}$ , as shown in the reaction:



Both, the removal of the water and the calcination processes mentioned occur in the preheating facility and the calciner. Nevertheless, the main chemical reactions take place in the rotary kiln. These reactions, which produce the calcium silicates, are a combination of endothermic and exothermic reactions occurring in a complicated chemical reaction sequence [1].

The formation of belite ( $\text{Ca}_2\text{SiO}_4$  or ' $\text{C}_2\text{S}$ '), aluminates and ferrites (mainly  $\text{Ca}_3\text{Al}_2\text{O}_6$  or ' $\text{C}_3\text{A}$ ' and  $\text{Ca}_4\text{Al}_2\text{Fe}_2\text{O}_{10}$  or ' $\text{C}_4\text{AF}$ ') is attained at temperatures between 800 - 1250 °C in the cold end of the rotary kiln. Afterwards, at higher temperatures than 1250 °C a liquid phase melt is formed. The formation of alite ( $\text{Ca}_3\text{SiO}_5$  or ' $\text{C}_3\text{S}$ '), which is the major component of the final clinker occurs at temperatures up to 1330 - 1450 °C [1], [4].

In the end, the solidification of the liquid phase at the end of the kiln and the fast clinker cooling in the cooler (so that alite is preserved) gives the final microstructure of the clinker produced.

Below, the clinker transformation reactions taking place in the raw meal are shown as a function of the temperature:

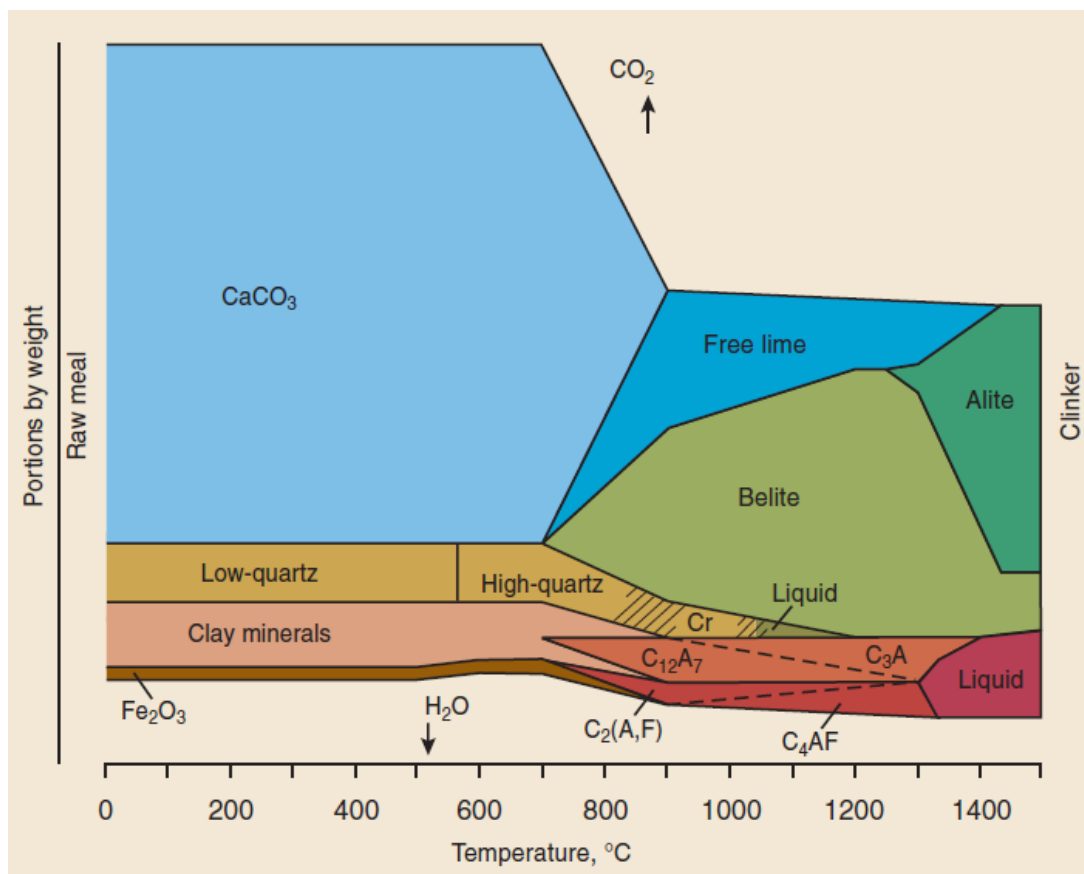


Figure 1. Chemical reactions occurring in the raw meal as a function of the temperature [1].

## 1.2 Cement production

The cement production can be separated in two different steps. In the first step clinker is produced from the raw materials. In the second step cement is produced from the clinker previously obtained.

Once the raw materials are extracted from quarries and received at the cement plant in a maximum size between 1 and 2 m, they are crushed until a proper particle size for the milling process is achieved. After that, the crushed minerals are prehomogenized, dried and conveyed to the raw mill in order to reduce the particle size to a top size of about 0,2 mm which is necessary for the pyroprocessing operation. Afterwards, the different materials are proportioned and homogenized.

A schematic diagram of the pyroprocessing process is shown underneath:

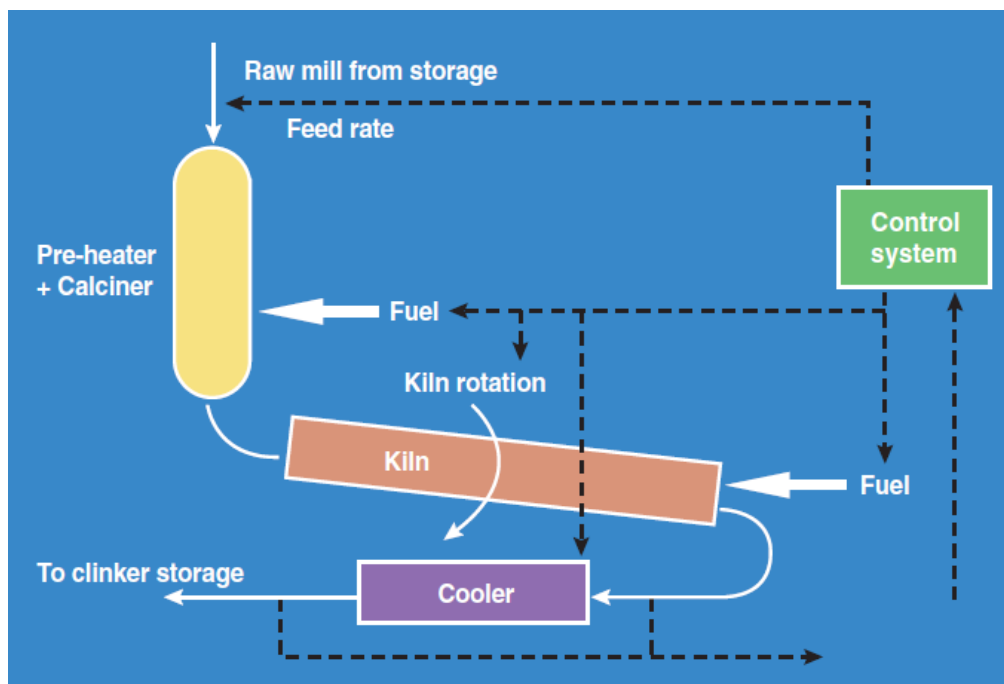


Figure 2. Sketch of the pyroprocessing operation [1].

Then, in the pyroprocessing operation, the raw meal is fed into the cyclone-based preheating facility, where it is heated up to around 850 °C before it enters to the calciner. In the calciner around 90% of the raw meal is calcined and afterwards the feed is led to the rotary kiln where a temperature of approximately 1500 °C is reached. In the rotary kiln a large amount of complex clinkering reactions are produced in the raw meal as a result of the heat, yielding to clinker.

The rotary kiln is slightly inclined so that the materials inside it flow from one end to the other. After leaving the rotary kiln, the clinker is introduced to the cooler, where is quickly cooled to 100 °C by using cold atmospheric air, freezing in the high temperature crystalline structure.

Finally, the clinker is blended with gypsum (calcium sulphates), additional cementitious materials (blast furnace slag, coal fly ash, natural pozzolanas) or inert materials (limestone) in the adequate proportions in the cement grinding mill, where all the components are milled to the desired particle size, mixed and homogenized until a grey fine powder is obtained [2].

### 1.2.1 Preheating facility

Nowadays, the preheating facility is based in a multi-stage cyclone preheating tower, together with a calciner where most of the calcination process takes place. However, it has not always been this way.

Before the Lepol kiln was invented in 1928, which used the exhaust gases from the rotary kiln to preheat the raw meal and improve the heat exchange and consequently the thermal efficiency of the kiln, all the kilns operated without preheating facilities. But it was in 1934 when the first cyclone preheated kiln was patented [1]. After that, the best improvement made to the preheating facility was the addition of the calciner, which permitted the calcination of the raw meal before it enters to the kiln using the hot gases from the cooler so that more fuel can be used in the kiln leading to an increase of the production rate.

At the moment at least six preheating system configurations exist depending mainly on the position of the calciner and their selection depend on the requirements of the cement plant and involve a large number of considerations. A schematic diagram of the In-Line Calciner preheating system configuration is showed below:

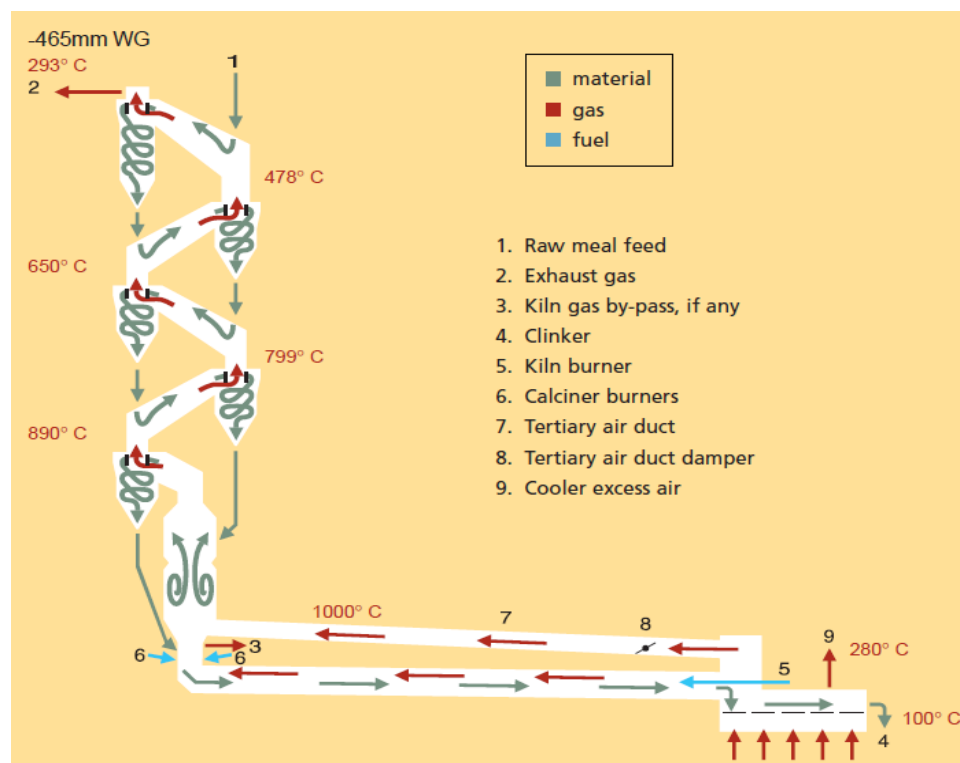


Figure 3. In-Line Calciner kiln system with 5-stage preheater. Typical temperatures in the system are also showed together with the negative pressure in the exhaust gas exit [5].

The preheating cyclone tower usually consists of 4 to 6 vertical stages, where the exhaust gases from the combustion and calcination processes enter each stage from the stage below whereas the raw meal enters from the above stage. In practice, the raw meal increases between 150 - 250 °C its temperature in every stage.

Each stage is composed of a cyclone and a riser duct where the heat exchange between the gas and particles take place. Due to the pulverized state of the raw meal and its consequently huge heat exchange area, when the particles are equally distributed across the duct both particles and gas equal their temperatures immediately. After that, the particles suspension enters the cyclone where particles are separated from the gas. The particles fall to the stage below and the exhaust gas goes upwards to the above stage.

The design of the cyclones in the preheating tower is different for each stage in order to maximize its efficiency.

The selection of a preheating configuration embraces the number of strings and the number of cyclone stages. On one side, the number of strings used (one, two or three) depends on the production rate. On the other side, the number of stages depends on the moisture content in the raw meal, investment cost, electricity and fuel price and other operating conditions.

### 1.2.2 Problems with bulk solids

When bulk solids are handled in silos, hoppers or bins, a bad design of them can lead to a decrease of the product quality or the productivity. It also occurs in the design of a new preheater based in particle beds. These consequences are due to many flow obstruction problems which can come about.

Furthermore, concerning the raw meal, experiences from the cement industry show that blockages caused by congested particles are frequently taking place, especially at temperatures above 600 - 700 °C.

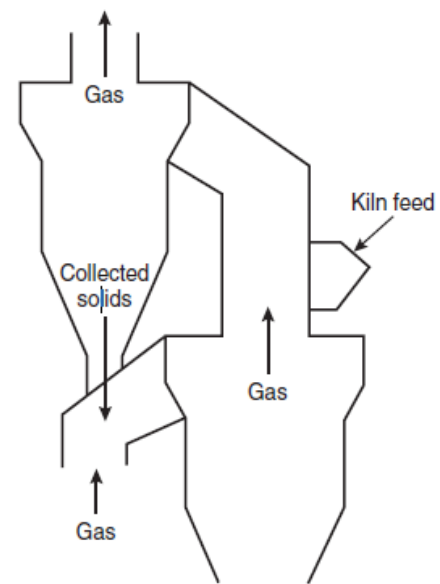


Figure 4. Schematic view of the two top stages in the cyclone preheating tower [1].

The following illustration shows some of these operation problems which can appear during the handling of bulk solids in silos or hoppers:

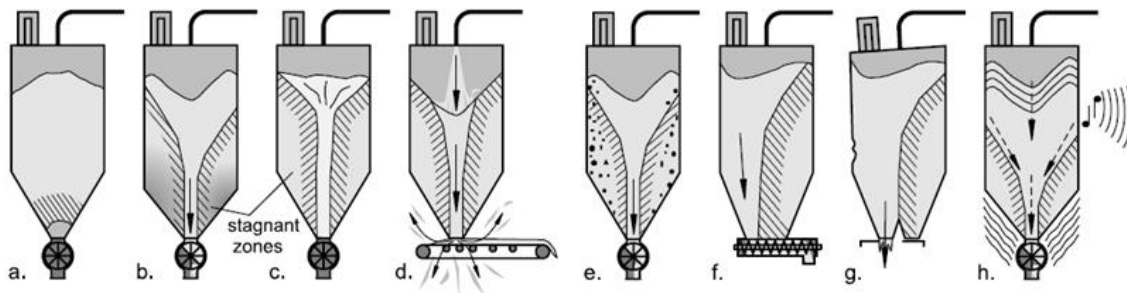


Figure 5. Possible operation problems when handling bulk solids: a. arching, b. funnel flow, c. ratholing, d. flooding, e. segregation, f. non-uniform discharge with screw feeder, g. buckling caused by eccentric flow, h. vibrations (quaking and noise) [6].

The outlined operation problems are caused not only by the poor design of the equipment, but also from the flow properties of the bulk solid. It is for this reason that the flow properties of the bulk solid to handle have to be studied and determined so that a steady particle flow can be attained by means of a correct design of the geometry of the equipment as the hopper slope or the outlet size. These parameters can be correctly determined from the yield loci obtained with the shear tests, which will be further explained.





## 2. Flowability

As stated before, a study of the flowability or the flow properties of a bulk solid must be done to design correctly the handling equipments in order to avoid or minimize operation problems.

It is widely known that the flow properties of a bulk solid depend on many parameters [6]:

- Chemical composition of the particles.
- Particle size distribution.
- Particle shape and type.
- Temperature.
- Moisture content.
- Vibration.
- Alkaline content.
- Equipment design and surfaces.

However, it is not currently possible to determine numerically the flow properties of bulk solids taking into account all that parameters. Thus, experimental suitable testing methods must be developed and performed in order to:

- Investigate the possibility to describe the flowability with simple testing methods.
- Characterize the flow behavior of different kind of powders at different conditions.

The principles of the cohesion (and so, the flowability) of bulk solids, the flow properties of the bulk solids which can be experimentally determined and some of the suitable testing methods used to characterize the flow behavior of powders are described in this section.

### 2.1 Principles

#### 2.1.1 Adhesive forces

As mentioned before, some of the parameters that influence the flow behavior of bulk solids are the moisture content and the chemical composition of the particles. Thus, different chemical compositions and dampness leads to different adhesive forces depending mainly on the adhesive forces between the individual particles.

In fine-grained dry bulk solids, Van der Waals forces are the most important contribution to the adhesive forces. Otherwise, if moisture is present, small liquid bridges formed between the contact surfaces of the particles are the most significant [6]. Both types of adhesive forces depend on the individual particle size and the distance between the individual particles.

Besides, there are some bulk solids which gain strength when stored for a long time under compressive stresses. This is called time consolidation and the reasons are related to the effects of the adhesive forces. Consequently it is necessary to take into account the stress history when determining the flowability of bulk solids.

There are several mechanisms which lead to adhesive forces, which are [6]:

- Solid bridges formed by solid crystallizing when drying moist bulk solids and the moisture is a solution of a solid and a solvent (e.g. sand and salt water).
- Solid bridges formed by the own particle material, when some particles have been dissolved at the contact points by moisture and then this moisture is removed (e.g. moist sugar).
- Bridges due to sintering caused by the storage of bulk solids at temperatures close to the melting temperature (e.g. storage of plastics).
- Plastic deformation at the particle contacts due to external compressive forces, which increases the contact areas of the particles and leads to an increase of the adhesive forces.
- Chemical processes due to chemical reactions at the particles contacts.
- Biological processes (e.g. fungal growth).

Fine-grained bulk solids with a poor flowability caused by the adhesive forces are called cohesive bulk solids and they use to have unpredictable flow behaviors due to their trend to form agglomerates.

Concerning the Van der Waals forces between particles which lead to adhesive forces, Derjaguin (1934) and Lifshitz (1956) formulated their own estimative models which can approximate the values of the forces [7]. They found that the Van der Waals force estimation can be defined as the sum of all the molecules from the surface of the particles found face to face. They also established that the magnitude of the Van der Waals forces increases with the reduction of the particle size (as further explained in section 2.1.2) and that these forces become dominating compared to the weight of the particles.

### 2.1.2 Particle size

Although the adhesive force between two identical spherical particles is proportional to the particle diameter, experiences with bulk solids show that when decreasing the particle size, a decrease of the bulk solid flowability occurs due to an increase of the sum of the adhesive forces. It is for this reason that a bulk solid flows worse when the particle size is reduced.

At the same time, it can also be theoretically demonstrated. Using the definition of the tensile strength of a bulk solid (if we assume that it corresponds to the sum of the adhesive forces between the individual particle contacts:  $F_Z = n \cdot F_H$ ), it is obtained that the tensile strength is inversely proportional to the particle diameter (i.e. the flowability decreases when the particle size of the powder is reduced):

$$\sigma_t = \frac{F_Z}{A} \propto \frac{n \cdot F_H}{n \cdot d^2} \propto \frac{d}{d^2} \propto \frac{1}{d}$$

Where:  $\sigma_t$  is the tensile strength,  $F_Z$  is the tensile force at failure,  $A$  is the area of the failure plane,  $n$  is the number of individual particle contacts inside the area  $A$ , and  $F_H$  is the adhesive force between two particles of diameter  $d$ .

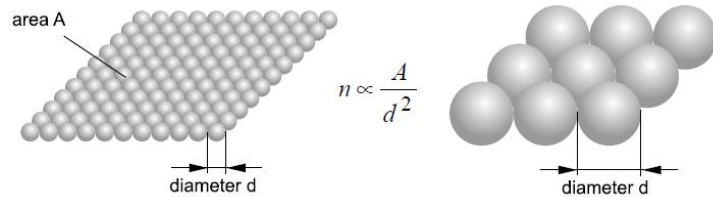


Figure 6. Fine and coarse particles. It is shown that the number of area contacts is inversely proportional to the square of the particle diameter, since the smaller the particles are, the more particles can be found [6].

Even so, there are some exceptions to this flow behavior like in case of flow agents. Flow agents are additions to fine-grained bulk solids of even more fine powder in order to improve the flow behavior of the bulk solid due to a reduction of the interparticle adhesive forces. Moreover, flow agents work as lubricants and increase the interparticle distances. Therefore, an addition of a small percentage of flow agent yields to a slightly smaller mean particle size, but an increase of the flowability is achieved unlike stated before due to their work as lubricants and their increase of the interparticles distances.

### 2.1.3 Forces and stresses exerted

There are two kinds of forces which can be exerted on bulk solids: the normal force  $F_N$  acting perpendicular to a certain area  $A$ , and the shear force  $F_S$  acting parallel to the area  $A$ . When a force does not fit any of both just mentioned, it can be split up in a perpendicular force and a parallel force yielding to a normal component and a shear component of that force respectively.

In order to remove the dependence of the area in the forces, is necessary to define the stresses. Stresses are the relationship between forces and the dimensions of the area where they are exerted. Therefore, the normal stress  $\sigma = F_N / A$  and the shear stress  $\tau = F_S / A$  are defined. Compressive stresses correspond to positive values and tensile stresses to negative values.

Shear stresses are important because they are responsible of the relative movement of the particles to each other.

When exerting a vertical compressive normal stress  $\sigma_v$  to a bulk solid element arranged in a container, if we assume an infinite filling height and frictionless internal walls, the resulting horizontal tensile normal stress exerted by the container  $\sigma_h$  is lower than the vertical so that the stress ratio  $K = \sigma_h / \sigma_v$  can be defined.

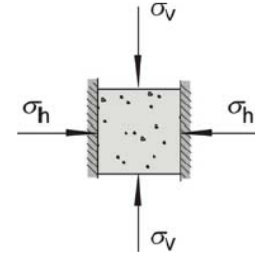


Figure 7. Bulk solid element with vertical stress exerted [8].

Besides, different stresses can be found in different cutting planes in a bulk solid. These normal stresses  $\sigma_\alpha$  and shear stresses  $\tau_\alpha$  acting on the different planes inclined by the angle  $\alpha$  can be theoretically calculated using the following expressions obtained from an equilibrium of forces [6]:

$$\sigma_\alpha = \frac{\sigma_v + \sigma_h}{2} + \frac{\sigma_v - \sigma_h}{2} \cos 2\alpha \quad \tau_\alpha = \frac{\sigma_v - \sigma_h}{2} \sin 2\alpha$$

If the values of  $\sigma_\alpha$  and  $\tau_\alpha$  calculated for all the possible angles  $\alpha$  are plotted in a  $\sigma$ - $\tau$  diagram a circle is obtained. This circle is called Mohr stress circle and represents all the possible stress conditions.

The radius of the Mohr stress circle is  $\sigma_r = (\sigma_v - \sigma_h) / 2$  and the center of the circle is placed at  $\sigma_m = (\sigma_v + \sigma_h) / 2$  and  $\tau_m = 0$ . Consequently, a Mohr stress circle has always two points of intersection with the  $\sigma$ -axis which define the circle called the principal stresses. The major principal stress corresponds to  $\sigma_1$  and the minor principal stress corresponds to  $\sigma_2$ .

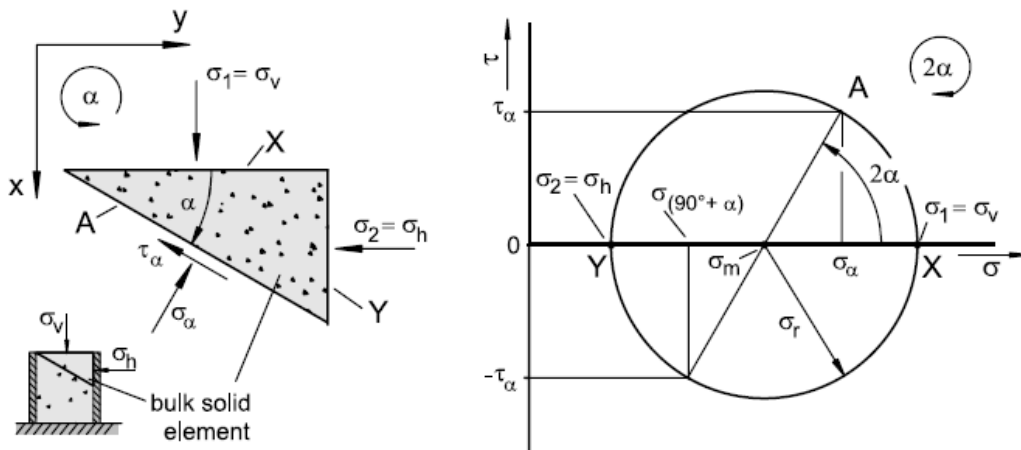


Figure 8. Equilibrium of forces on a cutting plain of a bulk solid element and the Mohr stress circle [8].

Mohr circles are highly important for the correct design of silos or hoppers since the effective angle of internal friction is determined from their representation (it will be further seen in section 2.2.4).

### 2.1.4 Bulk density

The bulk density  $\rho_b$  is the ratio of the mass of a certain quantity of bulk solid  $m$  and its volume  $V$ . It is important to do not confuse the bulk density with the solid density of the individual particles  $\rho_s$ .

Bulk density is always lower than solid density due to the existence of voids between the individual particles in a bulk solid. The relationship between bulk density and solid density depends on the porosity  $\varepsilon$ , which is defined as the ratio of the volume of the voids between the individual particles and the total volume of the bulk solid. If the fluid between the individual particles is a gas, the bulk density can be approximated to (where  $\rho_f$  is the density of the fluid):

$$\rho_b = (1 - \varepsilon) \cdot \rho_s + \varepsilon \cdot \rho_f$$

The bulk density depends on the consolidation stress acting in the bulk solid, especially in fine-grained bulk solids which can be highly compressed due to its small particle size that allows a higher packing of the individual particles. An increase on the consolidation stress leads to a decrease of the porosity and consequently an increase of the bulk density is observed. However, the bulk density increases until a certain limit, which corresponds to  $\rho_s$  ( $\varepsilon = 0$ ) is attained.

## 2.2 Flow properties

### 2.2.1 Flow function and time flow function

A specimen of bulk solid can be compressed by a vertical consolidation stress  $\sigma_1$  and subsequently exert an increasing vertical compressive stress over it until the specimen breaks. The compressive stress to failure  $\sigma_c$  is called compressive strength or unconfined yield strength.

The experienced failure is also called incipient flow and it actually is a plastic deformation, i.e. an irreversible deformation. Therefore, a yield limit exists for each specific bulk solid, and the bulk solid starts to flow when the compressive stress reaches this limit.

Like other properties mentioned before, the yield limit of a bulk solid depends on the stress history, in this case the previous consolidation. Greater consolidation stresses yield to greater bulk densities and unconfined yield strengths.

Therefore, by varying the consolidation stresses exerted, different values of bulk density and unconfined yield strength are obtained. These values can respectively be plotted in a  $\rho_b$ - $\sigma_1$  diagram and a  $\sigma_c$ - $\sigma_1$  diagram. The curve in the  $\sigma_c$ - $\sigma_1$  diagram is called the flow function. An example of possible curves on both diagrams is showed in *Figure 9*:

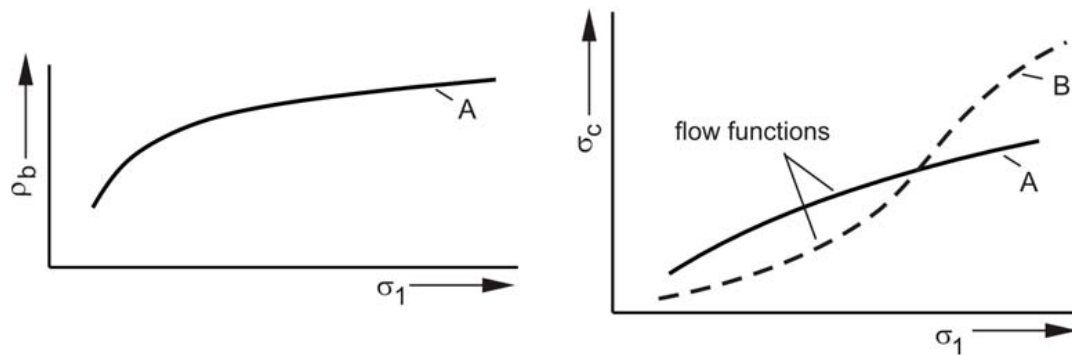


Figure 9. Bulk density - consolidation stress diagram and unconfined yield strength - consolidation stress diagram (flow functions). Note that flow functions like curve B are rarely obtained [8].

Schwedes (2000) stated that the flow function can only be properly determined using tests where both consolidation stress and unconfined yield strength are exerted in the same direction, due to anisotropic properties of the powders [9].

As stated before, some bulk solids gain strength due to the time consolidation or also called caking, e.g. the storage for a long time under a compressive stress.

Hence, compressing a specimen of bulk solid with a consolidation stress  $\sigma_1$  for a certain period of time  $t$  instead of a short period of time, it is obtained another unconfined yield strength  $\sigma_c$  value. Varying the consolidation stresses exerted on identical storage periods  $t$ , flow functions for each storage time can be determined. The flow functions for storage times  $t > 0$  are called time flow functions. Some examples of different time flow functions are showed in Figure 10:

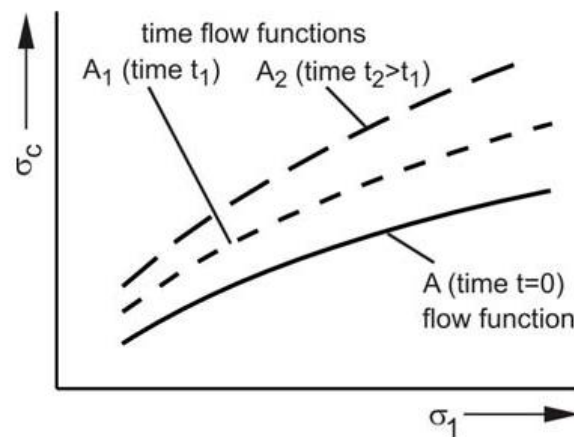


Figure 10. Flow function ( $t = 0$ ) and time flow functions at storage times  $t_1$  and  $t_2$  [8].

However, not all the bulk solids increase its unconfined yield strength when increasing the storage time. Some bulk solids do not have any changes in their unconfined yield strength along the time. Furthermore, each bulk solid undergo changes of different magnitude with time consolidation due to the different physical, chemical or biological processes which cause the consolidation (adhesive forces).

## 2.2.2 Numerical classification of flow behavior

The flow factor ratio  $ff_c = \sigma_1 / \sigma_c$  can be used to characterize numerically the flowability of several bulk solids, where greater values of the ratio represent a greater flowability of the powder. The numerical classification is the following [6]:

- $ff_c < 1$  Non-flowing
- $1 < ff_c < 2$  Very cohesive
- $2 < ff_c < 4$  Cohesive
- $4 < ff_c < 10$  Easy-flowing
- $10 < ff_c$  Free-flowing

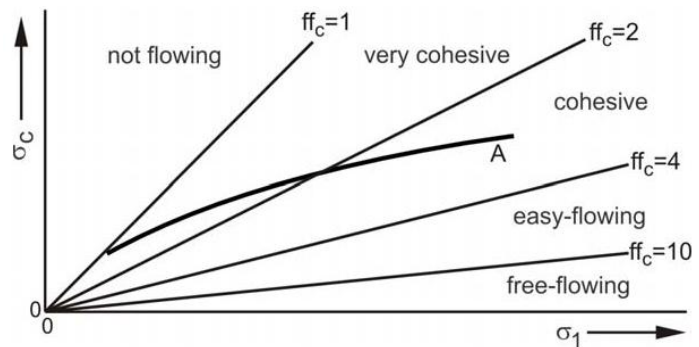


Figure 11. Flow function and boundaries of the numerical ranges of the classification of flowability [6].

As it can be clearly observed in *Figure 11* the flowability of a bulk solid depends on the consolidation stress  $\sigma_1$ .

The classification based on the flow factor ratio can also be used to evaluate the flowability of a powder depending on the time consolidation effect, where at greater consolidation times (for a certain constant consolidation stress), a worse flowability usually occurs.

Furthermore, there is another ratio called Hausner ratio which can be used to characterize the flow behavior of bulk solids, although it depends on a lot of parameters and not always provide reliable results [10]. The Hausner ratio  $HR = \rho_t / \rho_{ae}$  is the ratio between the bulk density of fine powders after prolonged tapping of the sample and the aerated density (initial density), and expresses the reduction of the volume of a packed bed of particles. The classification is showed below [11]:

- $HR < 1,25$  Not cohesive (free flowing)
- $1,25 < HR < 1,4$  Intermediate flow behavior
- $1,4 < HR$  Cohesive (non-free flowing)

Hence, both classifications can be used to evaluate the bulk solids flowability depending on the desired parameters which need to be studied for a better understanding of the flow behavior of a certain powder. The flow factor ratio classification will be used with the results experimentally obtained in this thesis to analyze the dependence of the temperature on the raw meal flowability (section 5.1.3).

### 2.2.3 Yield limit

When determining the unconfined yield strength the walls are assumed frictionless and the effects of the gravity are neglected. Hence, both vertical stress and horizontal stress are constant in the entire bulk solid specimen so that the stresses can be represented in the Mohr stress circle, which is identical at each position.

In the consolidation process the shear stresses in both horizontal and vertical cutting planes are assumed as  $\tau = 0$ . Therefore, the vertical stress  $\sigma_v$  and the horizontal stress  $\sigma_h$  equal respectively to the major and minor principal stresses ( $\sigma_1$  and  $\sigma_2$ ) so they can be plotted in the  $\sigma$ - $\tau$  diagram since the Mohr stress circle is already defined.

After removing the walls and increasing the vertical stress, the horizontal stress equals to zero, and identically as the consolidation process the principal stresses can be plotted in each vertical stress value until the failure of the specimen. In that moment the yield limit is reached so its representation in the diagram must be tangent to the last Mohr stress circle.

There is also the possibility of applying the increasing vertical stress without removing the walls which contain the specimen. In this case the horizontal stress is not equal to zero, and the principal stresses can be plotted so the Mohr stress circle is defined. The Mohr stress circle which corresponds to incipient flow must be also tangent to the yield limit.

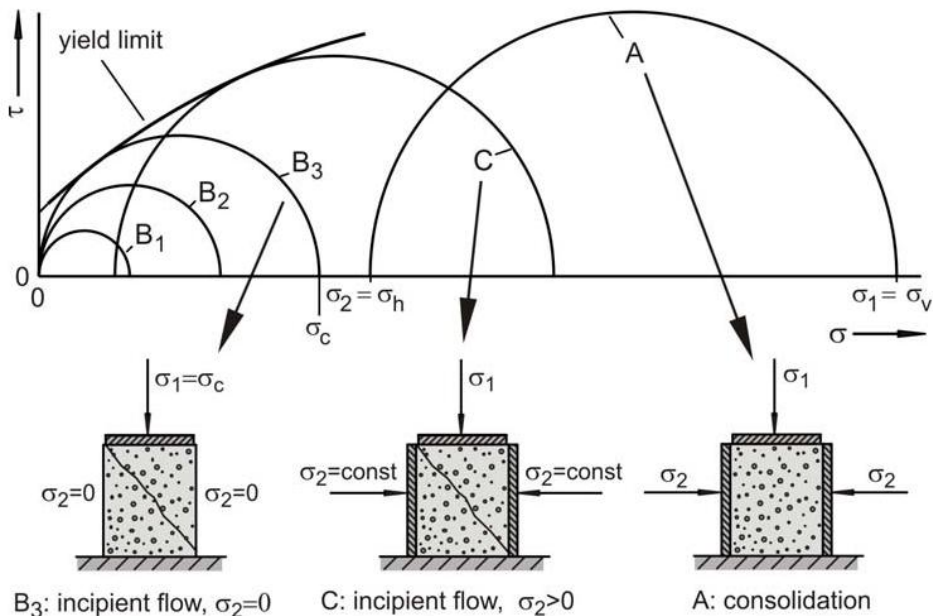


Figure 12. Representation of the yield limit using the Mohr stress circles [8].



## 2.2.4 Yield locus and time yield locus (shear tests)

Otherwise than using uniaxial compressive tests to measure the yield limit or also called yield locus, shear tests are more widespread for this purpose since Mohr stress circles can be directly determined from the measured data.

In these kind of tests a bulk solid specimen is consolidated (so-called preshear) by a vertical consolidation normal stress  $\sigma_{pre}$  and after that is sheared with an increasingly shear stress  $\tau$  until a constant shear stress  $\tau_{pre}$  is attained so a steady-state flow occurs. At this moment, a constant bulk density is also achieved. The preshear ends after the shear deformation is reversed until a value equal a zero. The shear stress  $\tau_{pre}$  and the bulk density  $\rho_b$  obtained are characteristic for the normal stress  $\sigma_{pre}$  exerted.

Afterwards, the normal stress applied to the specimen is reduced to a lower value  $\sigma_{sh}$ , and the top particles begin to move against each others with a constant velocity caused by the shear stress  $\tau$  exerted on the bulk solid specimen (so-called shear to failure). This shear increases until a value  $\tau_{sh}$  where the incipient flow is attained.

Plotting the obtained values for the preshear and shear to failure (with several normal stresses  $\sigma_{sh}$ ) processes in a  $\sigma$ - $\tau$  diagram the yield locus is determined.

An example of the results obtained in these tests is showed underneath:

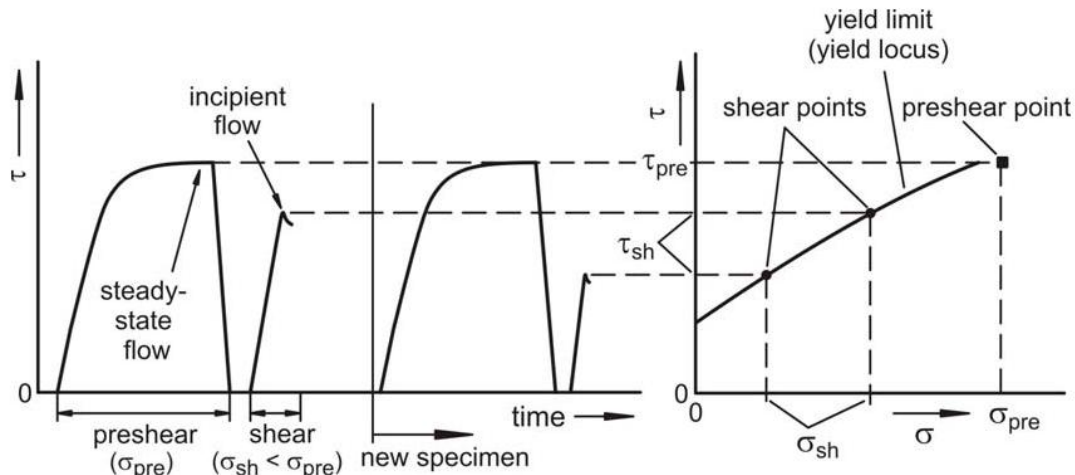


Figure 13. Representation of the yield locus determined with shear tests [8].

Relevant parameters which define the flow behavior of a bulk solid can be obtained from the yield locus.

In analogy to the uniaxial compression, the consolidation stress  $\sigma_1$  correspond to the major principal stress of the steady-state flow Mohr stress circle. This Mohr circle is tangential to the yield locus intersecting with it at  $(\sigma_{pre}, \tau_{pre})$ . The unconfined yield strength  $\sigma_c$  corresponds to the major principal stress of the shear to failure Mohr stress circle. This circle is defined by a minor principal stress equal to zero and is also tangential to the yield locus.

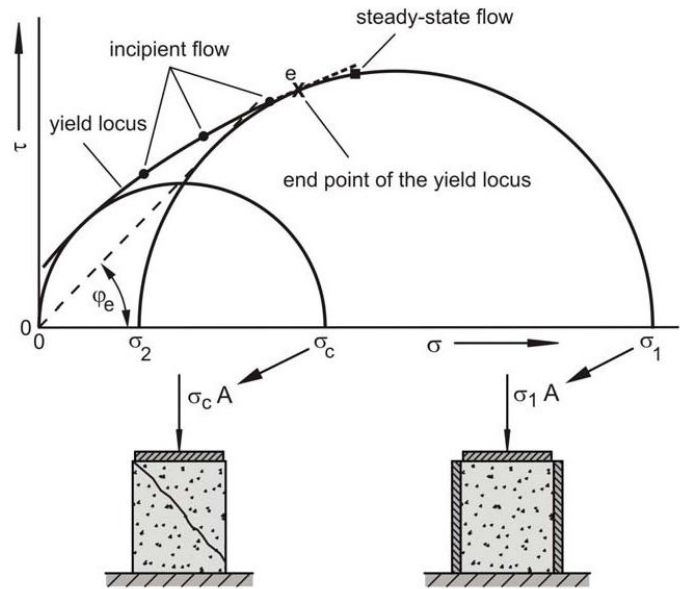


Figure 14. Analogy of the yield locus to the uniaxial compression procedure, effective yield locus and effective angle of internal friction [8].

Furthermore, a tangent line to the steady-state flow Mohr stress circle can be drawn from the origin of the  $\sigma$ - $\tau$  diagram. It is called effective yield locus. The angle  $\phi_e$  defined between the effective yield locus and the  $\sigma$ -axis is called effective angle of internal friction and it has a relevant importance on the design of silos or hoppers.

Ashton et al. (1965) developed the Warren Spring equation [12]. This equation is the most valid to describe the shape of a plotted yield locus of cohesive and non-cohesive powders as stated by Stainforth & Berry (1973) [13]:

$$\frac{\tau}{C}^n = \frac{\sigma + T}{T}$$

Where:  $n$  is the shear index,  $C$  is the cohesion of the powder and  $T$  is the tensile stress. All the parameters can be determined from the graph:  $C$  corresponds to the intercept of yield locus on the  $\tau$ -axis and  $T$  corresponds to the intercept of yield locus on negative values of  $\sigma$ -axis. All the parameter should be expressed in the same stress units.

Using shear tests it is also possible to study the influence of time consolidation on the yield locus. In this case the bulk solid is presheared as explained and after a consolidation normal stress  $\sigma$  during a desired period of time  $t$ , it is sheared to failure. The consolidation stress must be the same as the consolidation stress  $\sigma_1$  determined from the yield locus in order to have the same major principal stress both in preshear and consolidation processes. The yield loci obtained for different storage times  $t > 0$  are called time yield locus. Time yield loci are defined for the consolidation period of time and the consolidation stress applied. Some examples of time yield locus are showed in Figure 15:

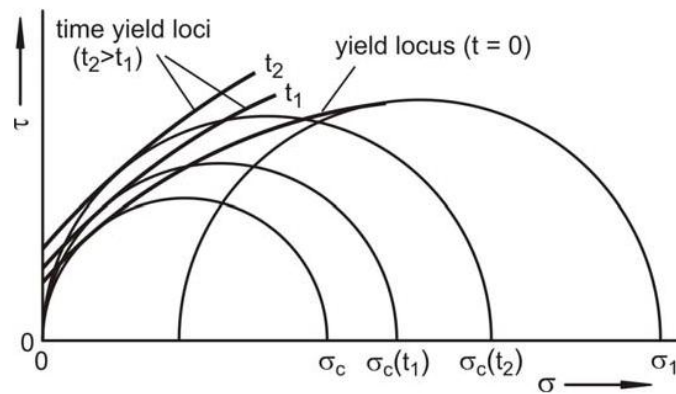


Figure 15. Yield locus ( $t = 0$ ) and time yield loci at storage times  $t_1$  and  $t_2$  [8].

### 2.2.5 Wall friction

Wall friction, i.e. the friction between a bulk solid and the surface of a solid wall containing it, is another important property when designing the walls of a silo, a hopper or other equipments where the powder flows along a surface.

In order to determine the wall friction, a specimen of bulk solid is held with the wall normal stress  $\sigma_w$  and after that shifted in relation to the wall surface with a constant velocity so that the wall shear stress  $\tau_w$  between the specimen and the wall material selected can be measured. This procedure is carried out decreasing the wall normal stresses and the wall shear stress depends on the wall normal stress exerted. The values obtained can be plotted in a  $\sigma_w$ - $\tau_w$  diagram, where the resultant curve is called wall yield locus.

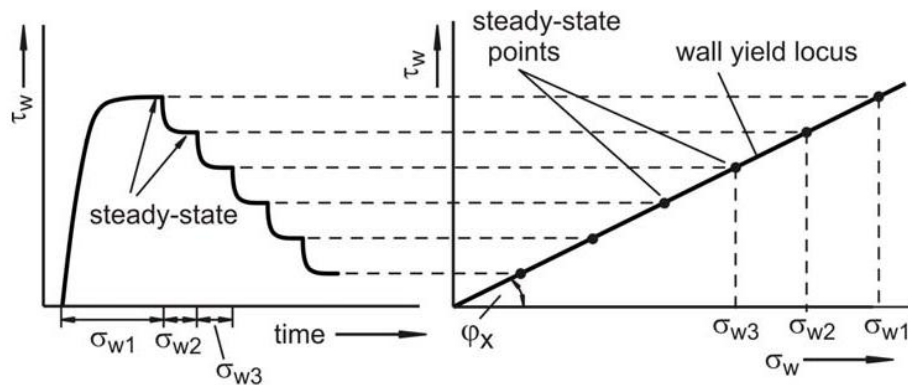


Figure 16. Representation of the wall yield locus obtained with the wall friction procedure [8].

Specifically the important parameters that determine wall friction are the wall friction coefficient  $\mu$  and the wall friction angle  $\phi_x$ . The wall friction coefficient is the ratio between the wall shear stress and the wall normal stress. The wall friction angle is the slope of a line drawn from the origin of the diagram to a chosen point of the wall yield locus. When the wall yield locus is curved, the wall friction angle depends on the wall normal stress.

There are some materials which use to adhere at the walls and this is denoted when the wall yield locus intersects the  $\tau$ -axis at values unequal to zero. This shear stress  $\tau_{ad}$  is called adhesion.

## 2.3 Testing methods

Even though the classical theory of bulk solids was developed in the second half of the 20th century through experiments using mainly Jenike shear tests [14], the establishment of modern technologies led to a big variety of suitable methods for the studying of the flowability of bulk solids. Some of the most used and/or most interesting testing methods are explained as follows.

### 2.3.1 Uniaxial compression test

The uniaxial compression test is the test used to determine the flow function of a bulk solid as explained previously. The fine-grained bulk solid sample is introduced into a hollow cylinder where the vertical consolidation stress is exerted during the desired period of time without wall friction (this ensures that the vertical stress is constant throughout the bulk solid specimen). Once the bulk solid specimen is consolidated, the hollow cylinder is removed and after the increasing vertical compressive stress is applied until the incipient flow is achieved.

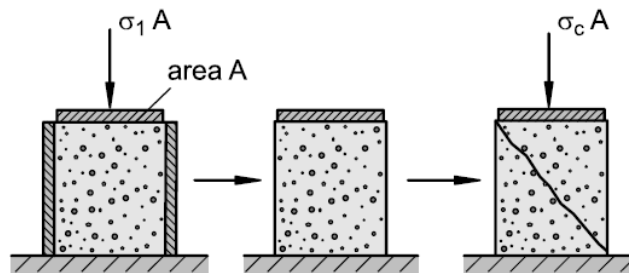


Figure 17. Procedure of the uniaxial compression test [6].

This test is not appropriate for coarse-grained bulk solids due to the low values of unconfined yield strength obtained. Besides, parameters like internal and wall friction cannot be obtained using this test unlike shear tests [6].

### 2.3.2 Jenike shear test

The Jenike shear test was the first shear test and was developed by Jenike (1964) [15].

The Jenike shear test cell is formed by a bottom ring, an upper ring and a lid. The lid is loaded with a normal force  $F_N$ . Then, the upper part of the cell is shifted by a motorized stem against the bottom part of the cell, which is fixed, leading to a shear deformation of the bulk solid specimen. Consequently, the force  $F_S$  necessary to attain the failure of the specimen is measured.

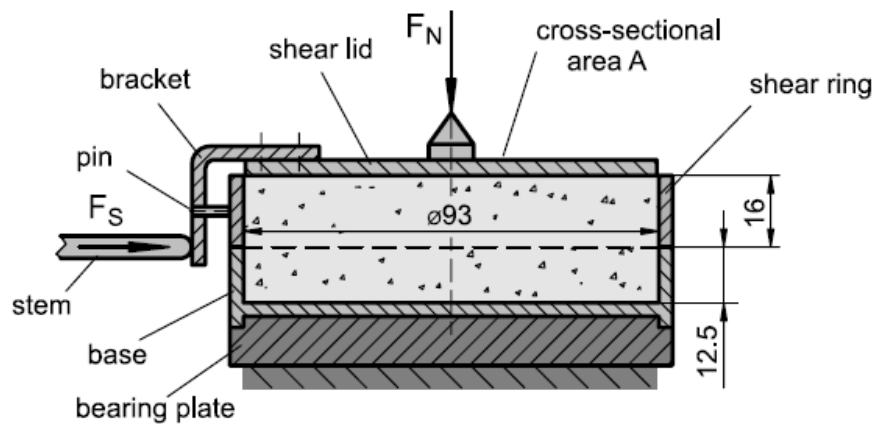


Figure 18. Cell of the Jenike shear test [6].

The procedure of the test is the execution of a preshear and a shear to failure processes. After finishing the test with one bulk solid specimen, it has to be removed and replaced for another.

The disadvantages of this test are that it requires a high level of training and skill, and the procedure is extremely slow and the person who carries it out has to be present all the time. Furthermore, the manual consolidation of the specimen can lead to experimental errors and bulk solids which need a large deformation to achieve the steady-state flow cannot be tested using this method [6].

### 2.3.3 Uniaxial shear test

The uniaxial shear test can be considered as a mixture of the two methods previously discussed. The bulk solid specimen is consolidated using a normal force  $F_V$  and once the lid of the cell is removed, the specimen is shifted horizontally by a pushing wall. The force  $F_M$  necessary for the failure of the specimen is measured so that the unconfined yield strength can be determined.

The disadvantage of this test is that due to anisotropic effects (like limestone samples do) caused because the direction of the stress applied is perpendicular at the consolidation, it is not possible assess the effects of the time consolidation on the flowability [6].

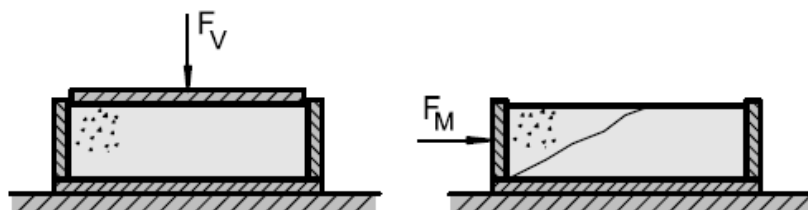


Figure 19. Procedure of the uniaxial shear test [6].

### 2.3.4 Angle of repose measurement

There are at least eight methods for measuring the angle of repose (also divided into static and dynamic methods), and each one give slightly different results of the angle of repose. However, the trends of the obtained results when analyzing the dependence of the angle of repose on a certain parameter are nearly the same [16].

However, the most extended is the poured angle of repose measurement, where the angle of repose  $\alpha_M$  corresponds to the angle of an uncompacted powder conical heap formed after the procedure of the test is done. The heap is obtained after a known mass of the bulk solid has been poured through a funnel which can remain static or be moved upwards while the bulk solids is poured so that the distance between the funnel and the conical heap remains constant.

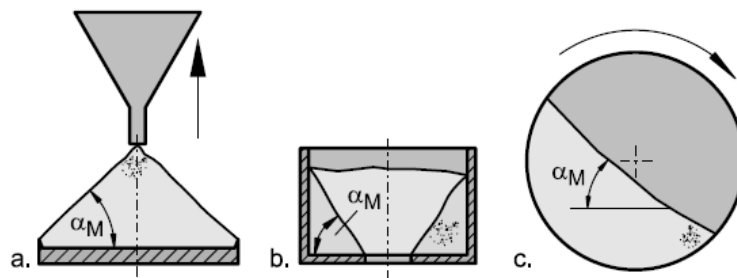


Figure 20. Some of the methods for measuring the angle of repose: a. poured angle of repose; b. drained angle of repose; c. dynamic angle of repose [6].

Depending on the results obtained, Carr (1965 & 1970) and Raymus (1985) established [15]:

- |                                 |  |
|---------------------------------|--|
| • Angle of repose < 30 °        | Good flowability                                 |
| • 30 ° < Angle of repose < 45 ° | Some cohesiveness                                |
| • 45 ° < Angle of repose < 55 ° | True cohesiveness                                |
| • 55 ° < Angle of repose        | High cohesiveness, i.e. very limited flowability |

Nevertheless, Brown and Richards (1970), Geldart et al. (1990), Antequera et al. (1994) and Cain (2002) preferred the classification in cohesive powders and non-cohesive powders considering the boundary between them on the 40 ° value [11], [15].

The advantage of this method is that it is quite simple and fast to perform and does not need trained operators, so it can be used as a control procedure in the industry. Nevertheless, the angle of repose measurement strongly depends on the design of test devices and the procedures like the falling distance, the quantity of the sample or the method used to quantify the value of the angle of repose obtained [17]. Furthermore, when cohesive powders are tested, irregular heaps can be formed, which makes it difficult to find a single angle that describes the shape of the pile.

For the correct design of the handling equipment of bulk solids, the calculated angle of hopper to the horizontal  $\pi/2 - \theta$  (determined from the effective angle of internal friction) has to be larger than the measured poured angle of repose and the sliding angle of repose in order to ensure a correct operation [13].

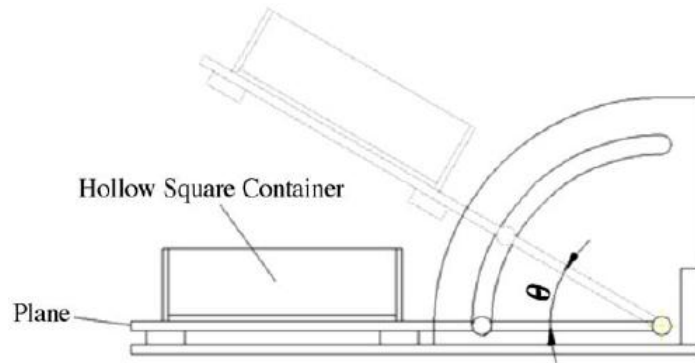


Figure 21. Schematic diagram for measuring the sliding angle of repose [16].

Trying to remove dependences caused by the different used devices in the angle of repose procedure, Geldart et al. (1990) [15], [17] developed a standardized robust testing device and its procedure for the angle of repose measurement. During more than fifteen years, the equipment has been re-examined and improved passing through several stages until a reliable testing device for both cohesive and non-cohesive powders was achieved. The most recent version of the device is called *Mark 4 Powder Research Ltd. AOR Tester* and it is showed as follows:

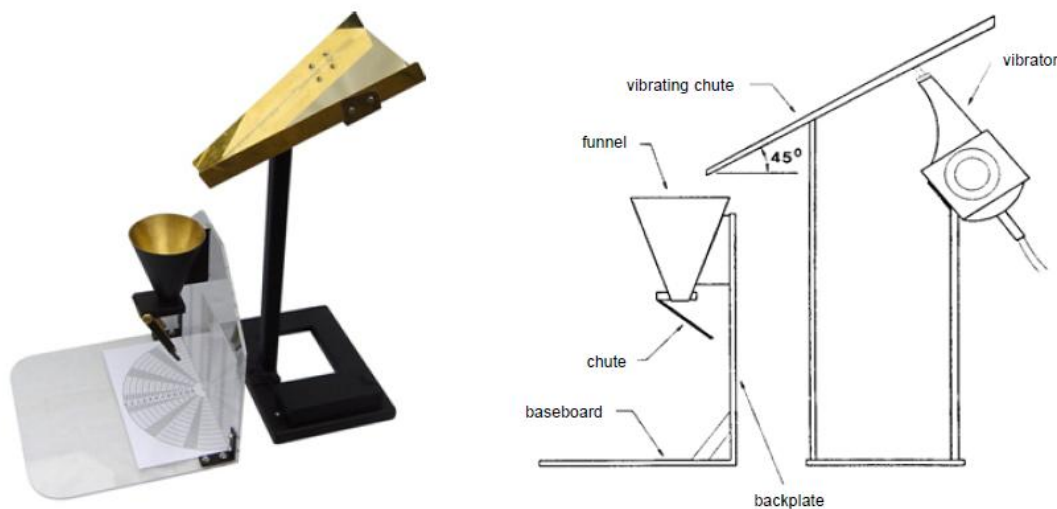


Figure 22. Mark 4 Powder Research Ltd. AOR Tester [15], [17].

Furthermore, the developed procedure is the following:

- 100 grams of powders (preferably) are weighed and put into a metal beaker.
- If the powder seems to be free-flowing, the powder sample is poured slowly onto the upper converging chute, taking about 20 seconds to pour all the powder. If the powder shows some cohesiveness, the vibratory motor is switched on.
- The powder flows towards the upper chute and falls into the metal hopper and finally reaches the lower chute which directs the powder against the vertical wall.
- The semi-cone formed should have a well formed apex, and in that case, the angle of repose is calculated from a table.



### 2.3.5 Cohesion tests

On one hand, the Warring Spring Bradford cohesion test consists of a cylindrical test cell where the bulk solid specimen is introduced. After the specimen is consolidated applying a vertical force  $F_V$ , a spoked wheel monitored by a computer is introduced into the bulk solid until the top edge of the vanes is leveled with the surface of the specimen. Afterwards, the vaned paddle is applies a gradually increasing torque over the cylindrical column of powder. At the beginning, the torque applied by the spoked wheel is resisted by the shear resistance of the bulk solid, but a torque which cannot be resisted by the specimen and the wheel begins to rotate exists. The maximum torque  $M_M$  measured at the failure of the specimen is used to determine the shear stress to failure.

On the other hand, the same principle is used in the flowability test. In this test, the bulk solid specimen is consolidated exerting the normal force  $F_V$  on the top plate when the stirrer is already inside the bulk solid specimen. After the consolidation, the top plate is raised and the stirrer is slowly rotated. The maximum torque measured at failure  $M_M$  is used to determine the flowability of the specimens.

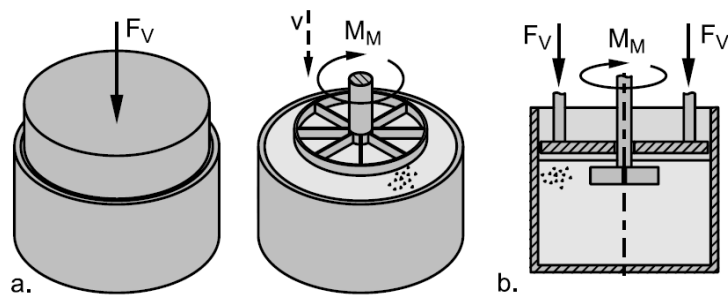


Figure 23. a. Warren Spring Bradford cohesion test, b. flowability test [6].

The disadvantage of this method is that it can only be considered as a qualitative comparison test in terms of cohesion between different bulk solids. The reason of this is that the force is locally applied by the vanes of the stirrer (the deformation depends on the radius) and the stresses in the shear plane of failure are not known [6]. Although this method measures the cohesion of a bulk solid, i.e. the resistance to shear, it can be regarded as the inverse of the flowability [18].

The advantage of the cohesion shear test is that it gives very sensitive results and has a high reproducibility due to that fact that the spoked wheel is monitored by a computer.

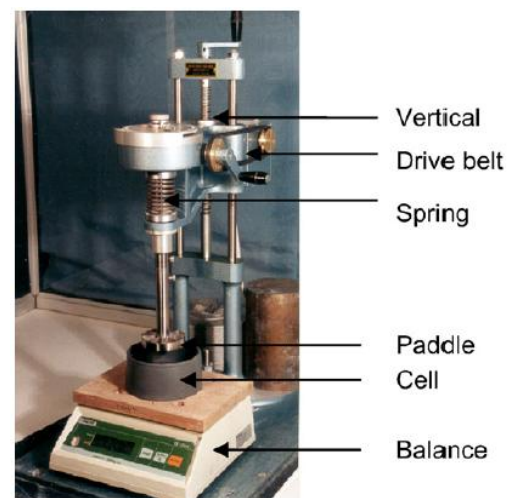


Figure 24. Warren Spring Bradford cohesion test device [18].



### 2.3.6 Torsional shear test

The torsional shear test (similarly to the cohesion shear test) consists of a cylindrical test cell where the bulk solid specimen is introduced. First the specimen is consolidated by applying a normal force  $F_N$  using a roughened lid and afterwards the lid is rotated so that a shear deformation occurs and the torque needed for the failure  $M_M$  is measured. The shear stress to failure can be determined from the measured torque.

Besides, another kind of torsional shear test with a split level shear cell exists. This cell consists of two parts (a base and a shear ring) allowing rotation of the shear ring relative to the base.

In both kind of torsional shear tests, the bulk solid specimen is presheared and sheared to failure, so the yield locus can be determined.

The advantage of the torsional shear test is that it provides quantitative information of the flowability of the bulk solid and the effect of time consolidation can be correctly stated. Nevertheless, it is known that the results obtained from this method can differ from the ones obtained with the Jenike shear test [6]. Similarly to the cohesion shear test, this test gives very sensitive results and has a high reproducibility due to the computer monitored test procedure.

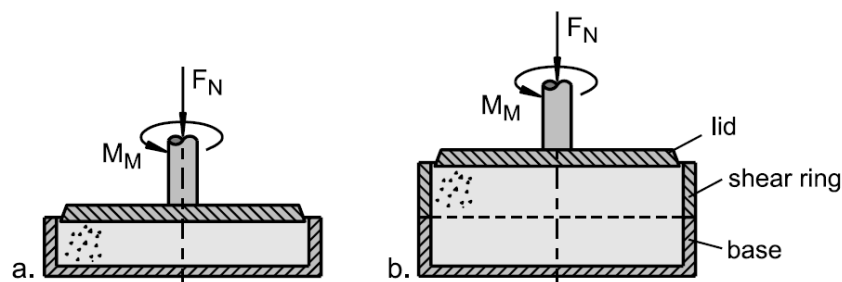


Figure 25. a. Cell of the torsional shear test, b. torsional shear test with a split level shear cell [6].



### 3. Previous research

A lot of experimental researches on the flow properties of powder have already been done, especially in the pharmaceutical industry, the food manufacturing industry and the chemical industry, where the cement manufacturing is included [19], [20].

On one side, the purpose of these investigations was to study the flow behavior of several substances of interest so that a better design of the handling facilities and a consequently better performance can be attained. On the other side, the purpose was either to evaluate new testing methods comparing the results with results obtained using established methods or to establish new theoretical considerations on the area. Some of the more relevant are shown in this section.

#### 3.1 Classification of powders

Geldart (1973) proposed that based on the flow behavior of powders fluidized by gases, powders can be classified by four groups defined by the mean particle size and the density difference between the particle density and the fluidized density. This classification proposed by Geldart was the following [21]:

- Group A: Suffer a dense phase expansion after minimum fluidization and before the bubbling starts.
- Group B: Bubble at the minimum fluidization velocity.
- Group C: Have a low mean particle size and are difficult to fluidize.
- Group D: Have a large mean particle size or density (or both) and spout easily.

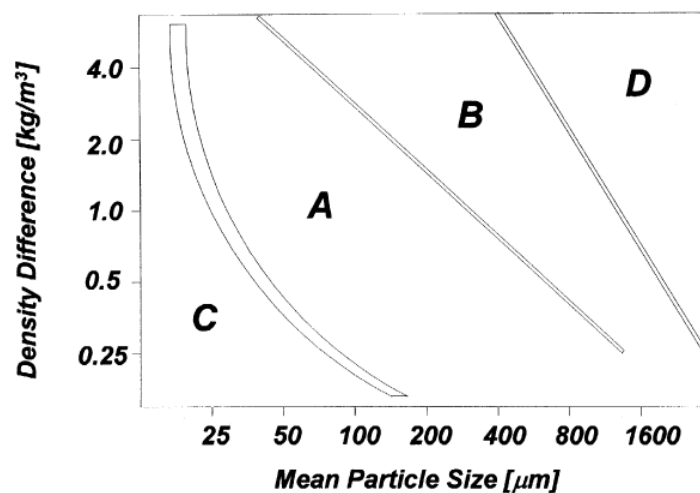


Figure 26. Schematic diagram of powder classification for fluidization by air proposed by Geldart (at ambient temperature) [22].

## 3.2 Flowability research

Concerning the influence of the particle size and shape, Podczek and Miah (1996) [23] determined the optimal concentration of magnesium stearate<sup>1</sup> needed to improve the flowability of several powders with different particle shape and size, using an annular shear cell to determine the flowability. The used parameters to analyze the flowability were the angle of internal friction ( $\delta$ ) and the Jenike's flow factor ( $ff$ ). The lowest values for the angle of internal friction and the highest values for the Jenike's flow factor correspond to the better flowability.

Table 1. Particle size and shape of the studied powders [23].

Powder	$d_{vs}$ [ $\mu\text{m}$ ]	Shape (BP)
Pregelatinized starch	103.2	Angular
Paracetamol	537.6	Angular
Calcium carbonate	4.6	Cubic
Potassium chloride	481.1	Cubic
Maize starch	49.2	Round
Microfine cellulose	363.3	Round
Microcryst. cellulose	107.7	Rod shaped
Acetylsalicylic acid	721.7	Needle shaped

$d_{vs}$ , Edmundson's weight mean of the surface distribution.

In the results obtained from the performed experiments they could see that both particle size and particle shape have an important influence in the flow behavior of powders, where the flowability for unlubricated powders (in terms of the flow factor) increases from needle shaped, cubic shaped, angular shaped to round shaped particles. Nevertheless using an optimal concentration of magnesium stearate, needle shaped can behave similarly to round shaped particles. Moreover, and improvement of the flowability after the addition of magnesium stearate was obtained in all the studied powders.

Table 2. Results of the flow characteristics of the studied powders [23].

Powder	Unlubricated powder		Lubricated powder			
	$\delta$ [°]	$ff$	$\delta_{min}$ [°]	MgSt <sub><math>\delta</math></sub> [%]	$ff_{max}$	MgSt <sub><math>ff</math></sub> [%]
Pregelatinized starch	55.41	2.27	43.30	1.25	8.95	1.25
Paracetamol	45.00	8.78	37.95	0.75	28.27	0.75
Calcium carbonate	56.23	1.81	39.35	1.00	8.67	1.25
Potassium chloride	43.77	5.75	41.67	1.25	9.67	1.25
Maize starch	48.36	9.68	41.35	0.75	48.45	0.75
Microfine cellulose	46.67	9.20	41.99	0.25	> 50	1.25
Microcryst. cellulose	50.43	7.66	48.21	0.25	> 50	1.25
Acetylsalicylic acid	54.48	1.58	49.61	0.25	> 50	0.25

MgSt, optimum magnesium stearate concentration.

<sup>1</sup> Magnesium stearate is, nowadays, the most frequently used additive to improve the flowability of powders. It was stated by Gold et al. (1968) [23] that magnesium stearate reduces the adhesion of the particles due to long-range Van der Waals forces between the particles.

Concerning the effect of consolidation and time consolidation on bulk solids, Teunou et al. (2000) [24] studied this effect in the obtained flow functions from three different powders: flour, tea and whey-permeate. Four different consolidating stresses were used which represent the stresses in a silo of 15 m high and 3 m of diameter: 3 kPa, 5,75 kPa, 9,87 kPa and 14 kPa. The testing method used to determine flow function was the Jenike shear test.

The obtained time flow functions are shown:

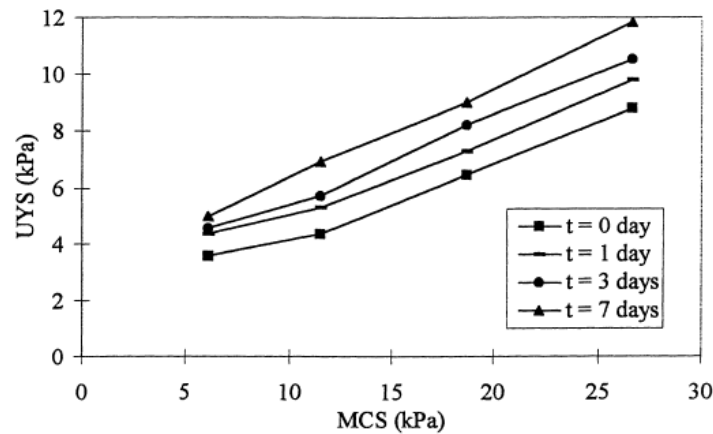


Figure 27. Time flow functions obtained with flour powder [24].

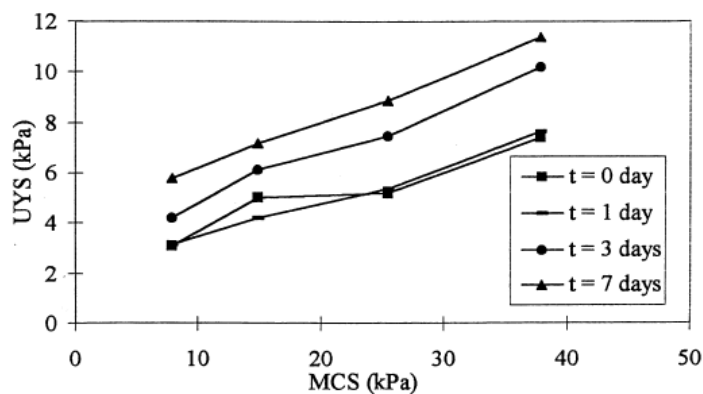


Figure 28. Time flow functions obtained with tea powder [24].

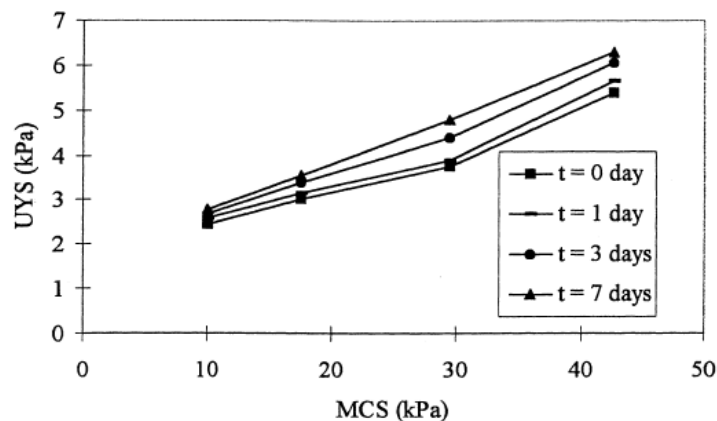


Figure 29. Time flow functions obtained with whey-permeate powder [24].

Concerning the dependence of moisture on bulk solids flowability, Teunou et al. (1999) [13] studied the dependence of the relative humidity on the flowability of four different food powders (flour, skim-milk, whey-permeate and tea) using a annular shear cell and a Jenike shear cell. The results showed that, in general, the flowability decreases when increasing the relative humidity due to an increase of the adhesive forces:

However, to understand the flow behavior of each powder, other parameters like the critical relative humidity, the water sorption isotherms or the particle size had to be taken into account.

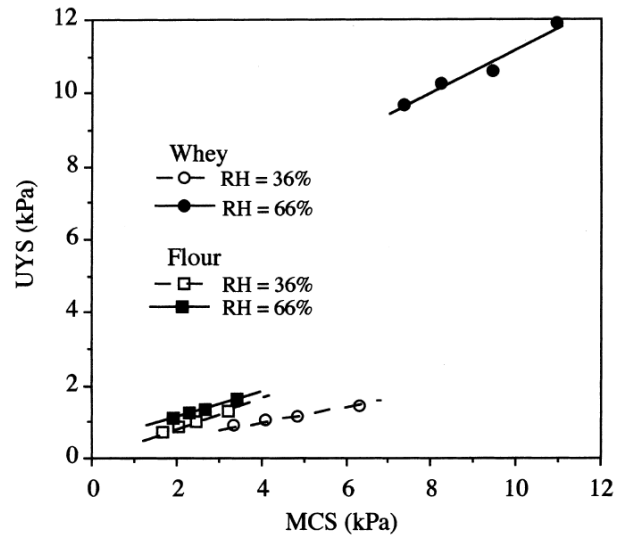


Figure 30. Instantaneous flow functions of flour and whey-permeate powder at 36 % and 66 % of relative humidity at 20 °C [13].

Wang et al. (2010) [16] studied the flow behavior of pulverized coal samples of different particle sizes and also different moisture contents using three different methods on angle of repose measurement. The results concluded that in general the greater the moisture content is, the greater the angle of repose measured is, i.e. the smaller the flowability is:

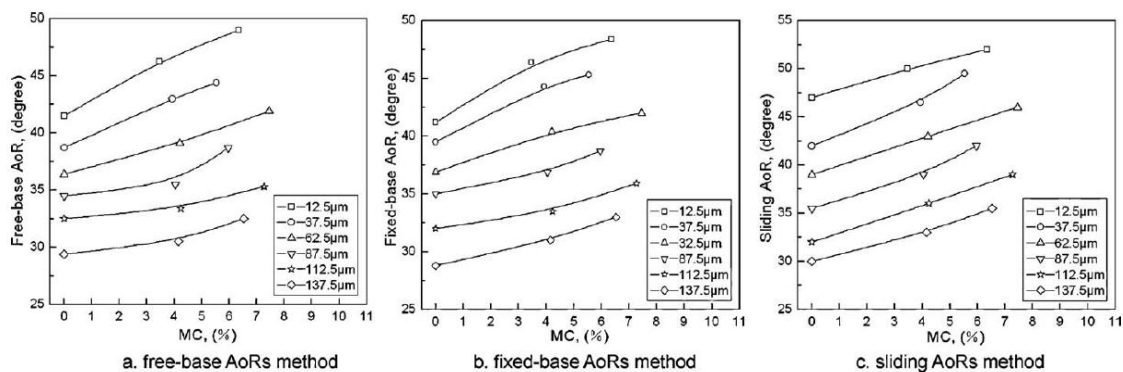


Figure 31. Variations of the angle of repose with moisture content (MC) for pulverized coal with different sizes measured with three different kind of angle of repose measurements [16].

Concerning the particle size effect, Wang et al. (2010) [16] found that for the smallest particles, the angle of repose decreased when increasing particle size, but after a critical value, which depends on the bulk solid density, the angle of repose increased. It was found that this behavior could be related to the particle classification proposed by Geldart.

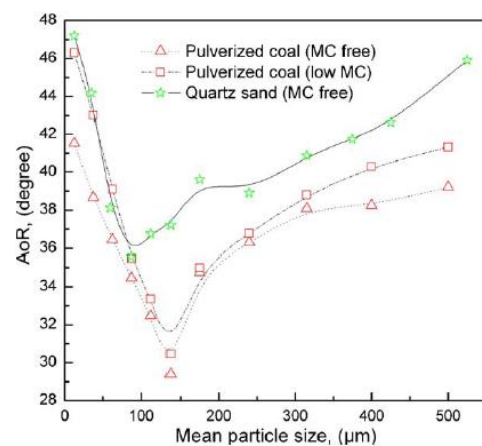


Figure 32. Variations of the free- base angle of repose measurement with the mean particle size [16].

Wouters and Geldart (1996) [15], [17] and later Geldart et al. (2006) [13] found a correlation between the Hausner ratio and the angle of repose using four different kinds of powders: sodium bicarbonate, equilibrium fluid cracking catalyst (FCC), sodium carbonate (soda ash) and lactose:

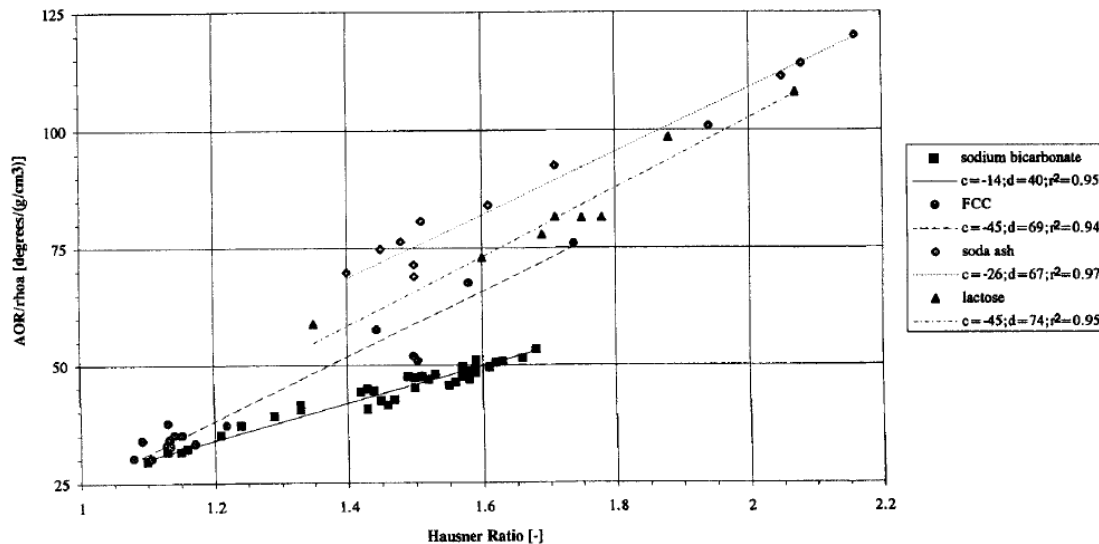


Figure 33. Correlation between the weighted angle of repose divided by the aerated bulk density ( $AOR/\rho_A$ ) and the Hausner ratio for the different studied substances [14].

Santomaso et al. (2003) [25] determined the poured density, the dispersed density, the tap density and the true density on more than ten different powders. After evaluating these densities through angle of repose measurements, the packing ratio to characterize the flow properties of bulk solids was suggested.

The Packing ratio was defined as the ratio between the dispersed density and the poured density.

This ratio was found to be more sensitive to flowability variations in the cases where the Hausner ratio could not distinguish between different samples. Furthermore, a linear correlation with the square root of the angle of repose was determined. However, the Packing ratio does not take into account the compaction so a combination of the Packing ratio and the Hausner ratio should be used.

In order to evaluate the Warren Spring cohesion test, Geldart et al. (2009) [18] found, using mixtures of alumina powders with different mean particles sizes, that a correlation between values of flowability calculated from the inverse of cohesion (determined using the cohesion test) and values of angle of repose exists.

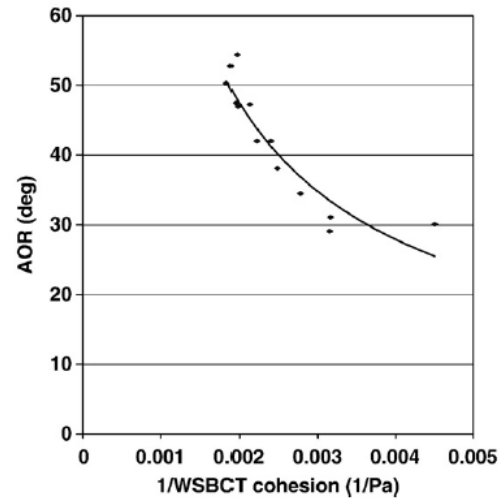


Figure 34. Angle of repose versus the inverse of the cohesion calculated with the Warren Spring cohesion test [18].

Additionally, Krantz et al. (2009) [26] also found correlations between the values of a torsional test and values obtained from other techniques like the angle of repose measurement, the avalanche angle measurement and the bed expansion ratio. They used two different formulations of coating powders: polyurethane and polyester-epoxy powders.

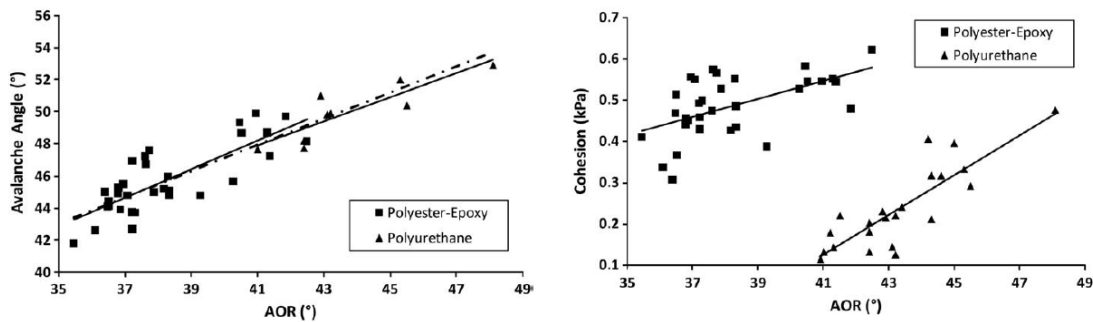


Figure 35. Angle of repose plotted against avalanche angle of repose and against cohesion [26].

Mohammed et al. (2011) [11] defined the weighted cohesion indicator ( $WS_A$ ) as the ratio between the cohesion ( $S$ ) obtained from a Warren Spring-University of Malaya cohesion test and the aerated bulk density ( $ABD$ ):

$$WS_A = \frac{S}{ABD}$$

Performing that modified Warren Spring cohesion test, performing a measure of the Hausner ratio and measuring the angle of repose on samples of silica gel and ballotini powders of different mean particle size, besides of taking into account the flowability classification on the Hausner ratio and the 40 ° criteria for the angle of repose, a classification of the flow behavior on the weighted cohesion indicator was determined [11]:

Table 3. Flowability classification of powders based on the weighted cohesion indicator ( $WS_A$ ) [11].

Flowability	$WS_A \times 10^3 \text{ (m}^2/\text{s)}$
Free-flowing	<0.11
Semi-cohesive	0.11–0.16
Cohesive	>0.16



Jiang et al. (2009) [27] proposed a new testing method to evaluate the flowability of bulk solids based on the flow of the powder in a vibrating capillary. Using this method, the flowability can be evaluated from several points of view. A schematic diagram of the vibrating capillary method device is depicted in *Figure 36*:

The principle of the vibrating capillary method consists of filling the glass tube with the powder to study, which has to be fully kept along the measurement. Afterwards, the capillary has to be horizontally vibrated by a piezoelectric vibrator. This vibration can be sinusoidal, rectangular, triangular or saw-tooth, amongst other shapes. Moreover, the frequency and the amplitude of the vibration can be automatically increased or decreased. Finally, the mass of particles discharged from the capillary end is measured by a digital balance, providing a profile of the mass discharged during the time that the performance of the testing method lasts [27].

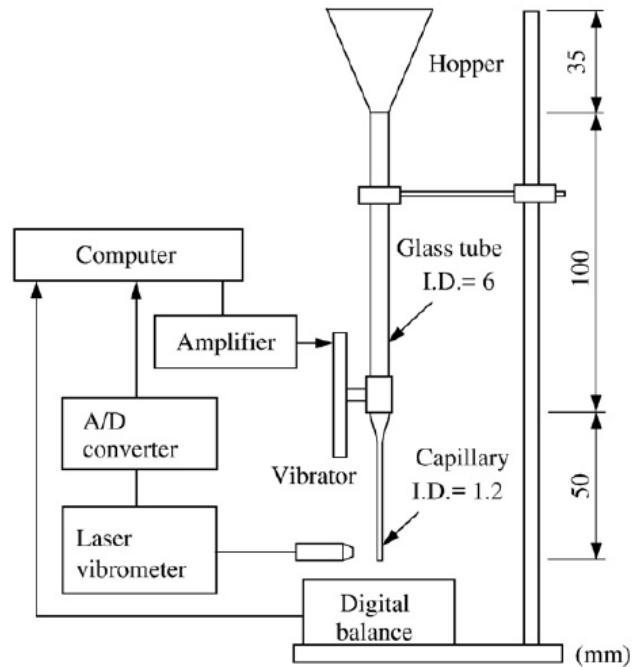


Figure 36. Schematic diagram of the vibrating capillary device [27].

Hassanpour and Ghadiri (2007) [28] introduced the indentation on a bulk solid bed as a new testing method to characterize the flowability of powders. The procedure of this testing method is rather similar to the uniaxial compression test, so it was shown that with some powders there was a correlation between this indentation and the uniaxial compression test, defining a constraint factor  $C$  as the ratio between the results obtained with the uniaxial compression test and with the indentation ball test.

The ball indentation test consists on a high precision spherical glass indenter which applies loads from 2 to 10 mN to the powder specimen, which has to be previously consolidated. The displacement of the indenter ( $h$ ) is continuously recorded in the computer and the maximum on the pressure exerted on the powder specimen belongs to the indentation hardness. A schematic diagram of the principle of the test is shown in *Figure 37*:

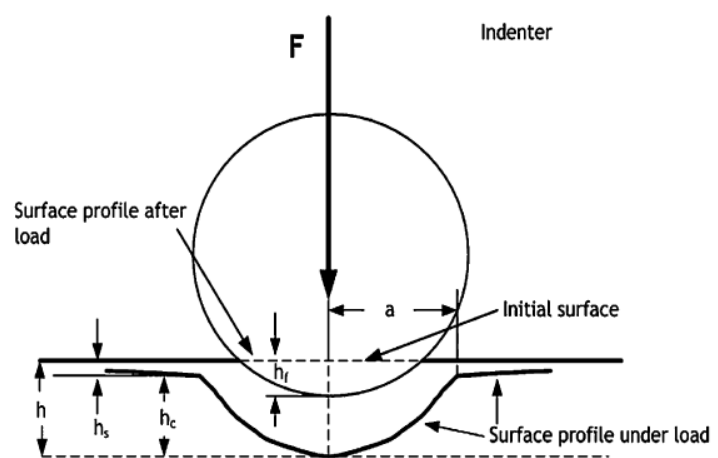


Figure 37. Schematic setup for ball indentation test [28].

Wang et al. (2008) [28] determined the constraint factor  $C$  in different samples:  $\alpha$ -lactose monohydrate, avicel (microcrystalline cellulose) and starch powder. In order to do that, the uniaxial compression test was performed with the ball indentation test device, as well as the indentation procedure. The determined unconfined yield strengths and indentation hardness's were used to determine the constraint factor  $C$ :

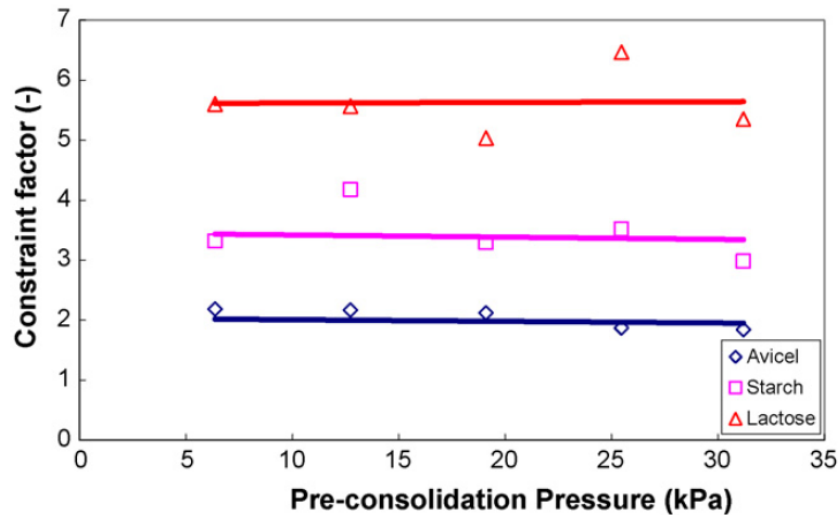


Figure 38. Relationship between the constraint factor and the pre-consolidation pressures for the materials studied [28].

Concerning the temperature effect on the bulk solids flowability, few experiments have been currently performed at elevated temperatures (like the ones which will be studied in this thesis).

Nevertheless, the highest temperature achieved in a shear test was performed by Pilz (1996) [29]. Shear tests with a kind of Jenike shear ceramic cell at temperatures up to 1000 °C were performed using an oven. The experiments were performed in two different ways:

- Preshearing the powder specimens outside the oven at room temperature and shearing inside the oven at 1000 °C.
- Performing the preshearing and shearing inside the oven at the same high temperature.

In order to obtain reliable results it was concluded that both preshear and shear processes must be done at the same high temperature inside the oven.

## 4. Material and methods

The flow behavior determination of raw meal will be performed using three different kinds of testing methods: the uniaxial shear test, the torsional test and the angle of repose measurement. A characterization of the raw meal used in the experiments as well as a description of each method is also given in this section.

### 4.1 Raw meal

The tests described in the following section have been carried out using a raw meal from *Cimpor* cement plant in Cezarina (Brasil) with case number 20110091. A characterization of the raw meal performed by *FLSmidth* is provided [30].

Concerning the flowability of this raw meal sample, using the Shear tester ASTM D6773-02 (Standard Shear Test Method for Bulk Solids Using the Schulze Ring Shear Tester) was used to determine the flow factor ratio  $ff_c$ , obtaining the following results at room temperature:

Table 4. Results obtained for the used raw meal with the Shear Tester (ASTM D6773-02) and the determined flow factor ratio  $ff_c$  [30].

ASTM D6773-02	
Major principal strength ( $\sigma_1$ )	8551 Pa
Unconfined compressive strength ( $\sigma_c$ )	2039 Pa
Flowability ( $ff_c$ )	<b>4,19</b>
Bulk density ( $\rho_b$ )	1286 kg/m <sup>3</sup>
Effective angle of internal friction ( $\varphi_e$ )	44,0 °

Thus, according to the flowability classification stated in section 2.2.2, the raw meal used in the further experiments can be considered as an easy flowing bulk solid at room temperature:

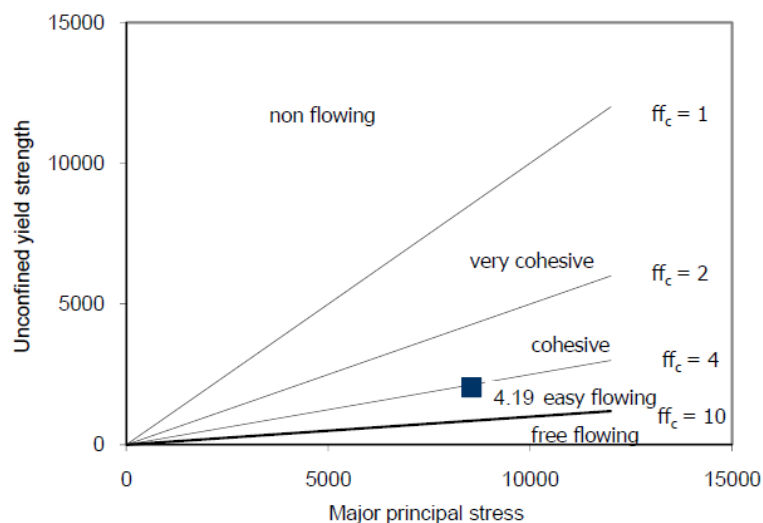


Figure 39. Raw meal flow factor ratio  $ff_c$  in the numerical flowability classification diagram [30].

The bulk densities at loose and packed conditions (ISO 787-11) are shown in the next table:

Table 5. Loose and packed bulk densities [ $\text{kg/m}^3$ ] of the raw meal used for the experiments [30].

	Loose	Packed
Bulk density	1040	1576

Concerning the raw meal particle size, the distribution and residue diagrams expressed as volume percent are shown:

#### DISTRIBUTION

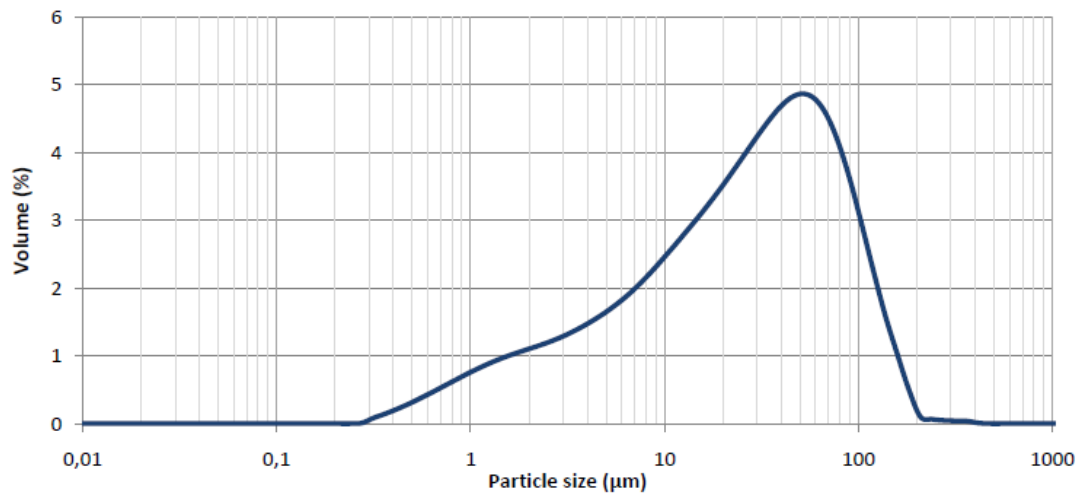


Figure 40. Raw meal particle size distribution (in volume percent) [30].

#### ROSIN-RAMMLER

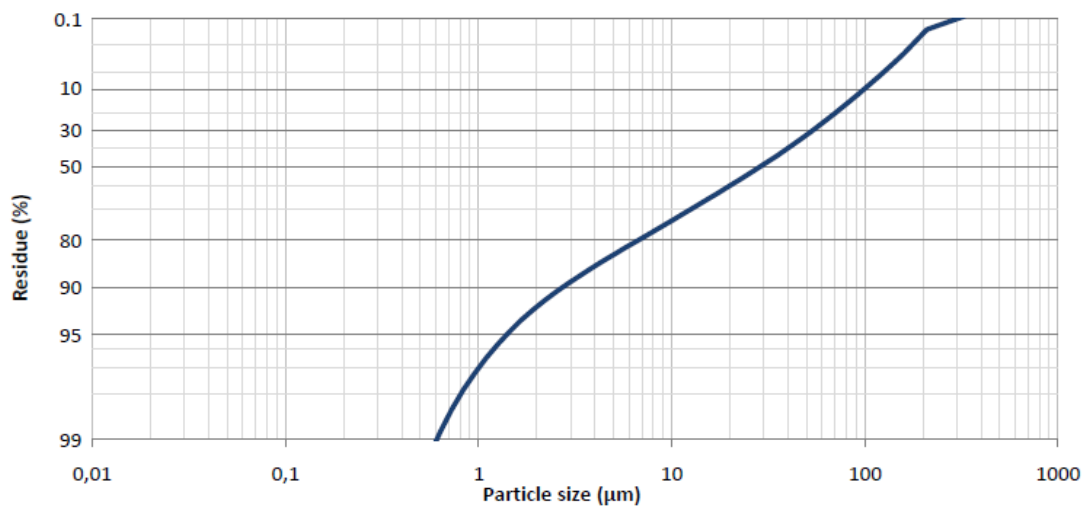


Figure 41. Raw meal particle size distribution (residue in volume percent) [30].

The Sauter mean particle size of the raw meal used in this thesis was determined from the particle size distribution data with the expression shown below, where  $x_i$  is the relative frequency of a certain particle diameter (in fraction of unity) and  $d_{si}$  is the particle diameter (in  $\mu\text{m}$ ) [18]:

$$d_s = \frac{1}{\sum_{i=1}^n \frac{x_i}{d_{si}}} = 7 \mu\text{m}$$

## 4.2 Uniaxial shear test

The uniaxial shear test was used to determine the unconfined yield strength on bulk solids at different operational conditions: stress history and temperature. Consequently, different flow functions were determined at each temperature. The principles of the test are the same as stated previously in section 2.3.3.

### 4.2.1 Experimental setup

In this test, a raw meal specimen was pushed using a monitored piston connected to a force sensor which provided the force necessary to achieve the structural failure of the specimen. This force to failure was used to calculate the unconfined yield strength and plot the flow function. The uniaxial shear test device is showed as follows:

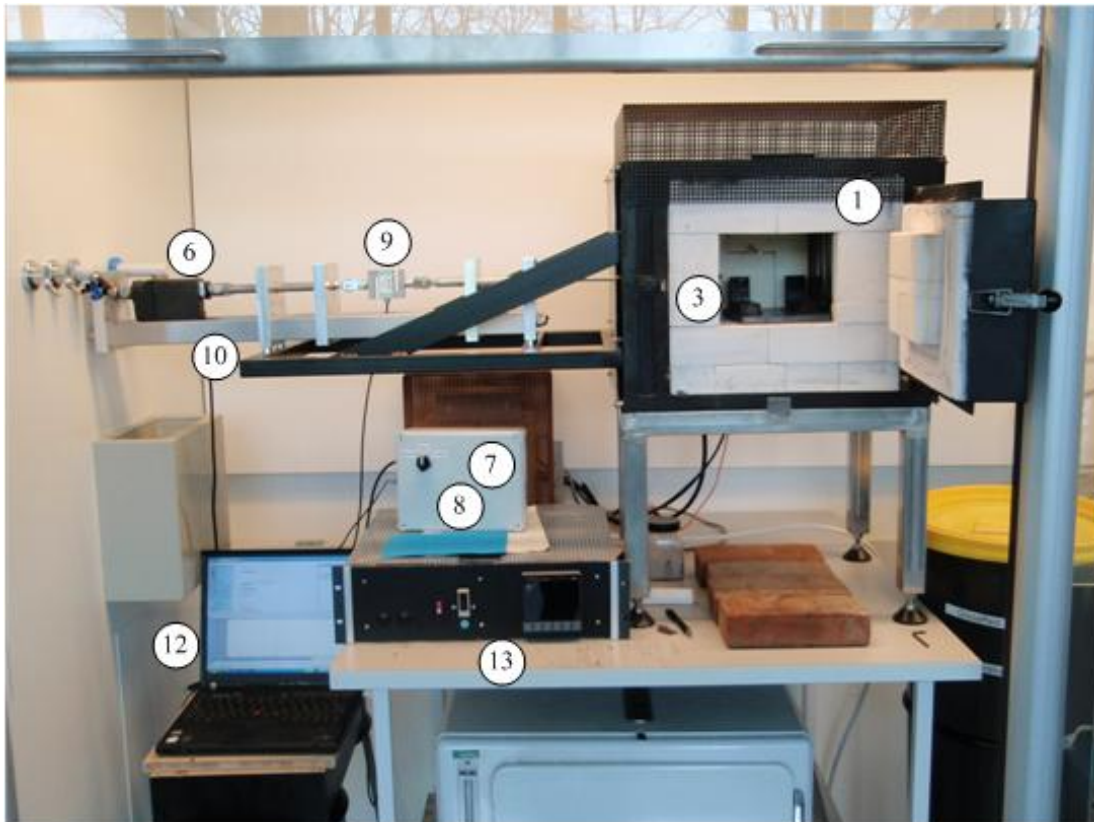


Figure 42. Uniaxial shear test device.

The uniaxial shear test consists of different parts which are explained below and referred to *Figure 42*, *Figure 43*, *Figure 44* and *Figure 45* for a better understanding:

1. *Muffle oven*: Oven built with refractory bricks which make it able to reach high temperatures. A temperature sensor is incorporated inside the oven in order to control the temperature. There is a hole in a wall where the piston which pushes the test cell enters into the oven.
2. *Test cell*: Metal cell specially designed for this testing method. It consists of a fixed part where the raw meal sample is introduced and a movable pushing wall which compresses the bulk solid specimen until its failure. The cell was initially built of steel S355, but after having problems due to corrosion at high temperatures, another cell of stainless steel 253MA was built, obtaining a better oxidation resistance at high temperatures. The size of the hole of the test cell is 140 mm x 100 mm x 3 mm.



*Figure 43. Uniaxial shear test cell.*

3. *Cell holder*: Piece of metal placed inside the oven which fixes the test cell always in the same position and consequently allows reproducibility between the different measures.
4. *Consolidation lids*: There are three different metal consolidation lids corresponding to normal consolidation stresses of 2,79 kPa, 1,87 kPa and 0,94 kPa. Their consolidation area is 70 cm<sup>2</sup> (100 mm x 70 mm) with a height of 36 mm, 24 mm and 12 mm respectively.



*Figure 44. Consolidation lids for the uniaxial shear test (2,79 kPa, 1,87 kPa and 0,94 kPa).*

5. *Metal fork and metal rod*: Tools specially designed to safely handle the potentially hot metal cell and the consolidation lids at high temperature. The metal fork fits with the test cell handling holes. The metal rod fits with the lid handling hoop.

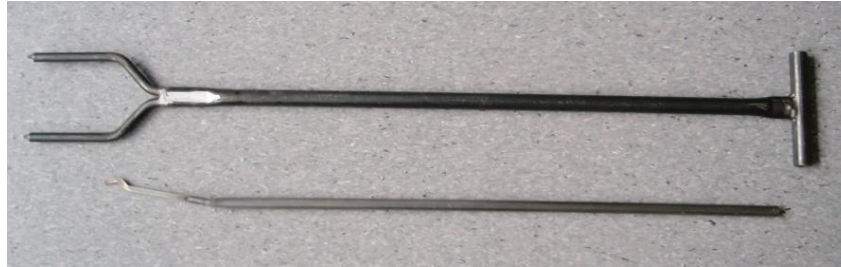


Figure 45. Metal fork and metal rod for the uniaxial shear test.

6. *Actuator LA23 (Linak)*: Small and strong push or pull linear motor, up to 2500 N. It is connected to the piston which moves the pushing wall of the test cell.
7. *TR-EM-288 DC-Motor controller 12-24V 15A*: Controller which starts the motor. It has three possible configurations: backwards, stop and forward.
8. *EM-236 interface unit (Linak)*: It adjusts the settings of the actuator and it is found inside the motor controller box (number 6).
9. *S Beam Model TCTN-9110 transducer Tension/Compression (Nordic transducer)*: Force sensor that measures the resistance of the piston to move. The facility is provided with a sensors which capacity is 0-50 N.
10. *Support*: Metal support which holds the motor and guides the piston towards the oven. It also carries the force sensor.
11. *Sensor Interface with Configuration and Evaluation Software LCV-USB2 (Lorenz Messtechnik GmbH)*: It is connected between the sensor and the PC. By means of this, analog sensor signals are digitized and transferred to the PC where they can be visualized by the software.
12. *LCV-USB-VS2 Software V1.12 (Lorenz Messtechnik GmbH)*: Measured data can be visualized and analyzed in a PC with the VS2 software. The software also stores measured data in both Excel-files and BMP-files. The software was set to work with a 100 samples/s sampling rate and a 4 values moving average in order to reduce the noise of the system.
13. *Oven controller*: Controller which turns on/off the oven and allows the temperature control inside the oven.



## 4.2.2 Experimental procedure

The experimental procedure to perform the uniaxial shear test is divided in three parts:

- Loading of the sample into the test cell.
- Carrying out of the test operation.
- Cleaning of the cell.

### 4.2.2.1 Loading

First of all, the lid was put into the place in the test cell where the specimens to be analyzed would be loaded later in order to get the cell ready for its use. The pushing wall had to be shifted next to the lid and, without moving the pushing wall, the lid was removed.

After that, 150 g of raw meal were weighed using a scale and introduced into the empty space in the test cell. The cell was manually shaken so that the powder got evenly distributed in its space, trying to obtain a uniform specimen height. When shaking the cell it was very important to hold the pushing wall immobile so that the substance volume did not change.

### 4.2.2.2 Test operation

After the bulk solid specimen was correctly loaded, the oven could be turned on. When the desired operational temperature was achieved in the oven, the test cell was introduced inside the oven using the metal fork. After waiting 10 minutes to allow the bulk solid specimen reach the operational temperature, the test operation could start.

First the bulk solid specimen had to be consolidated using one of the lids which corresponded to the desired consolidation stress to analyze. The lid had to be introduced into the oven and removed from it after the desired consolidation time using the metal rod.

Once the specimen had been consolidated, it was shifted horizontally by the action of the monitored piston which pushed the pushing wall. In order to perform this, the program *VS2 Lorenz Messtechnik GmbH* had to be initially started. Afterwards, the motor that moves the piston with a constant velocity of 1 mm/s<sup>2</sup> had to be switched on and, immediately after, the button *Measure Start* in the program menu *Meas./Diagram Mode* had to be pressed so that the horizontal force necessary to shift the piston with a constant velocity could be recorded and displayed in the computer. When the piston reached the end of its movement, the button *Measure Stop* in the program menu *Meas./Diagram Mode* was pressed to stop recording data. Then, the piston had to be moved back to the initial position using the backward motor configuration.

---

<sup>2</sup> In shear tests, small shear velocities (around 1 - 2 mm/s) should be applied. These velocities ensure enough time to observe clearly the results of the bulk solid specimen failure. Moreover, inertia forces and collisions between particles are avoided [6].



Finally, after turning off the oven and waiting until the cell had cooled down to approximately 550 °C, the test cell was removed from the oven using again the metal fork, and the cell was placed on some bricks for further cooling.

#### 4.2.2.3 Cleaning

After finishing the test operation, the bulk solid specimen was discarded in a metal container and the test cell was cleaned up using a brush to remove any remaining powder.

After waiting for approximately one day to allow calcium oxide in the container react with CO<sub>2</sub> from the air to form calcium carbonate, the waste material could be immobilized by addition of water so it could be regarded as construction waste.

### 4.2.3 Experiments

Raw meal flowability was studied using the uniaxial shear test at ambient temperature (22 °C), 200 °C, 400 °C, 550 °C, 700 °C and 850 °C in order to investigate the relationship between temperature and flowability. The experiments were done using three different consolidation stresses 0,94 kPa, 1,87 kPa and 2,79 kPa and a consolidation time of 10 minutes.

Experiments at each temperature and consolidation stress were repeated three times. This provides knowledge of the repeatability and deviation of the data even though this technique needs around 1 hour to obtain the force – time diagram in a certain operational condition.

Furthermore, the system behavior (i.e. the results of the test with the empty system) were determined at each temperature three times before carrying out the raw meal measurements and three times after, in order to take into account the possible friction changes occurring in the metal test cell along the experience at high temperature.

Besides, in order to obtain the area of contact between the raw meal and the pushing wall (needed for the unconfined yield strength determination), the height of the raw meal specimens were determined from 15 points in the particle bed one time at each consolidation stress and temperature. This determination was also used to study the variation of the bulk density with the temperature.

A sketch of the distribution of the 15 points on the raw meal specimen where the height was measured is shown in *Figure 46*:

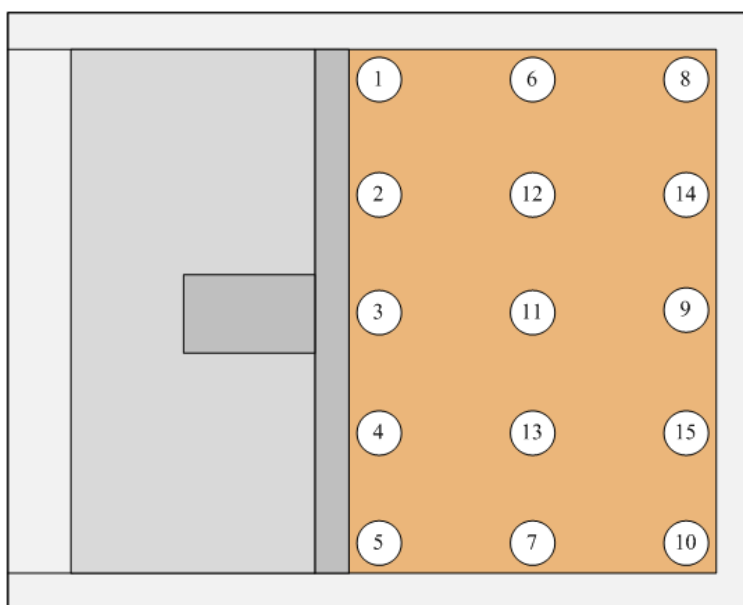


Figure 46. 15 points used to determine the height of the raw meal specimens used in the uniaxial shear test cell.

It should be noted that the height of raw meal specimens in contact with the pushing wall should have been determined for each measurement in the uniaxial shear test work process. However, due to methodical limitations it was determined (after all the measurements were done) only once at each consolidation stress and temperature. For this reason not only the points from 1 to 5 are used to calculate the average area of contact with the pushing wall, but also the rest of them were used because of the irregular height distribution of the powder at each repetition.

#### 4.2.4 Calculation and statistical analysis

The theoretical profile of the results obtained with the uniaxial shear test is shown so it can be explained how they were treated and analyzed.

Considering that the data obtained from the uniaxial shear test is expressed in mV/V, a conversion to a force unit (N) was previously needed to be done. The calibration curve for the 50 N sensor is represented in the next figure and provides the correlation between the two parameters.

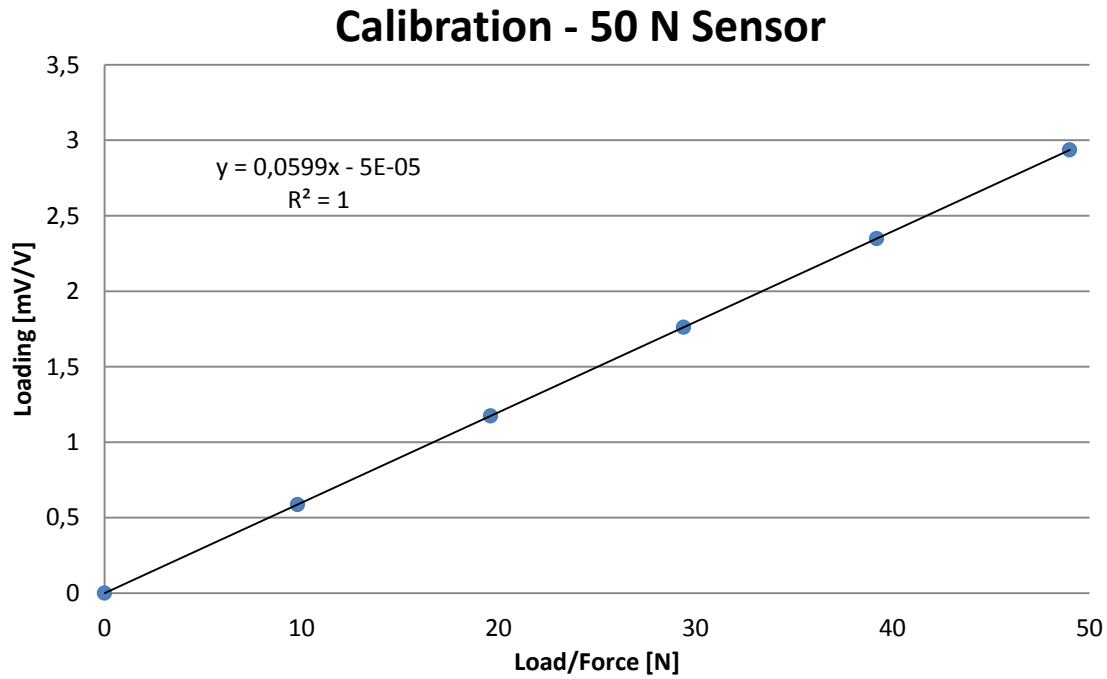


Figure 47. Calibration curve of the 50 N sensor used in the uniaxial shear test.

According to the calibration curve, the relationship between the loading (L) and the force (F) is shown as follows:

$$L \text{ mV/V} = 0,05992 \cdot F \text{ N} - 4,7562 \cdot 10^{-5}$$

Once the conversion to force units is done, the theoretical general profile of the results obtained during the uniaxial shear test is shown in the next figure:

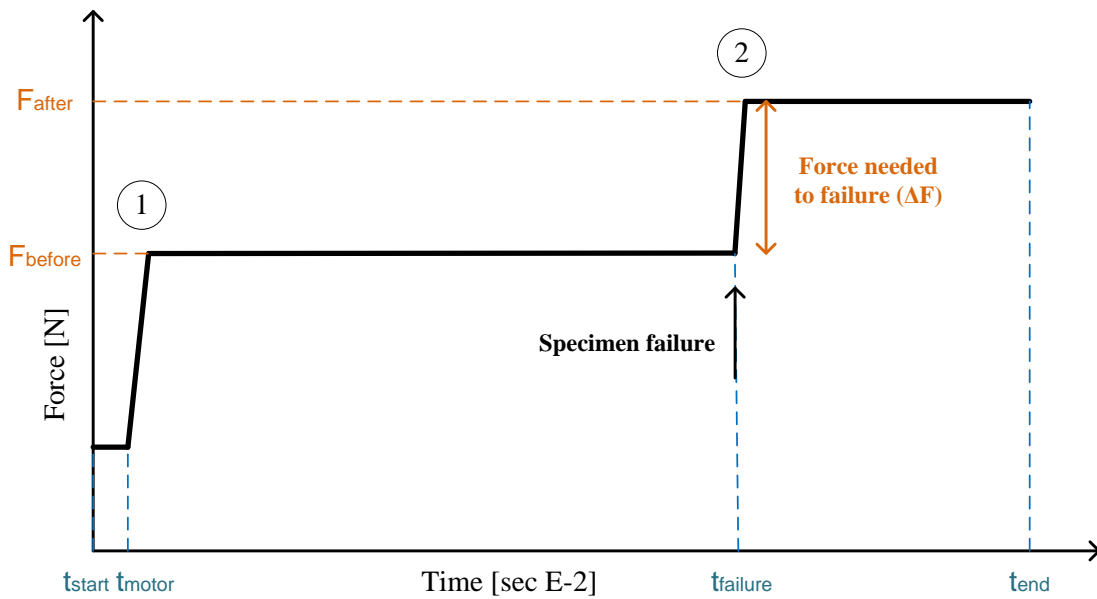


Figure 48. Representation of the theoretical profile of the uniaxial shear test results.

The theoretical profile consists on a force - time diagram which shows an initial slope (position 1 in *Figure 48*) when the piston, which shifts the sample, begins to move (not relevant) and another slope (position 2 in *Figure 48*) when the failure of the specimen occurs. It is the height of the specimen failure slope ( $\Delta F$ ) which shows the force needed to break the bulk solid specimen. However, in practice the real slopes from position 2 were not as well defined as the theoretical profile shows but they were always determined from a force minimum to a force maximum at the moment of the failure.

After obtaining at a certain temperature the values of the force needed to break the raw meal specimen at each consolidation stress and the force needed to move the pushing wall in the empty system, the treatment of the obtained data could be made.

Initially the system behavior without raw meal, i.e. the force needed to start moving the pushing wall in the test cell due to the friction of both parts of the cell (mobile and static), was studied. For the different repetitions ( $\Delta F_i$ ) the mean value ( $\Delta F$ ), the standard deviation ( $s$ ) and the coefficient of variation (CV) expressed as a % were calculated using the expressions showed below (where  $n$  means the number of repetitions) in order to study the variability on the obtained results [31]:

$$\Delta F = \frac{\sum_{i=1}^n \Delta F_i}{n} \quad s = \frac{\sqrt{\sum_{i=1}^n \Delta F_i^2 - \frac{(\sum_{i=1}^n \Delta F_i)^2}{n}}}{n-1} \quad CV = \frac{100 \cdot s}{\Delta F}$$

Subsequently, the mean value of the 15 specimen height measured values at each consolidation stress and temperature were done. In this case, regarding that they were determined only once, the standard deviation and the coefficient of variation were not calculated.

After that, in order to eliminate the mechanical term of the determined force to failure and obtain exclusively the force needed to break the raw meal specimen, the mean value of the force needed to push the wall in the empty system at a certain temperature was subtracted from each experimentally determined force to failure value with raw meal at the same temperature. Finally, in order to obtain the unconfined yield strengths ( $\sigma_c$ ), the result was divided by the area in contact with the pushing wall in the test cell ( $A_c$ ). This area corresponded to the mean value of the raw meal specimens heights (different for each consolidation stress) multiplied by the length of the specimen (100 mm):

$$\begin{aligned} \Delta F_{raw\ meal_i} \text{ N} &= \Delta F_{experimental\ determination_i} \text{ N} - \Delta F_{empty\ system} \text{ N} \\ \sigma_{c_i} \text{ kPa} &= \frac{\Delta F_{raw\ meal_i} \text{ N} \cdot 1000}{A_c \text{ mm}^2} \\ &= \frac{\Delta F_{experimental\ determination_i} \text{ N} - \Delta F_{empty\ system} \text{ N} \cdot 1000}{100 \text{ mm} * \text{height of the specimen mm}} \end{aligned}$$

For the unconfined yield strength calculated values, the mean value ( $\sigma_c$ ), the standard deviation (s) and the coefficient of variation (CV) were determined in order to study the results. Plotting the different consolidation stresses values and their respective unconfined yield strengths mean values, flow functions at a certain temperature and time consolidation were obtained.

At last, confidence intervals were calculated to compare the unconfined yield strengths between the different temperatures and determine if significant statistical differences exist. Confidence intervals<sup>3</sup> were determined with a 95% confidence level ( $\alpha = 0,05$ ) using the expression showed underneath where  $t$  is the student's  $t$  [31]:

$$\text{Confidence interval: } \sigma_c - t_{n-1; \frac{\alpha}{2}} \cdot \frac{s}{n}, \sigma_c + t_{n-1; \frac{\alpha}{2}} \cdot \frac{s}{n}$$

The student's  $t$  with  $n = 3$  and  $\alpha = 0,05$  equals to 4,30.

A similar statistical analysis was made to analyze the force needed to move the pushing wall in the empty system at the different temperatures. In that case the student's  $t$  with  $n = 6$  and  $\alpha = 0,05$  equals to 2,57.

### 4.3 Rheological shear test

The rheological shear test was used to determine the raw meal cohesion (resistance to shear) on bulk solids at different operational conditions (stress history and temperature) using a rheometer designed for the study of the viscoelasticity of polymers.

The first thought was to use the rheometer in order to perform the torsional shear test procedure previously described (section 2.3.6) in order to determine the yield locus. Nevertheless, it was not possible due to operational limitations of the rheometer software. The procedure finally accepted was the one used for the cohesion tests. The consequence of that was that the results could be only used as a comparison between the different studied conditions.

Even so, the running of the test cell was similar to the torsional shear test with a split level shear cell, where the raw meal specimen rotated only on its top half, dividing the specimen in two parts when the failure was obtained. This was achieved adding 4 vanes to the consolidation lid of the test cell and 4 small vanes to the bottom of the test cell.

---

<sup>3</sup> Condence intervals are used to estimate, with a chosen grade of accuracy, between which values will be comprised the real value of a group of measurements determined at the same conditions. Hence, the real values between different conditions can be evaluated. Confidence intervals provide grafically the same results numerically obtained with the tests of hypotesis (student's  $t$  test) [31].

### 4.3.1 Experimental setup

During the test, the vaned lid applied a gradually increasing torque on a bulk solid specimen until a torque value which cannot be resisted by the specimen was achieved. This torque to failure was used as an indicator of the bulk particle cohesion, also regarded as the inverse of the flowability. The rheological shear test device is depicted and described in the following:

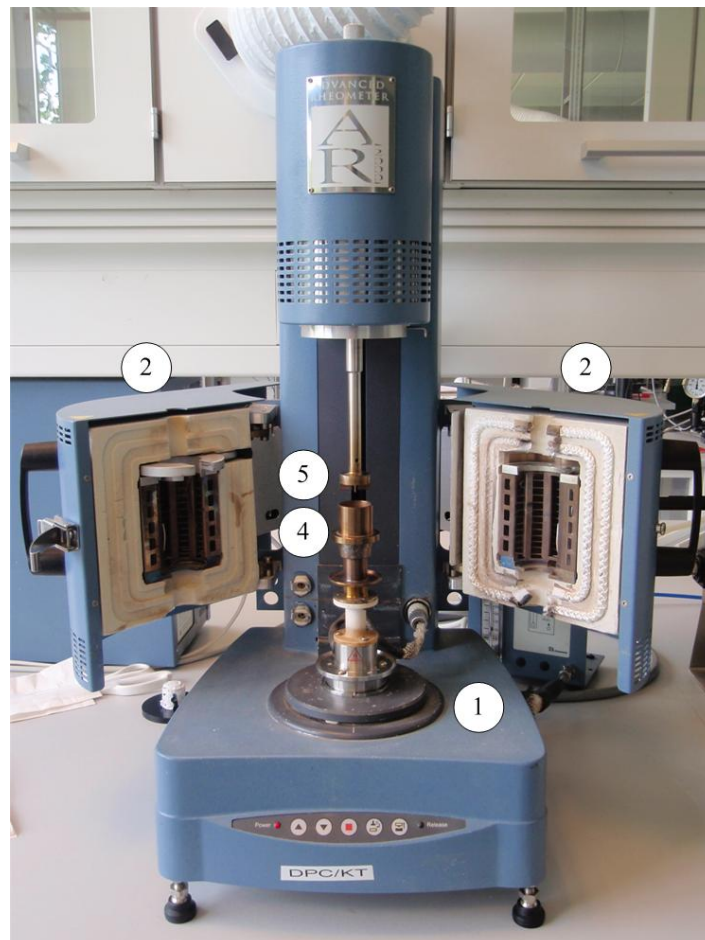


Figure 49. Advanced Rheometer AR 2000.

The rheological shear consists of the following parts, which are also referred to *Figure 49*, *Figure 50* and *Figure 51*:

1. *Advanced Rheometer AR2000 (TA Instruments)*: Rheometer designed for the study of viscoelasticity on polymers, but special cell and lid have been designed in order to make it capable of studying bulk solids flow behavior. All sensors needed are integrated in the device.
2. *Heater*: Heater capable of heating up to approximately 600 °C. A temperature sensor is placed inside the heater to control the temperature.

3. *Rheology Advantage Instrument Control AR*: All the adjustments and the test operation (consolidation and shearing of the sample) are controlled by means of this software. Measured data is visualized and can be analyzed in the PC. Data is stored in a Text-file.
4. *Test cell*: Metal cylindrical cell specially designed for this testing method. It contains 4 small vanes located at the bottom in order to fix the bulk solid specimen in the cell, avoiding the rotation of all the cylindrical column of powder. The cell is 22 mm high and the vanes are 2 mm high and 10 mm long. The inner and outer diameters are 25,2 mm and 29 mm respectively.



Figure 50. Test cell for the rheological shear test (front and risen views).

5. *Vaned lid*: Metal lid specially designed for this testing method. It contains 4 big vanes so that the torque which causes the failure of the specimen can be correctly determined. The diameter of the lid is 25 mm and the vanes are 6 mm high and 10 mm long.

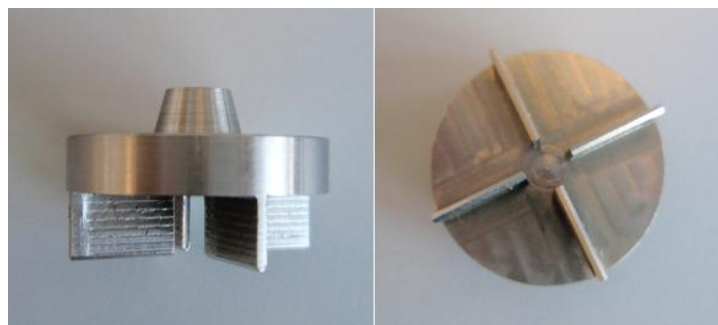


Figure 51. Vaned lid for the rheological shear test (front and risen views).

#### 4.3.2 Experimental procedure

Similarly to the uniaxial shear test, the rheological shear test procedure can be divided in four parts:

- Starting of the rheometer
- Loading of the sample into the test cell.
- Performance of the test operation.
- Cleaning of the cell.

#### 4.3.2.1 Starting

Initially, before starting the test, the rheometer had to be initialized. In order to do that, the pressure of the rheometer had to be set above 2 bar ( $\approx 2,2$  bar), the Nitrogen stream had to be opened and the hatches of the heater had to be opened as well. After that, the rheometer could be switched on and the program *Rheology Advantage Instrument Control AR* had to be started because all the work process was monitored by the computer.

Then, the test cell was placed in the rheometer and, before starting the measurements, the geometry of the test cell had to be chosen in the program menu *Geometry - Open geometry* (it was necessary to create the geometry the first time) and afterwards the zero gap had to be set in the program menu *Instrument - Gap - Zero gap* in order to calibrate the distance between the bottom of the test cell and the lid. Finally, a rotational mapping had to be performed by pressing the program menu *Instrument - Rotational mapping*.

#### 4.3.2.2 Loading

When the rheometer was ready for its use, 12 g of raw meal were weighed using a scale and introduced into the cylindrical test cell<sup>4</sup>. Then, the test cell was ready to be placed in its corresponding gap in the rheometer. The vaned lid was lowered until the top edge of the vanes is leveled with the surface of the specimen. Finally, the test cell was covered with aluminum foil in order to keep the rheometer clean after the measurement and the hatches of the heater were closed<sup>5</sup>.

#### 4.3.2.3 Test operation

Once the test cell is ready to be used, the heater could be turned on setting the desired temperature on the software. When the operational temperature was achieved, it was necessary to wait 5 minutes to allow the bulk solid specimen reach the operational temperature. Afterwards the test operation could start.

After that, the specimen had to be vertically consolidated using the vaned lid, exerting the desired consolidation stress during the desired consolidation time by decreasing the gap distance manually in the software. After the consolidation, the sample had to be sheared exerting an increasingly torque over the cylindrical column of bulk solid until its incipient flow (i.e. when the vaned lid started to rotate). This was performed using a Creep procedure with several steps of additional 200  $\mu\text{N}\cdot\text{m}$

Finally, after turning the heater off and waiting until the cell temperature has been cooled down to approximately 35 °C, the test cell was removed from its position in the rheometer.

<sup>4</sup> It is important to use a sufficient amount of bulk solid in order to avoid the contact between the vanes of the vaned lid and the small vanes on the bottom of the test cell. Therefore the minimum operating distance corresponds to 9 mm

<sup>5</sup> Dust is released from the test cell during the experiments



#### 4.3.2.4 Cleaning

After finishing the test operation, the bulk solid specimen was discarded in a metal container and the test cell was cleaned up using a brush to remove any remaining powder.

### 4.3.3 Experiments

In the rheological shear test, raw meal flowability was studied with experiments carried out at 25 °C, 100 °C, 300 °C and 500 °C so that the dependence between temperature and the raw meal flowability can also be studied in this testing method. The experiments were done using the normal stresses 2 kPa, 4 kPa, 6 kPa and 8 kPa for a consolidation time of 5 minutes.

Experiments at each temperature and consolidation stress were performed three times with the purpose of obtaining solid data even though this technique needs around 2 hours to obtain the value of a measure in a certain operational condition.

Due to lack of time, the experiments at 300 °C and 500 °C were performed exerting only consolidation stress of 2 kPa and 8 kPa. Besides, the experiments at 300 °C and 500 °C with a 2 kPa consolidation stress were performed two times instead of three.

### 4.3.4 Calculation and statistical analysis

After obtaining a certain temperature the values of the torque needed to break the raw meal specimen at each consolidation stress, a statistical analysis of the results can be made.

For the different repetitions ( $T_i$ ) the mean ( $T$ ), the standard deviation ( $s$ ) and the coefficient of variation (CV) expressed as a % were calculated using the same expressions used to analyze the data obtained with the uniaxial shear test (where  $n$  means the number of repetitions) in order to study the variability on the obtained results [31]:

$$T = \frac{\sum_{i=1}^n T_i}{n} \quad s = \sqrt{\frac{\sum_{i=1}^n T_i^2 - T^2 \cdot n}{n-1}} \quad CV = \frac{100 \cdot s}{T}$$

Finally, confidence intervals were calculated to compare the obtained torques between the different temperatures and determine if significant statistical differences exist. Confidence intervals were determined with a 95% confidence level ( $\alpha = 0,05$ ) using the following expression where  $t$  is the student's  $t$  [31]:

$$\text{Confidence interval: } T - t_{n-1; \frac{\alpha}{2}} \cdot \frac{s}{n}, T + t_{n-1; \frac{\alpha}{2}} \cdot \frac{s}{n}$$

The student's  $t$  with  $n = 3$  and  $\alpha = 0,05$  equals to 4,30. In the cases where only two repetitions were made, the student's  $t$  with  $n = 2$  and  $\alpha = 0,05$  equals to 12,71.

## 4.4 Angle of repose measurement

The poured angle of repose measurement was used to determine the angle of repose at different temperatures, which can be linked with the flowability of bulk solids as established by Carr (1965 & 1970) and Raymus (1985) [15]. The principles of the measurement are explained in section 2.3.4.

The initial idea was to design a testing device similar to the standardized testing device *Mark 4 Powder Research Ltd. AOR Tester* developed by Geldart et al. (1990) [15], which was previously shown. Unfortunately, it was not possible because of the physical limitation of the oven: the inside volume is too small and there is no room for such device.

### 4.4.1 Experimental setup

In the poured angle of repose measurement, a certain mass of raw meal was poured over a face down ceramics cup. The angle of repose formed by the conical heap of powder was used to qualitatively determine the flowability of the raw meal at different temperatures. The angle of repose measurement equipment is shown below:

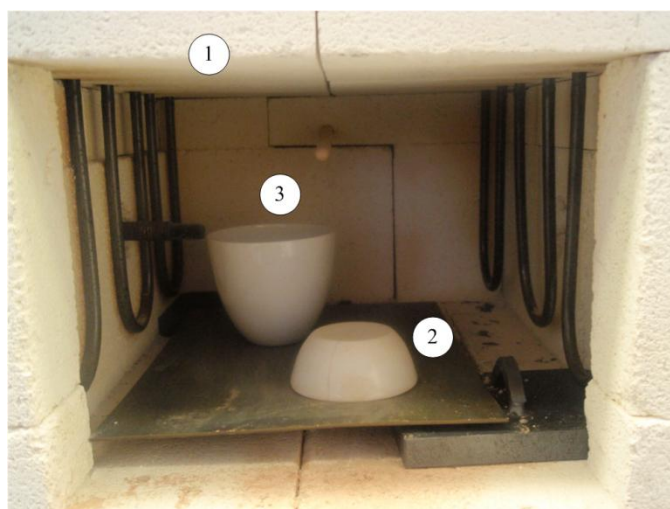


Figure 52. Angle of repose measurement equipment.

The angle of repose measurement consists of the following parts, which are also referred to Figure 52:

1. *Muffle oven*: Oven built with refractory bricks which make it able to reach high temperatures. A temperature sensor is incorporated inside the oven in order to control the temperature. It is the same oven than used in the uniaxial shear test.
2. *Ceramic crucible placed face down*: Ceramics crucible used as a base where the raw meal particles are poured on.
3. *Pouring ceramic crucible*: Ceramics cup used to heat the raw meal up and to pour it over the ceramics cup positioned face down.

## 4.4.2 Experimental procedure

The angle of repose measurement procedure can be divided in two parts:

- Performance of the test operation.
- Cleaning of the cell.

### 4.4.2.1 Test operation

Initially, 20 g of raw meal were weighed and introduced into the pouring ceramic crucible. Then, the oven was turned on and when the desired temperature was achieved into the oven, the pouring ceramic crucible containing the raw meal was introduced inside the oven using crucible tongs. After waiting 10 minutes to allow the raw meal particles reach the operational temperature, the pouring ceramic crucible was shaken to break the possibly formed soft cohesive agglomerates. The raw meal sample was poured over the ceramic crucible placed face down without stopping the shaking of the pouring cup.

Finally, after turning off the oven and waiting until the temperature had cooled down to approximately 200 °C, a picture of the formed powder conical heap was taken so that the angle of repose could be graphically determined.

### 4.4.2.2 Cleaning

After finishing the test operation, the bulk solid specimen was discarded in a metal container and the ceramic crucibles were cleaned up using a brush to remove any remaining powder.

After waiting for approximately one day to allow calcium oxide in the container react with CO<sub>2</sub> from the air to form calcium carbonate, the waste material was immobilized by addition of water so it could be regarded as construction waste.

## 4.4.3 Experiments

The raw meal angle of repose (and flowability) was studied using the angle of repose measurement at ambient temperature (22 °C), 200 °C, 400 °C, 550 °C, 700 °C and 850 °C so that the effects of the temperature on the raw meal flowability can be studied.

The experiments at each temperature were repeated three times. This provides knowledge of the repeatability and deviation of the data.

#### 4.4.4 Calculation and statistical analysis

The theoretical shape of the powder conical heap formed during the performance of the angle of repose measurement is shown underneath:

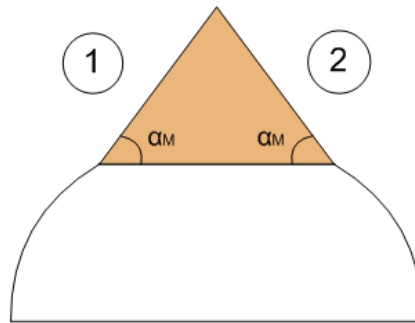


Figure 53. Theoretical shape of the conical heap of raw meal obtained with the angle of repose measurement.

As it can be observed, two angles of repose (angle 1 and angle 2) can be determined from each measurement. However the projection of the conical powder heap rarely matched with a triangle.

On one hand, both sides trended to be irregular (not straight). On the other hand, hardly never the apex of the conical heap was sharp, but it was ragged. Both facts made the determination of the angle of repose difficult. It is for this reason that two ways to determine the angle of repose were carried out so that it could be evaluated the acceptance of each one:

- *Analysis A*: Determination of the angle of repose of the triangle formed from the base of the conical heap to its apex.
- *Analysis B*: Determination of the angle of repose on the base of the conical heap.

Both ways to determine the angle of repose are represented below using an example for a better understanding:

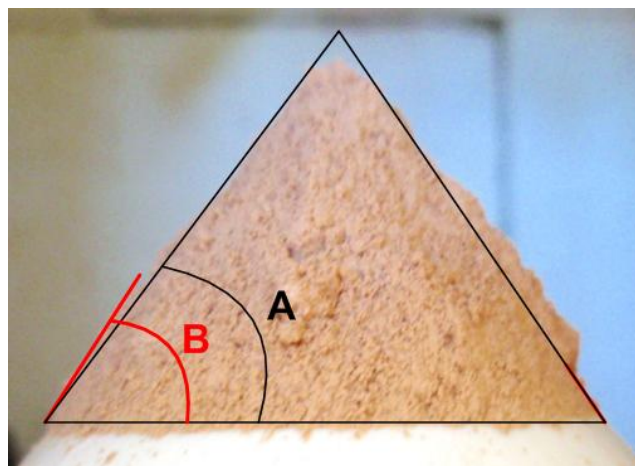


Figure 54. Two ways to determine the angle of repose: A: Angle of repose of the entire triangle, B: Angle of repose of the base of the conical heap of powder.

For the different repetitions at each temperature ( $\alpha_{Mi}$ ) the mean ( $\alpha_M$ ), the standard deviation ( $s$ ) and the coefficient of variation (CV) expressed as a % were calculated using the same expressions used to analyze the data obtained with the two previous tests (where  $n$  means the number of repetitions) in order to study the variability on the obtained results [31]:

$$\alpha_M = \frac{\sum_{i=1}^n \alpha_{Mi}}{n} \quad s = \sqrt{\frac{\sum_{i=1}^n \alpha_{Mi}^2 - \frac{(\sum_{i=1}^n \alpha_{Mi})^2}{n}}{n-1}} \quad CV = \frac{100 \cdot s}{\alpha_M}$$

As done for the uniaxial shear test and rheological shear test results, confidence intervals were calculated to compare the obtained angles of repose between the different temperatures and determine if significant statistical differences exist. Confidence intervals were determined with a 95% confidence level ( $\alpha = 0,05$ ) using the following expression where  $t$  is the student's  $t$  [31]:

$$\text{Confidence interval: } \alpha_M - t_{n-1; \frac{\alpha}{2}} \cdot \frac{s}{n}, \alpha_M + t_{n-1; \frac{\alpha}{2}} \cdot \frac{s}{n}$$

The student's  $t$  with  $n = 6$  and  $\alpha = 0,05$  equals to 2,57.



## 5. Results

In this section the results of the raw meal flow behavior test obtained using the three previously explained methods (uniaxial shear test, rheological shear test and angle of repose measurement) are provided. Note that the complete data is presented in the Appendix A.

### 5.1 Uniaxial shear test

#### 5.1.1 Bulk density

The bulk density at different temperatures and consolidation stresses is determined (from the measured specimen height values and the geometry of the cell) and studied as follows.

Hence, knowing the mass ( $m$ ) of raw meal used in each measurement, the area which the raw meal takes up in the test cell and the mean value of the 15 specimen height values previously measured at each operational condition, the bulk density ( $\rho_b$ ) can be measured with the next expression:

$$\rho_b \frac{g}{cm^3} = \frac{m_{raw\ meal} \ g}{V_{raw\ meal} \ cm^3} = \frac{150 \ g}{7 \ cm \cdot 10 \ cm \cdot height\ of\ the\ specimen \ cm}$$

It should be noted that in the determination of the specimen height mean value at 850 °C, not all of the 15 measured points were used for the calculation. The reason was that at this temperature some raw meal particles stuck to the consolidation lid and, therefore, they were removed from the particle bed when lifting the consolidating lid off the test cell leading to erroneous values of the specimen height. Specifically 6, 1 and 2 values from the 15 measured points were rejected from the measurements at 0,94 kPa, 1,87 kPa and 2,79 kPa respectively.



Figure 55. Removal of raw meal from the uniaxial shear test cell at 850 °C (left). Raw meal stuck to the consolidation lid at 850 °C (right).

The calculated bulk densities for each consolidation stress and temperature are plotted in a bulk density – consolidation stress diagram and a bulk density – temperature diagram:

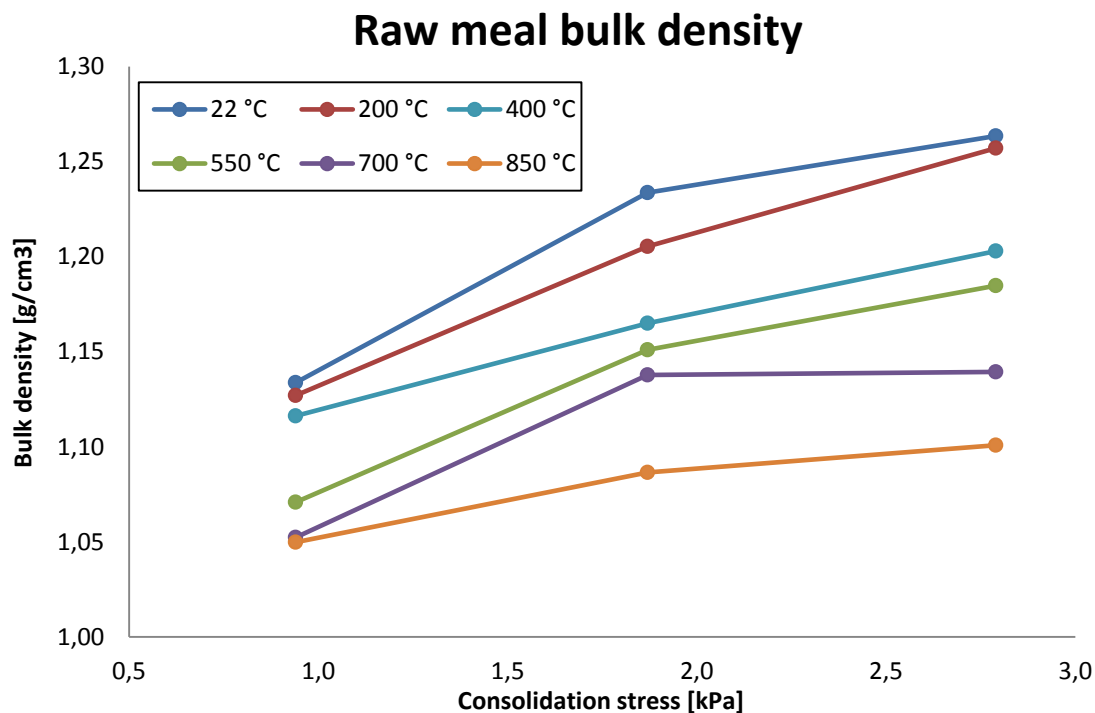


Figure 56. Raw meal bulk density in the uniaxial shear test as a function of the consolidation stress at the different temperatures.

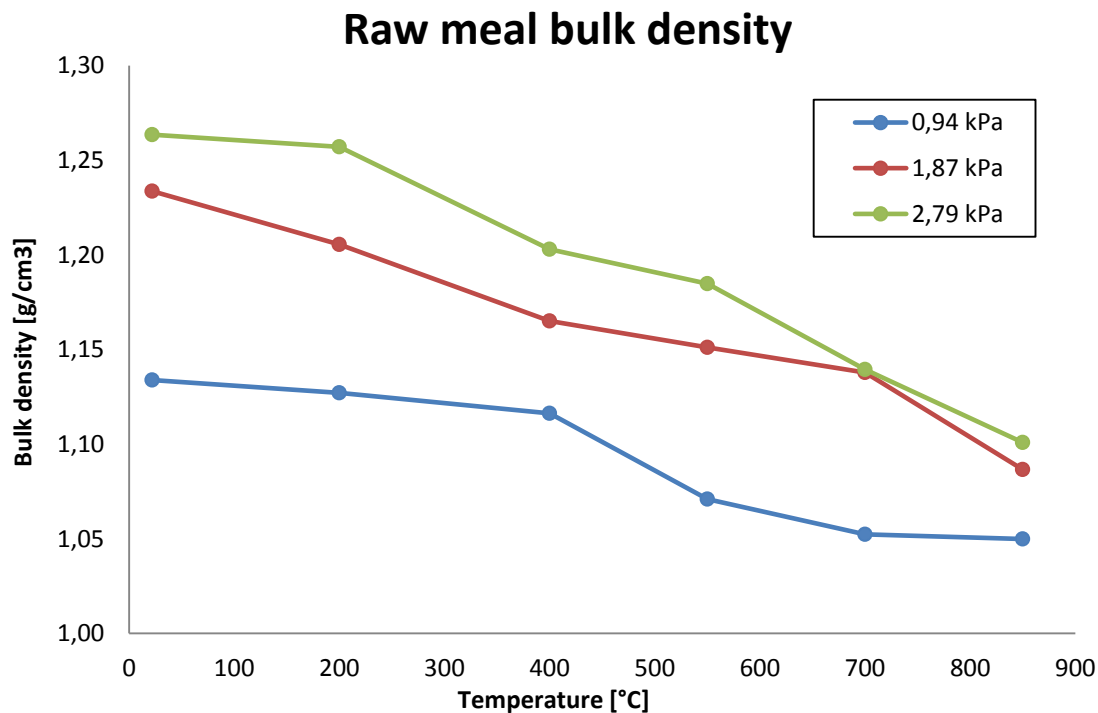


Figure 57. Raw meal bulk density in the uniaxial shear test as a function of the temperature at the different consolidation stresses.



On one hand the results show an increase of the bulk density with the consolidation stress as expected since an increase on the consolidation stress leads to a decrease of the porosity of the particle bed, increasing the bulk density.

On the other hand, a decrease on the bulk density is observed when increasing the temperature. The reason of this temperature effect could be that before the raw meal specimens were consolidated, they were placed 10 minutes heating up inside the oven. Therefore, at higher temperatures the raw meal could have gained more strength before the consolidation than at lower temperatures, making it more difficult to compress the high temperature specimens and consequently leading to a decrease of the bulk density.

### 5.1.2 System behavior

The force needed to start moving the pushing wall in the empty uniaxial shear test cell in all the experiments at the different temperatures are shown in the next graph together with the mean value in order to get a better overview of the measured data:

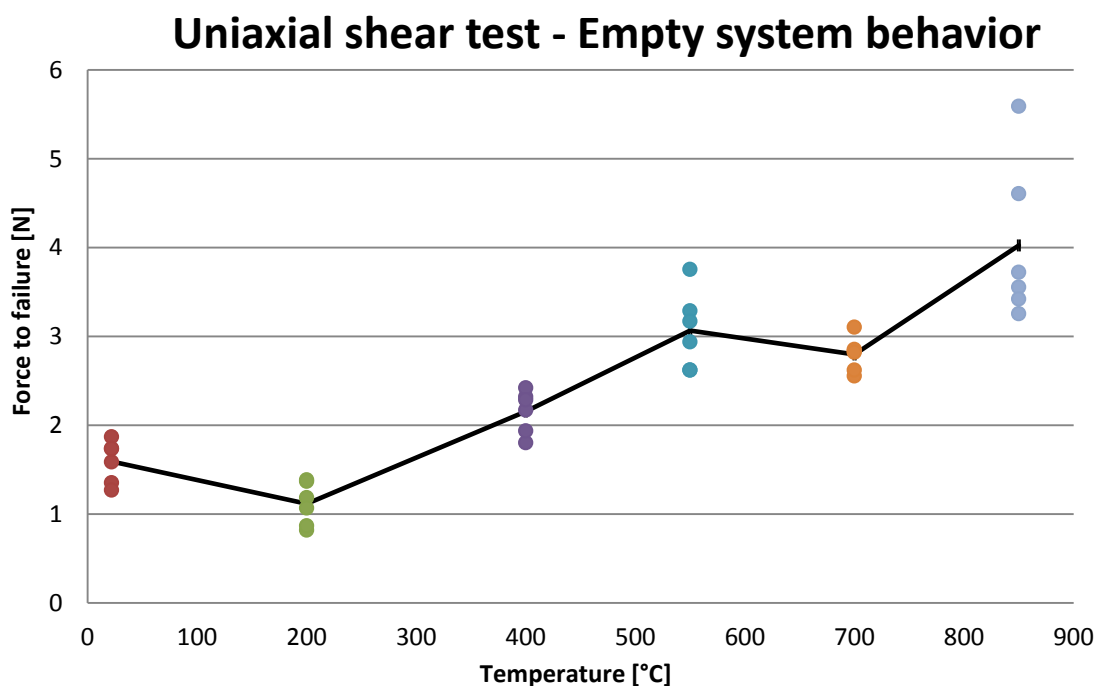


Figure 58. Dependence of the force needed to move the pushing wall in the empty uniaxial shear test system as a function of the temperature.

In general terms an increase of the force needed to start moving the mobile part of the cell (the pushing wall) is observed when increasing the temperature. The reason for this increase is that when increasing the temperature an increase on the friction between the metal surfaces is obtained due to the thermal expansion of the steel at higher temperatures and possibly due to a slightly stickiness between the mobile and fixed parts.

The coefficient of variation varies from 6,97 % to 22,39 %, where the latter belongs to the highest temperature (850 °C). As this coefficient of variation matches with the highest force, the standard deviation of the 850 °C measurements is moderately high (almost 1N).

### 5.1.3 Raw meal flow functions

The determined unconfined yield strength at each temperature are plotted in the following figures as a function of the consolidation stress together with their mean value, i.e. different flow functions at each temperature are shown. Besides, the boundaries of the numerical ranges of the classification of flowability depending on the flow factor ratio  $ff_c = \sigma_1 / \sigma_c$  (explained in section 2.2.2) are also drawn in the flow functions so that a better understanding of the raw meal flowability can be achieved.

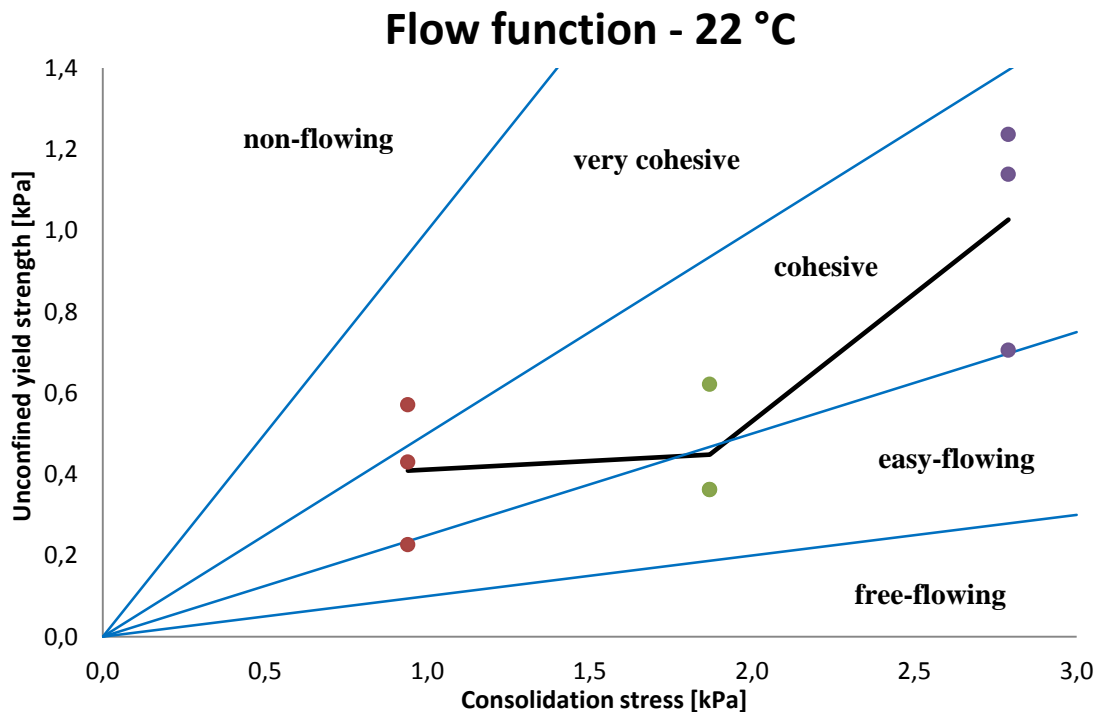


Figure 59. Raw meal flow function obtained with the uniaxial shear test at 22 °C (10 minutes consolidation).

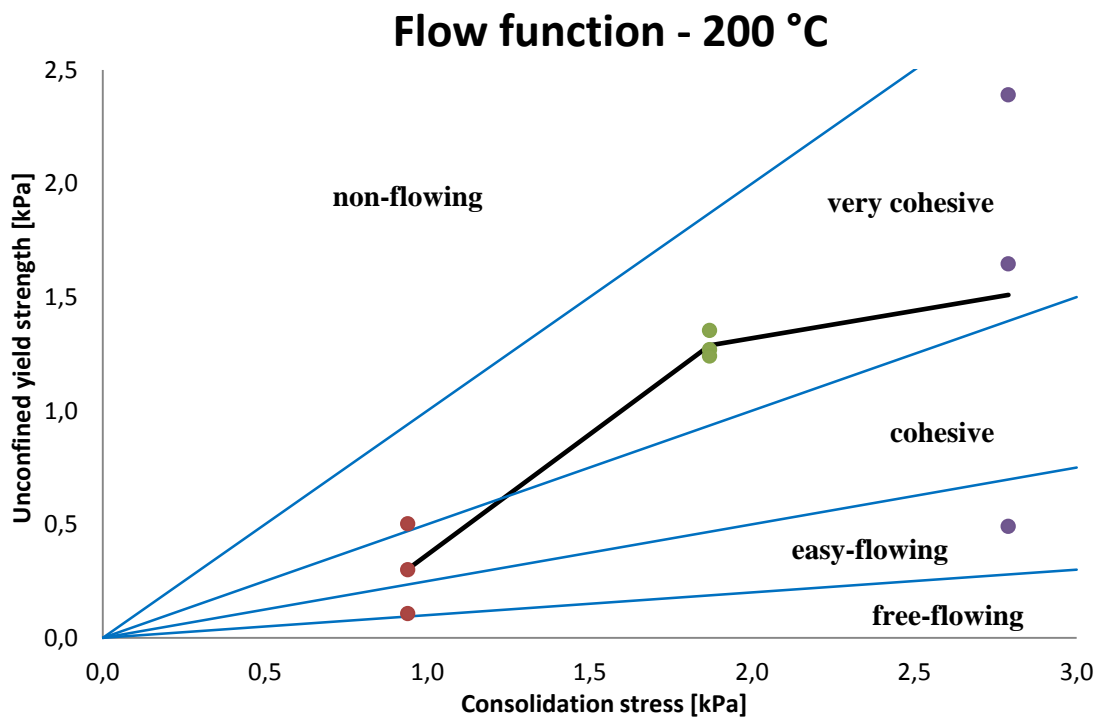


Figure 60. Raw meal flow function obtained with the uniaxial shear test at 200 °C (10 minutes consolidation).

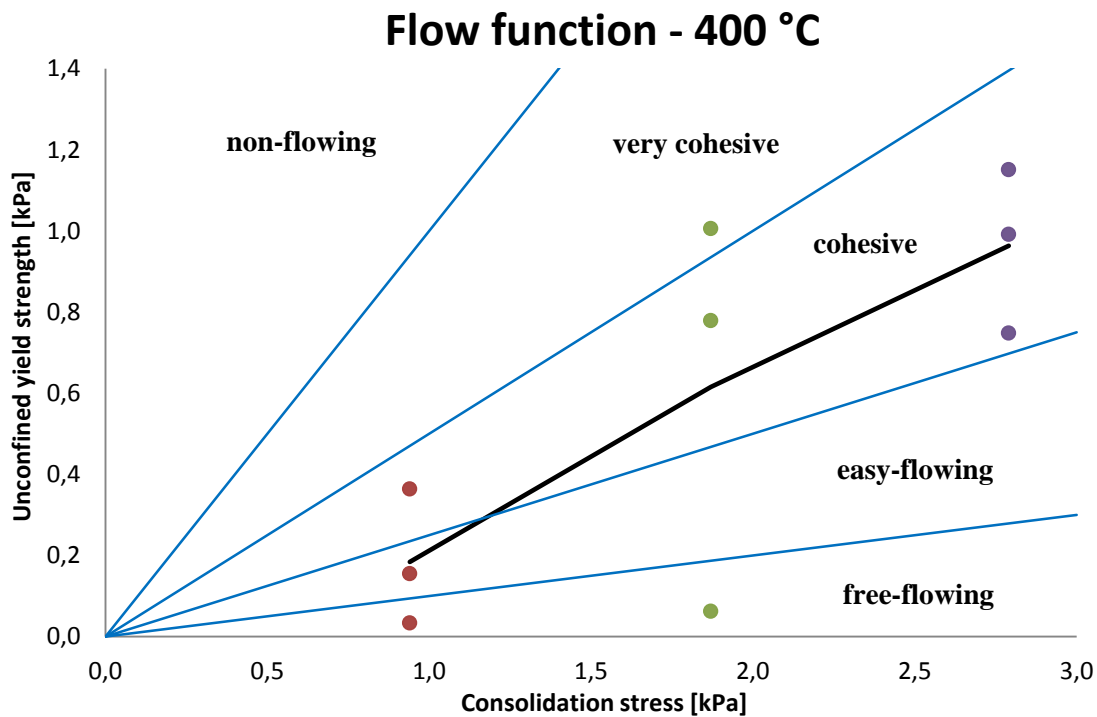


Figure 61. Raw meal flow function obtained with the uniaxial shear test at 400 °C (10 minutes consolidation).

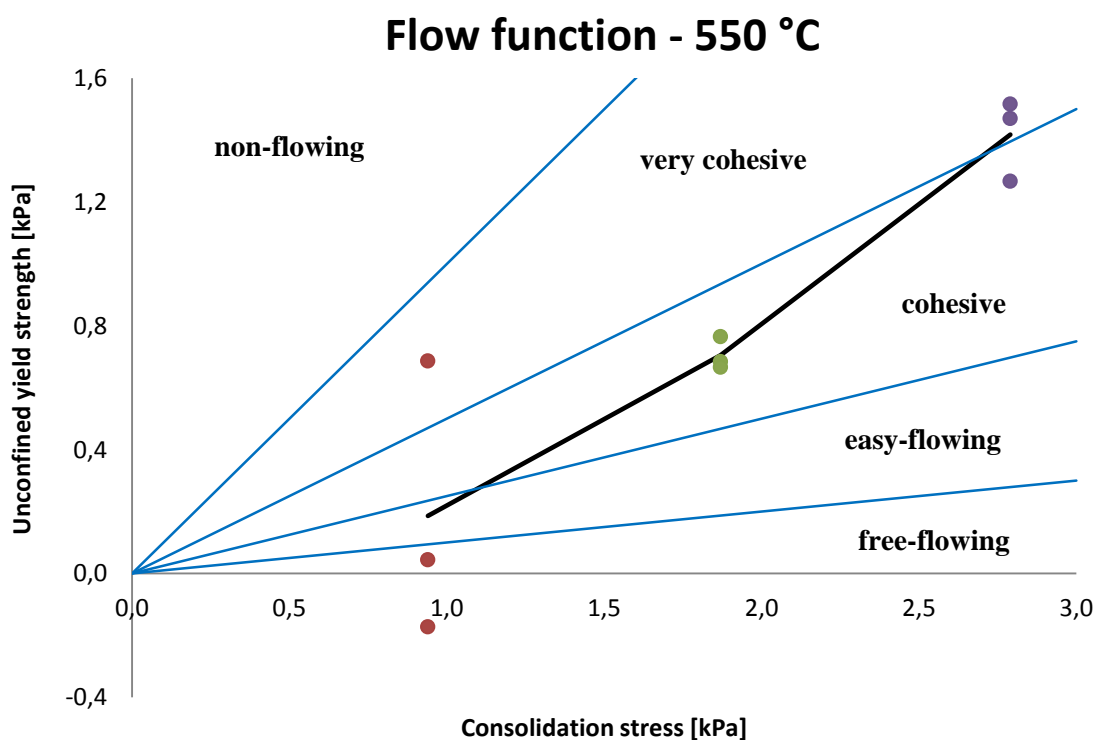


Figure 62. Raw meal flow function obtained with the uniaxial shear test at 550 °C (10 minutes consolidation).

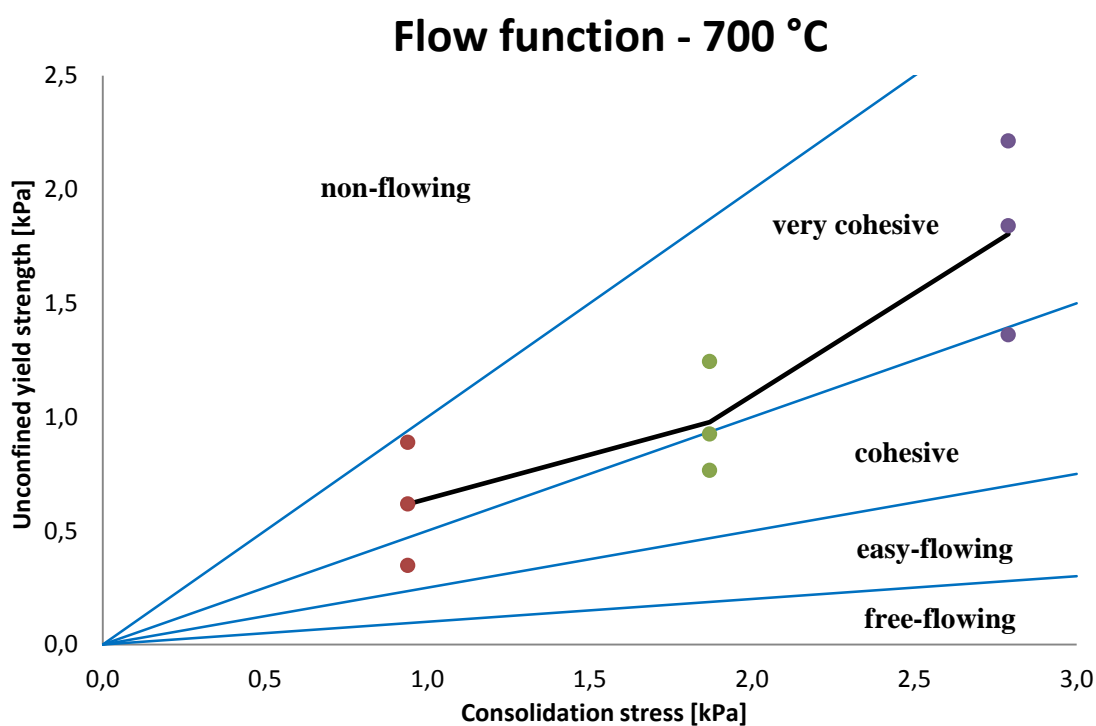


Figure 63. Raw meal flow function obtained with the uniaxial shear test at 700 °C (10 minutes consolidation).

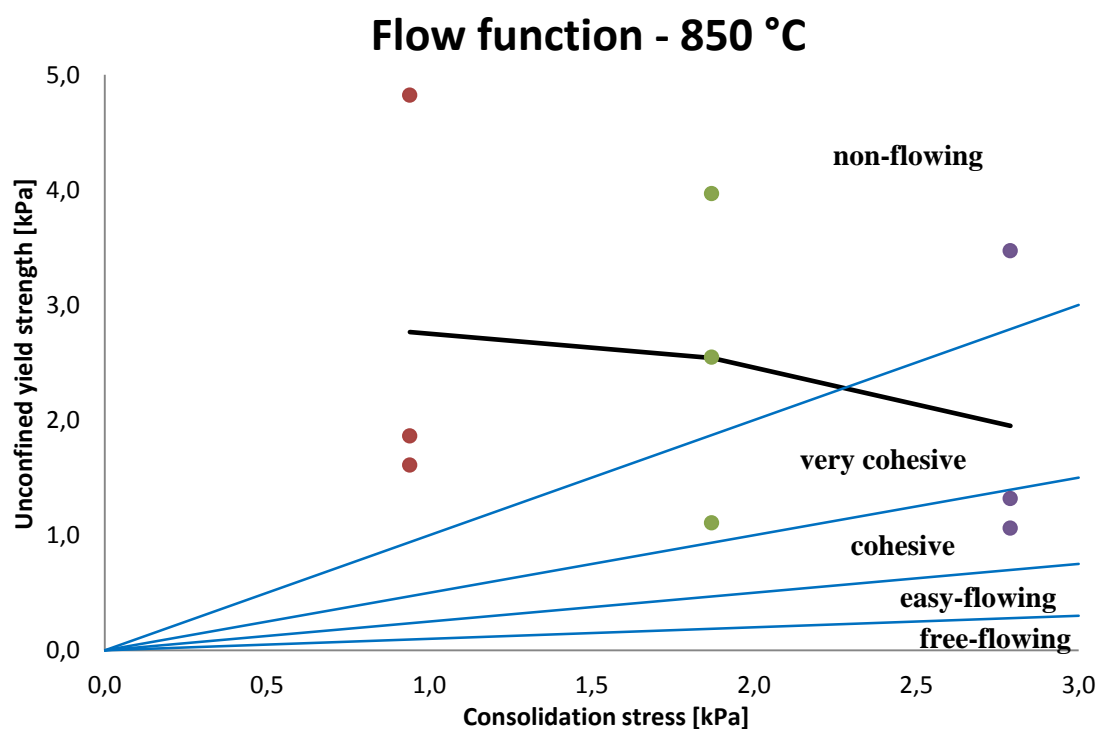


Figure 64. Raw meal flow function obtained with the uniaxial shear test at 850 °C (10 minutes consolidation).

Furthermore, for a better comparison of the unconfined yield strengths determined at the different studied temperatures, the mean values of the previously showed flow functions are outlined in the same graph:

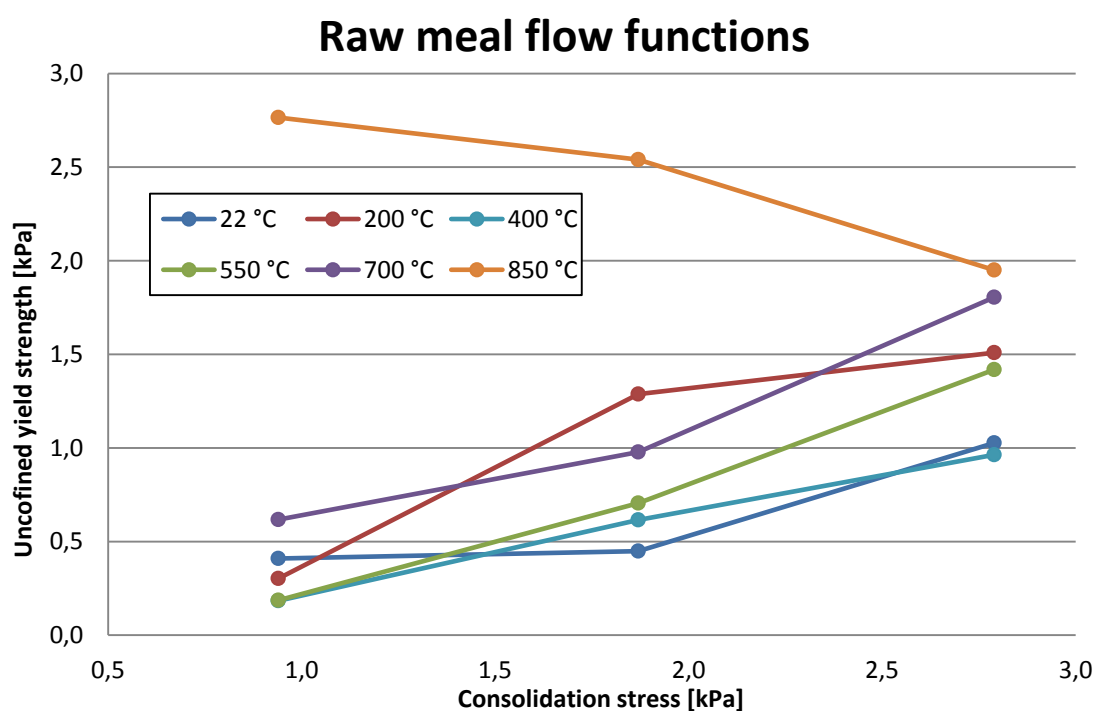


Figure 65. Raw meal flow functions at the different temperatures (10 minutes consolidation).

Initially is important to comment that in the 550 °C flow function there is a negative unconfined yield strength value. The reason for this is that the mean value of the force needed for the empty system (3,065 N) was higher than the force needed for the failure in that unconfined yield strength value (2,720 N). Nevertheless, that value do not have to be regarded as an error since there were two individual values of the force measured in the empty system which were lower than the 2,720 N (2,620 N obtained twice). Thus, the negative value is a result of the combination of a low force measured with powder and a high force measured in the empty system.

Concerning the results shown, the unconfined yield strength seems to remain practically constant until 700 °C. Above that temperature (at 850 °C) the unconfined yield strength appears considerably higher than all the other results. This means that the raw meal flowability seems to decrease with the temperature, especially after a certain temperature value which match with the temperature where the calcination of the  $\text{CaCO}_3$  found in the raw meal takes place (700 °C – 850 °C)

On the other hand, as it can be observed and was previously expected, the unconfined yield strength increases with the consolidation stress, i.e. raw meal gains more cohesion the higher the consolidation stress previously exerted is. However, this trend does not occur on the 850 °C values, probably because of the experimental variability or errors of the results.

The coefficient of variation from this data are between 4,55 % and 239,83 %, with a mean value around 55 %. This means that the deviation of the flow function values obtained using the uniaxial shear test is rather high.

Moreover, concerning the numerical classification of the flowability depending on the flow factor ratio  $ff_c$ , in general terms the raw meal trends to fit in the *cohesive* range from 22 °C to 550 °C, at 700 °C fits in the *very cohesive* range and at 850 °C fits in the *non-flowing* range. It can also be observed that in some cases, when increasing the consolidation stress, the raw meal flow behavior changes from a higher to a lower flowability range. Surprisingly, this does not take place in the 850 °C flow function, probably because of the experimental variability or errors of the results as stated before.

In order to clearly appreciate the relationship between the raw meal flowability and the temperature, the unconfined yield strengths and their mean values are plotted against the temperature at each consolidation stress:

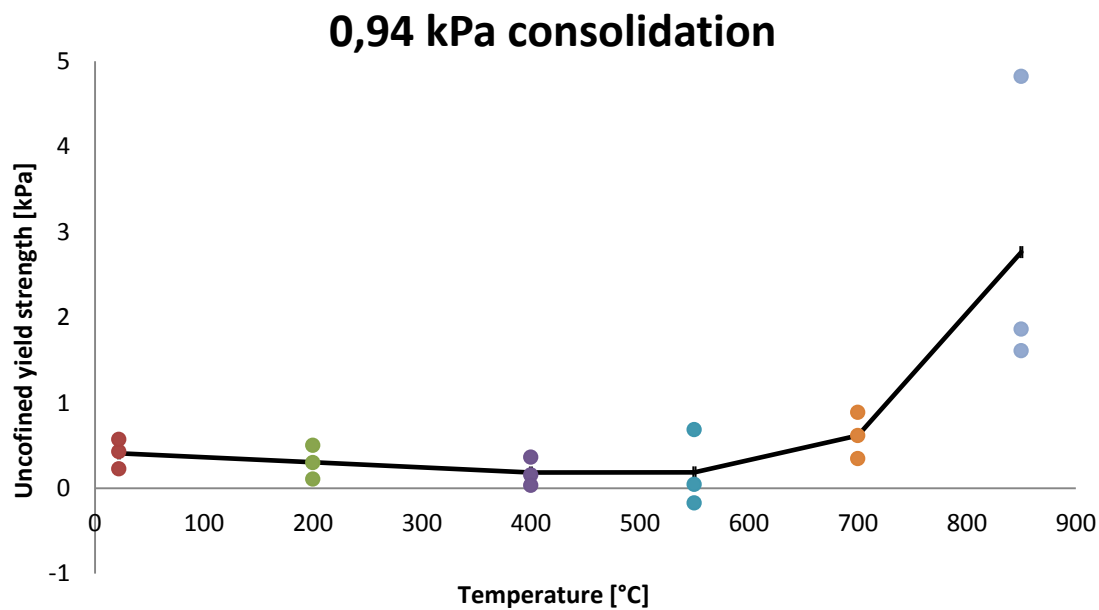


Figure 66. Raw meal unconfined yield strength as a function of the temperature after exerting the **0,94 kPa** consolidation stress in the uniaxial shear test.

The unconfined yield strength profile obtained when exerting a 0,94 kPa consolidation stress shows a nearly constant trend until 550 °C, at 700 °C particles start gaining strength and after that temperature the cohesion of the particles drastically rises.

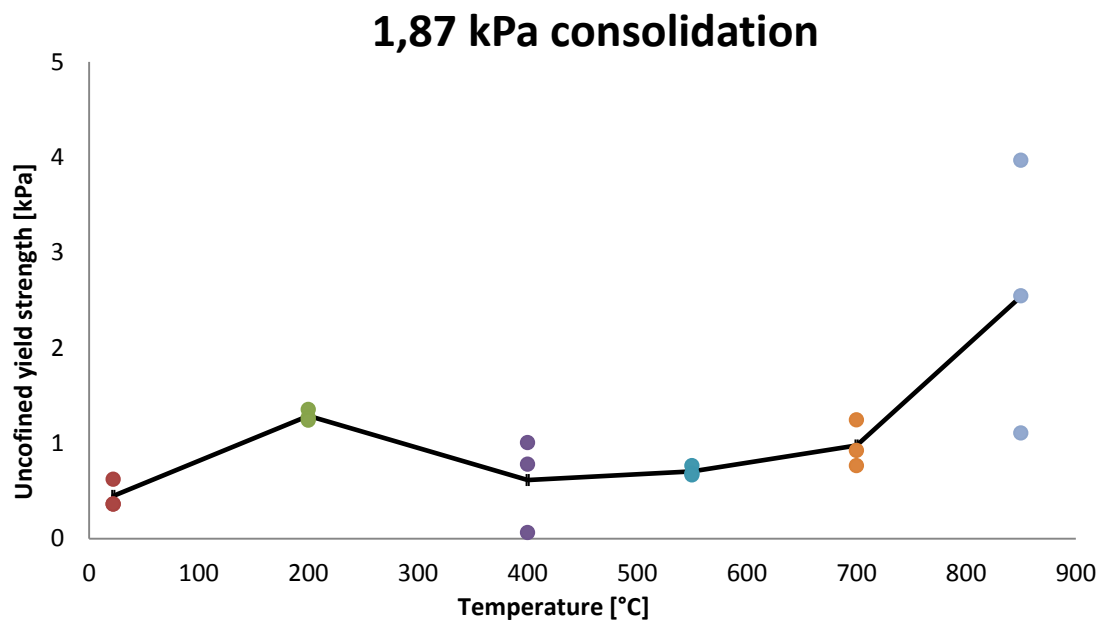


Figure 67. Raw meal unconfined yield strength as a function of the temperature after exerting the **1,87 kPa** consolidation stress in the uniaxial shear test.

When the 1,87 kPa consolidation stress is applied to raw meal, the trend observed in the unconfined yield strength as a function of the temperature seems quite similar to the one observed when exerting 0,94 kPa. Only the 200 °C unconfined yield strength differ from the trend previously commented.

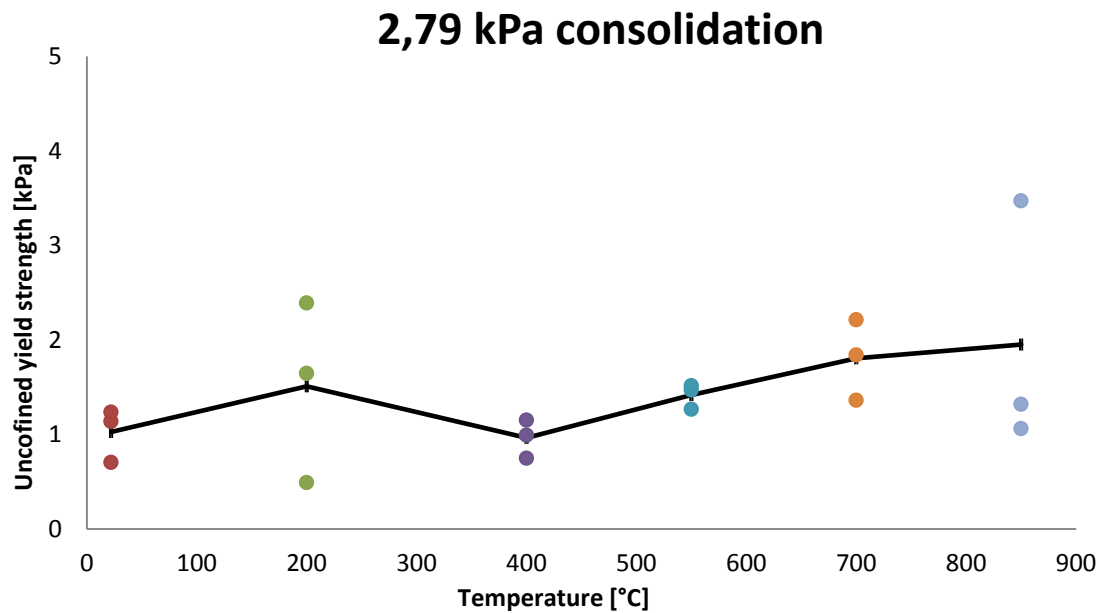


Figure 68. Raw meal unconfined yield strength as a function of the temperature after exerting the 2,79 kPa consolidation stress in the uniaxial shear test.

In the 2,79 kPa case previous consolidation stress determined values, the trend stated in both previously cases does not fit so nicely. On one hand, as it happened with the 1,87 kPa unconfined yield strength behavior, the 200 °C value deviates from the expected constant trend. On the other hand, as stated before, the 850 °C determined value seems to be lower than it should be expected due to possible errors or the variability or uncertainties of the results.

## 5.1.4 Other evidences

In this section other evidences of the raw meal flowability decrease with the temperature, which are not considered in the general results obtained, are shown. These are based on the force – time diagrams obtained directly from the measurements through the uniaxial shear test software VS2 Lorenz Messtechnik GmbH, and on the physical appearance of the raw meal specimens after the uniaxial shear tests were done.

### 5.1.4.1 Force – time diagrams

In order to support the theory of the trend in of the flowability remaining nearly constant until 700 °C, and then increases as the temperature reaches 850 °C, the force – time diagrams obtained directly from the uniaxial shear test device are discussed in the following.

Four force – time diagrams obtained all of them at 1,87 kPa are described in order to support the statement:



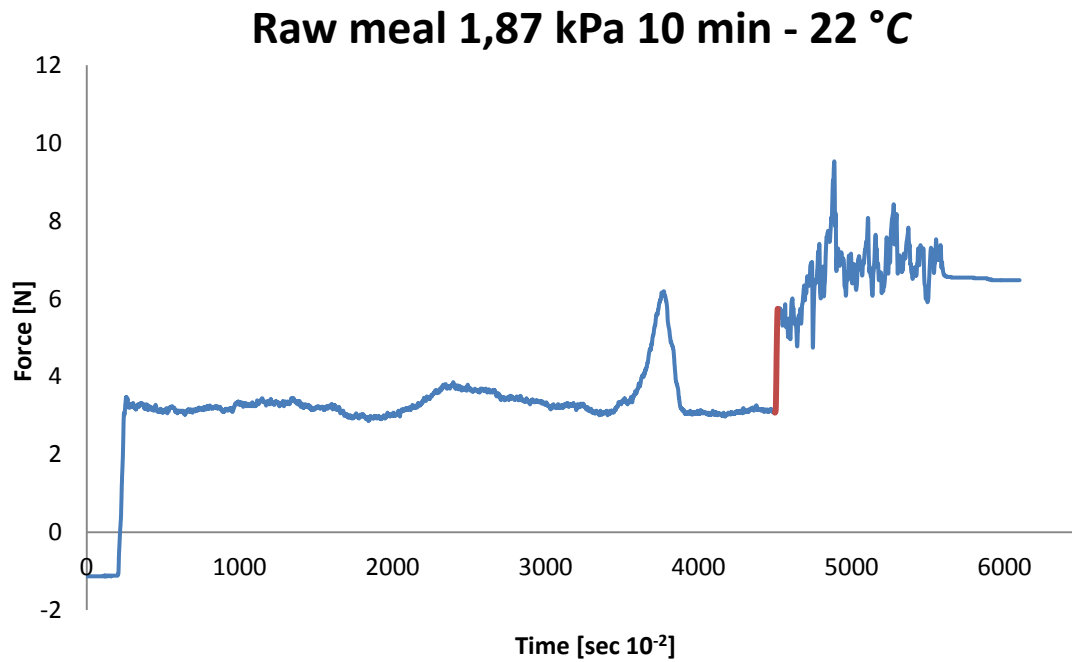


Figure 69. Results obtained with the uniaxial shear test at 220 °C. The raw meal specimen was compressed during 10 minutes with a 1,87 kPa consolidation stress. The force associated to the specimen failure is marked in red.

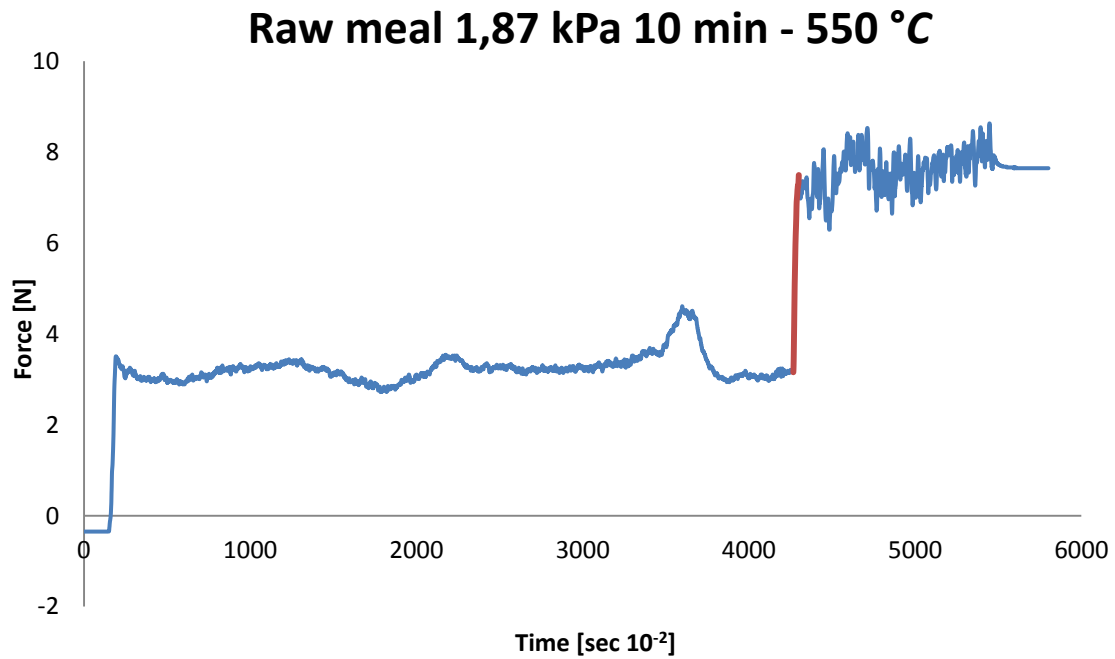


Figure 70. Results obtained with the uniaxial shear test at 550 °C. The raw meal specimen was compressed during 10 minutes with a 1,87 kPa consolidation stress. The force associated to the specimen failure is marked in red.

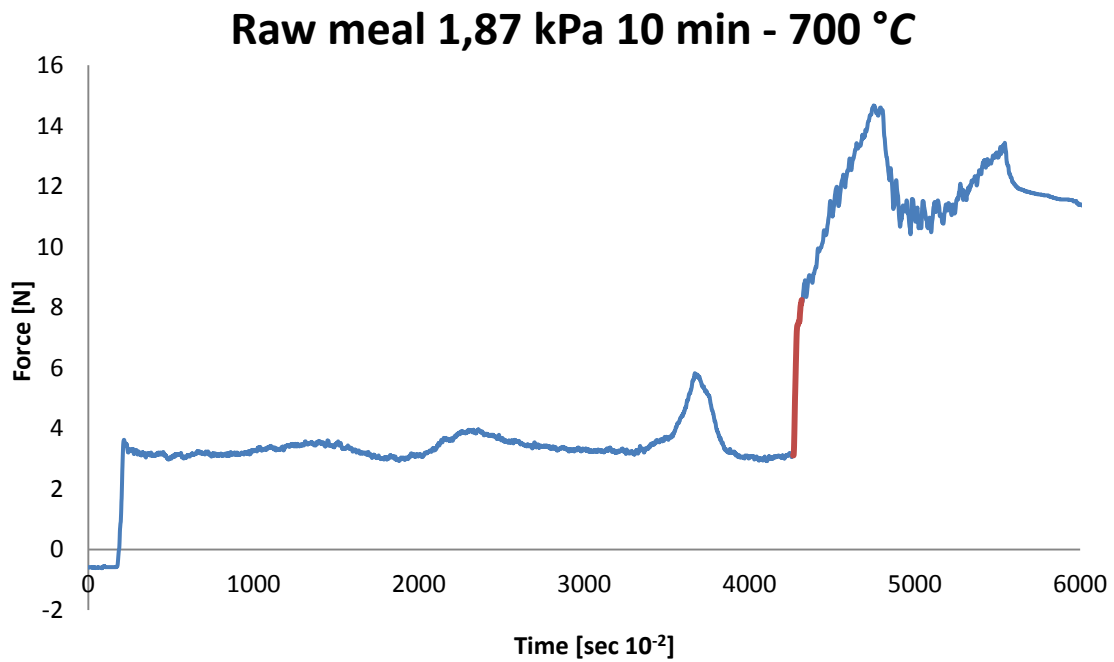


Figure 71. Results obtained with the uniaxial shear test at 700 °C. The raw meal specimen was compressed during 10 minutes with a 1,87 kPa consolidation stress. The force associated to the specimen failure is marked in red.

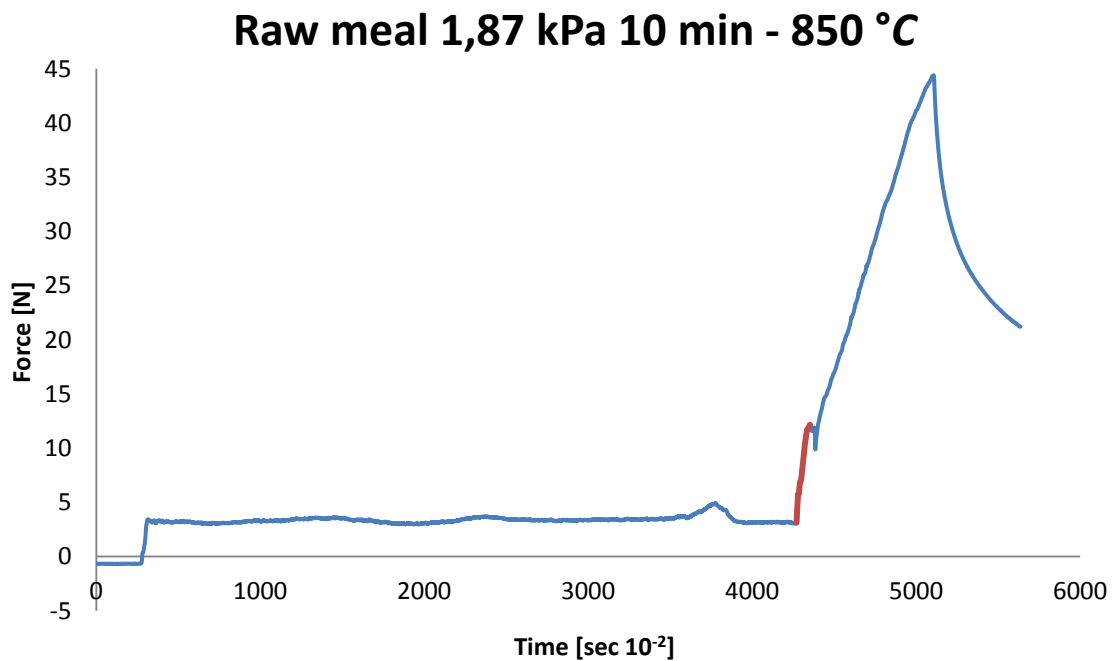


Figure 72. Results obtained with the uniaxial shear test at 850 °C. The raw meal specimen was compressed during 10 minutes with a 1,87 kPa consolidation stress. The force associated to the specimen failure is marked in red.

The force – time diagrams at 22 °C and 550 °C (*Figure 69 and Figure 70*) show that after the failure of the raw meal specimen, the force needed to continue shifting the particle bed remained practically stable. Subsequently, in the time – force diagram at 700 °C (*Figure 71*) a moderate increase of the force needed to keep on pushing the raw meal particle bed occurs. Finally, at 850 °C (*Figure 72*) the force – time diagram shows an large increase of the force needed to push the raw meal specimen after its failure.

Therefore, from the three last figures (*Figure 69, Figure 70, Figure 71 and Figure 72*) can be confirmed that until 550 °C the raw meal flowability is kept approximately constant, at 700 °C a remarkable decrease on the flowability occurs and at 850 °C, due to the calcination of the raw meal, a decrease of the raw meal flowability takes place.

Note that the force decrease at  $t \approx 5000 \cdot 10^{-2}$  s in all figures is caused by the stopping of the piston (ending of the test).

#### 5.1.4.2 Force – time diagrams

Finally, the physical appearance of the raw meal specimens after its determination in the uniaxial shear test supports the increment of the raw meal cohesion with the temperature.

The pictures show some raw meal powder thrown directly to the container where it was discarded after the experiments were done.

The first picture contains raw meal tested at temperatures below 700 °C (fine agglomerates) and raw meal tested at 700 °C (coarse powder agglomerates). The second one shows 3 big blocks of raw meal powder tested at 850 °C (can be also observed that it was calcined due to the different color), together with raw meal tested at lower temperatures.



Figure 73. Raw meal tested in the uniaxial shear stress at 700 °C (big aggregates marked in red) and at lower temperatures (fine powder aggregates).



Figure 74. Raw meal tested in the uniaxial shear stress at 850 °C (huge powder blocks marked in red) and at lower temperatures (fine powder).

## 5.2 Rheological shear test

The exerted torque needed for the failure of the raw meal specimen in the rheological shear test in all the repetitions at the different temperatures of interest and consolidation stresses are shown together with the mean value in the following figures:

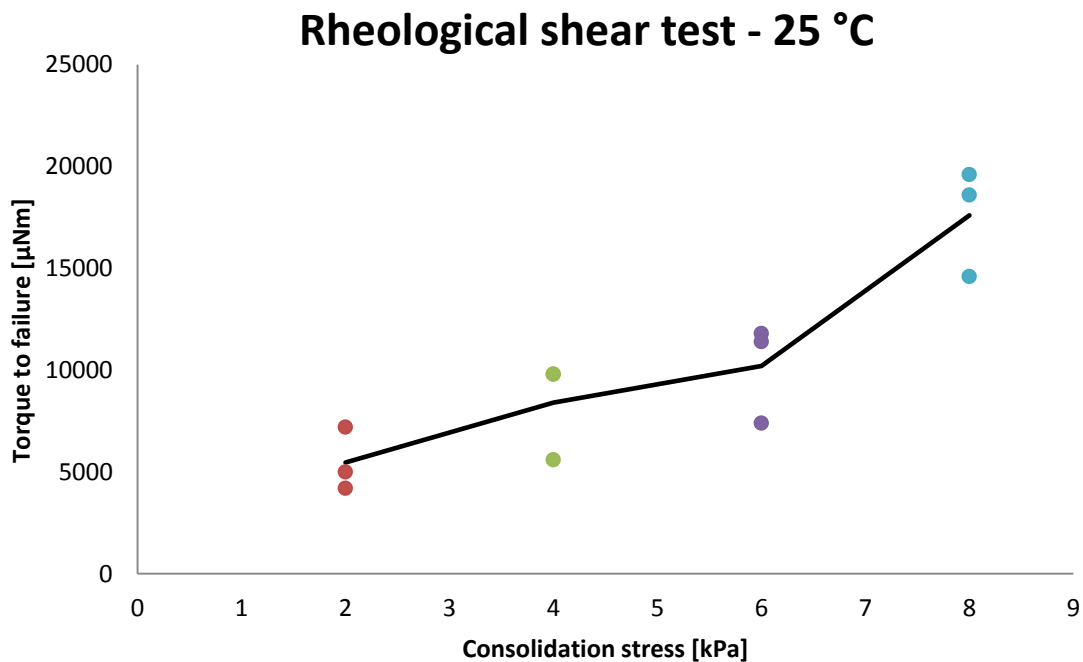


Figure 75. Torque needed to obtain the raw meal specimen failure in the rheological shear test at 25 °C as a function of the previous consolidation stress.

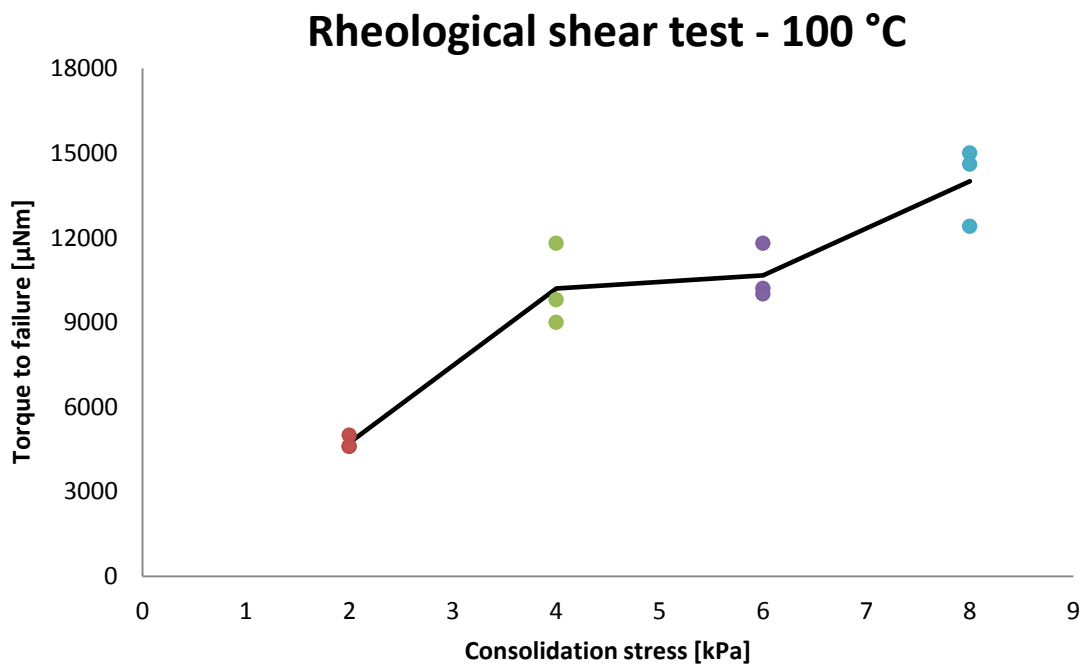


Figure 76. Torque needed to obtain the raw meal specimen failure in the rheological shear test at 100 °C as a function of the previous consolidation stress.

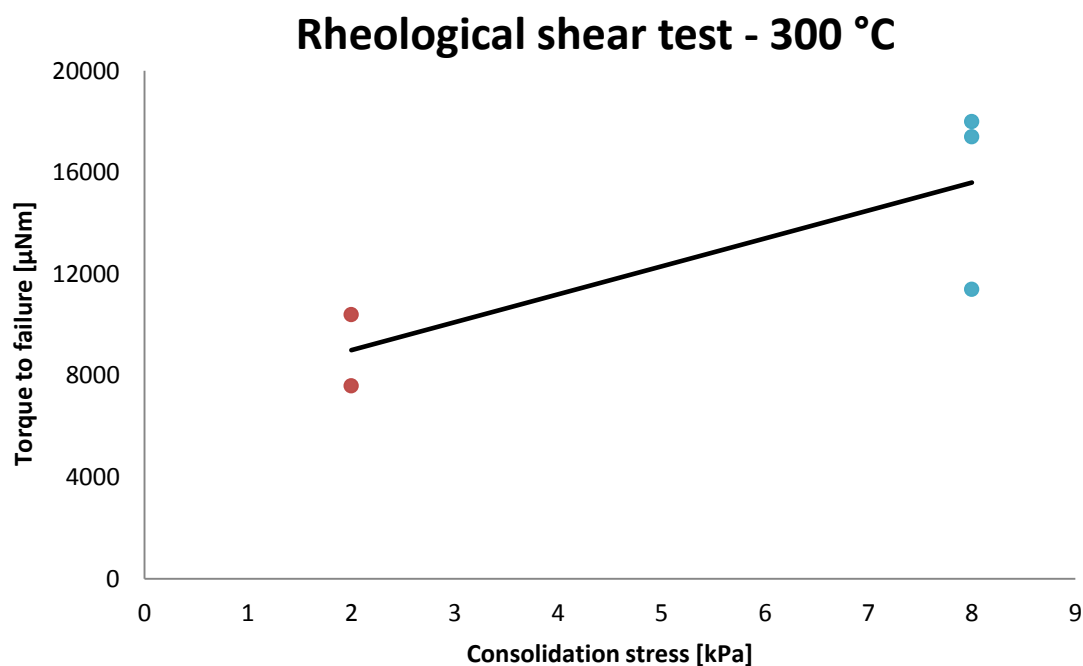


Figure 77. Torque needed to obtain the raw meal specimen failure in the rheological shear test at 300 °C as a function of the previous consolidation stress.

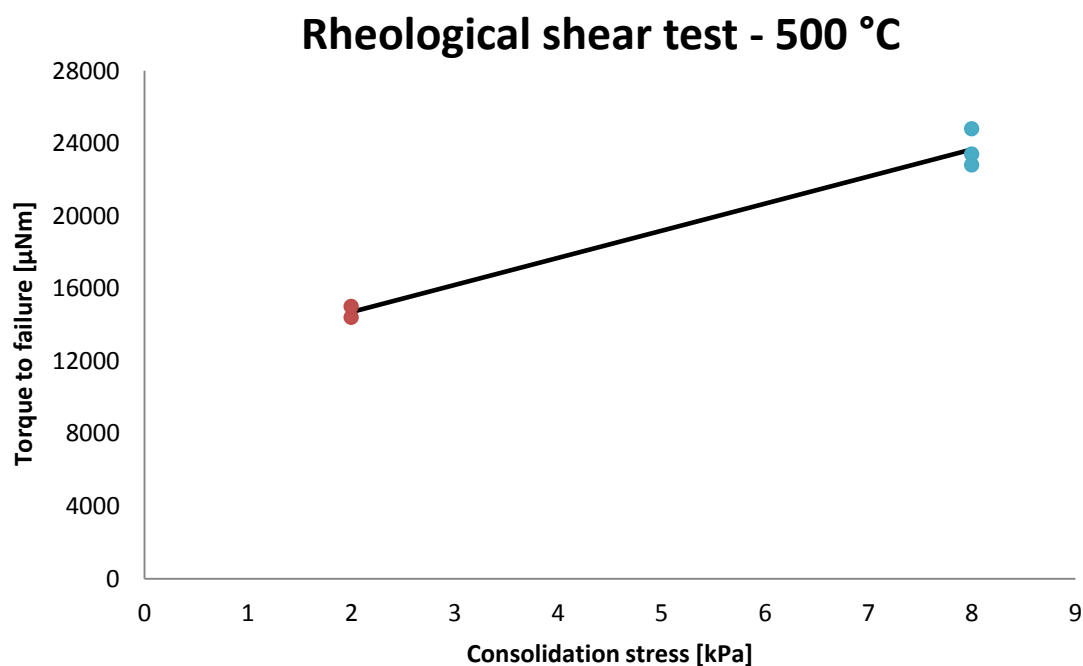


Figure 78. Torque needed to obtain the raw meal specimen failure in the rheological shear test at 500 °C as a function of the previous consolidation stress.

As observed, the torque needed to the failure of the raw meal specimens increases with the consolidation stress for all studied temperatures. The reason for this trend is, as stated previously, that bulk solids gain strength due to its previous consolidation, where greater consolidation stresses yield to greater bulk densities and strength (cohesion).

The coefficient of variation (and so the deviation on the measurements) varies with the temperature without following any pattern: the highest coefficients of variation belong to the 22 °C and 300 °C data, whereas the lowest belong to the 100 °C and 500 °C data.

In order to get a better overview of the relationship between the exerted torque to failure (and consequently the cohesion) and the temperature, the mean values illustrated above are plotted in the same graph so that the results can be more easily compared:

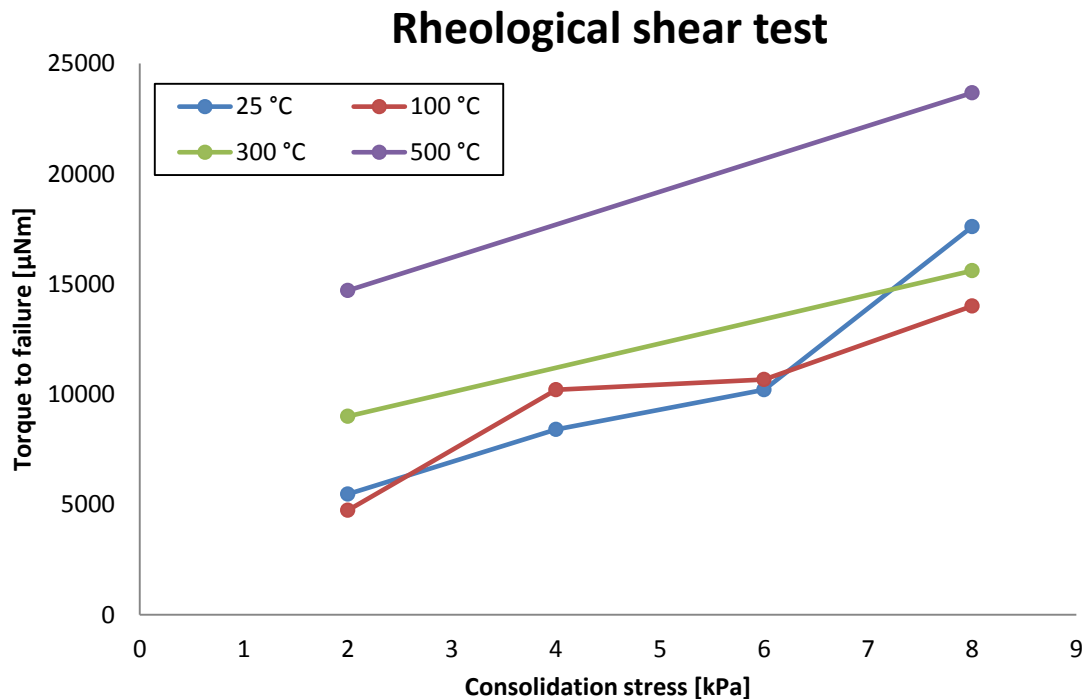


Figure 79. Torque needed to obtain the raw meal specimen failure in the rheological shear test at 25 °C and 100 °C as a function of the consolidation stress. The standard deviations are shown in the graph.

There does not seem to appear a relevant difference between the raw meal behavior between 22 °C, 100 °C and 300 °C. However, the measured torque to failure at 500 °C indicates a significant increase of the raw meal cohesion.

The measured torques to failure with their mean values are drawn as a function of the temperature at each consolidation stress:



## 2 kPa consolidation

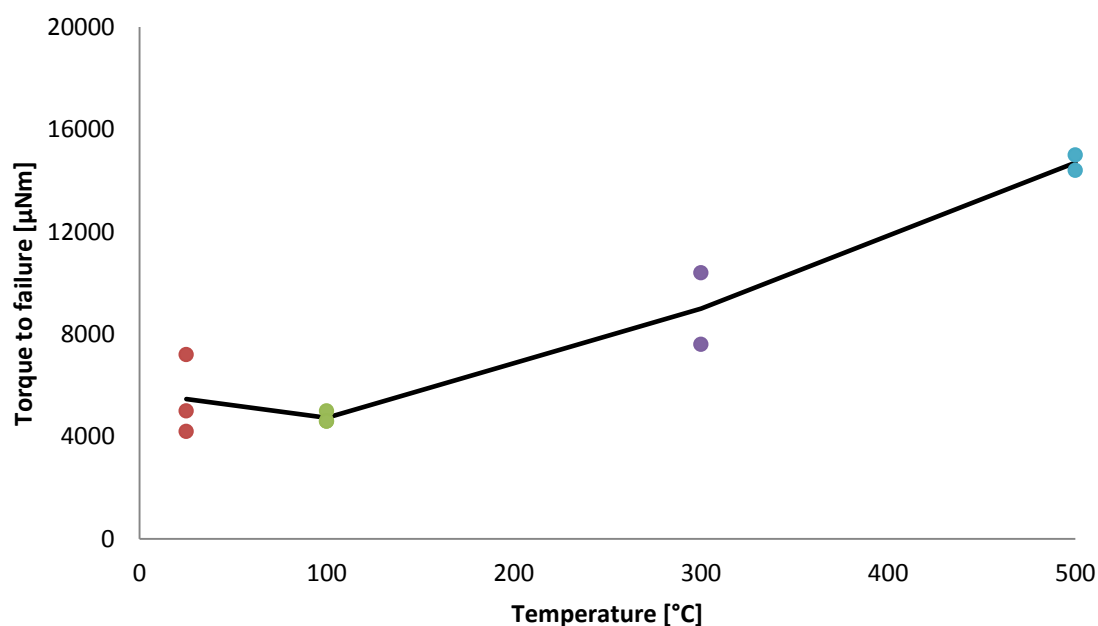
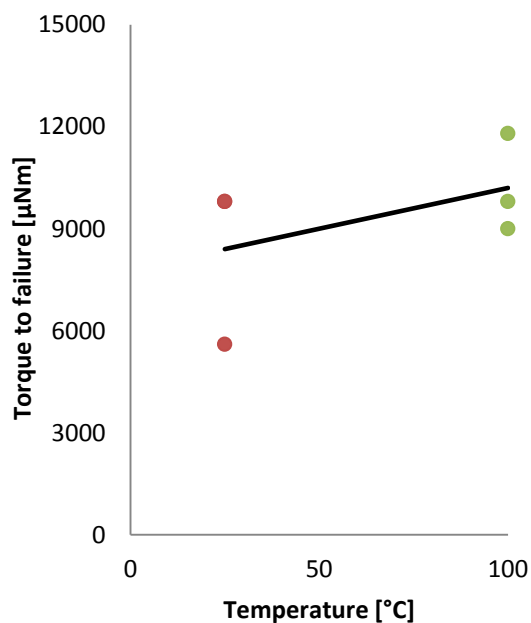


Figure 80. Raw meal torque to failure as a function of the temperature after exerting the **2 kPa** consolidation stress in the rheological shear test.

The torque to failure profile obtained when exerting a 2 kPa consolidation stress show that the raw meal cohesion remains similar when heating the raw meal up from 25 °C to 100 °C. However, the cohesion increases notably at 300 °C and even more at 500 °C.

## 4 kPa consolidation



## 6 kPa consolidation

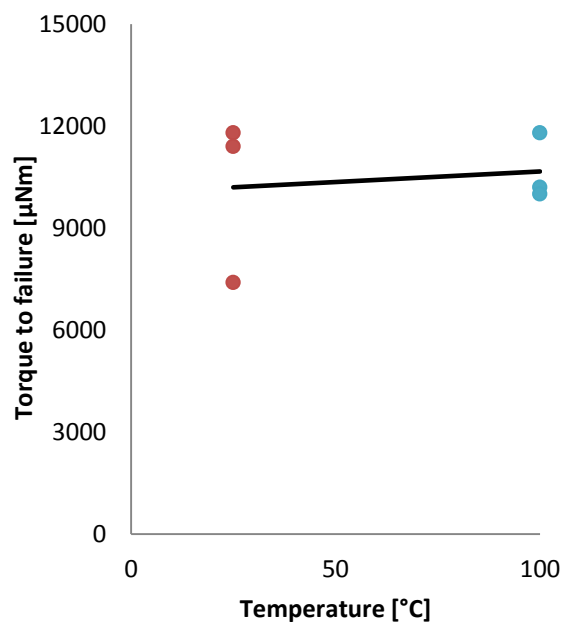


Figure 81. Raw meal torque to failure as a function of the temperature after exerting the **4 kPa** and **6 kPa** consolidation stresses in the rheological shear test.



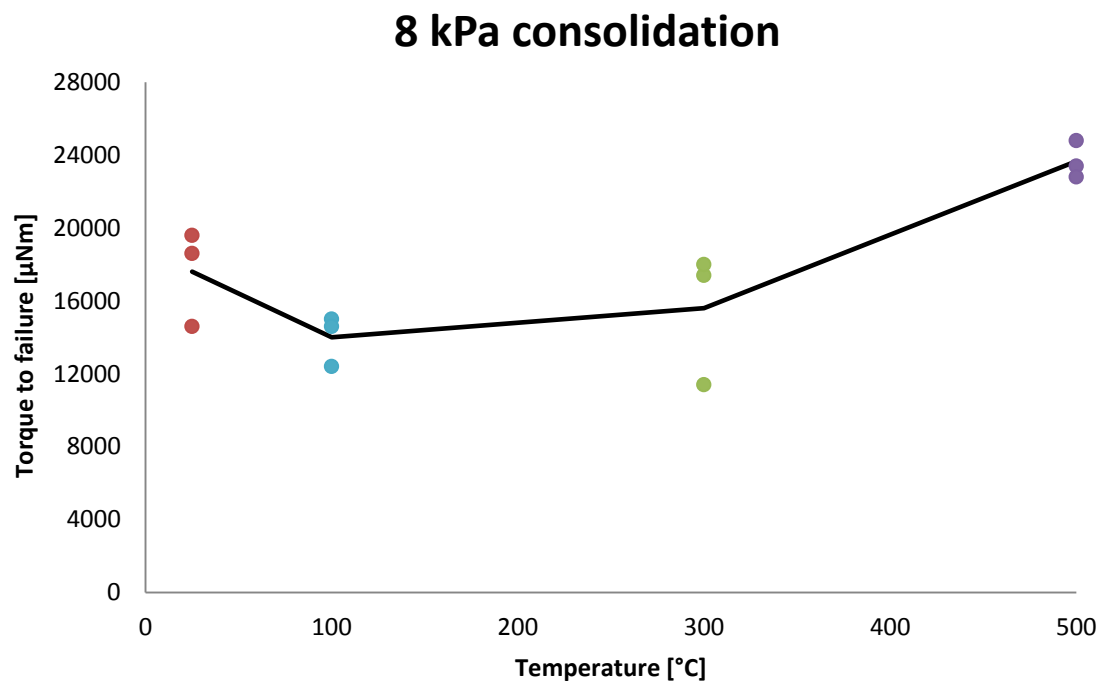


Figure 82. Raw meal torque to failure as a function of the temperature after exerting the **8 kPa** consolidation stress in the rheological shear test.

In this case, after exerting an 8 kPa consolidation stress, the trend indicates that until 300 °C the raw meal cohesion remains practically constant, and after that temperature (at 500 °C) a considerable increase of the cohesion takes place.

## 5.3 Angle of repose measurement

### 5.3.1 Analysis A

The measured angles of repose carrying out the Analysis A, which corresponds to the determination of the angle of repose of the triangle formed from the conical heap of raw meal to its apex. All the repetitions at the different temperatures of interest are plotted as follows:

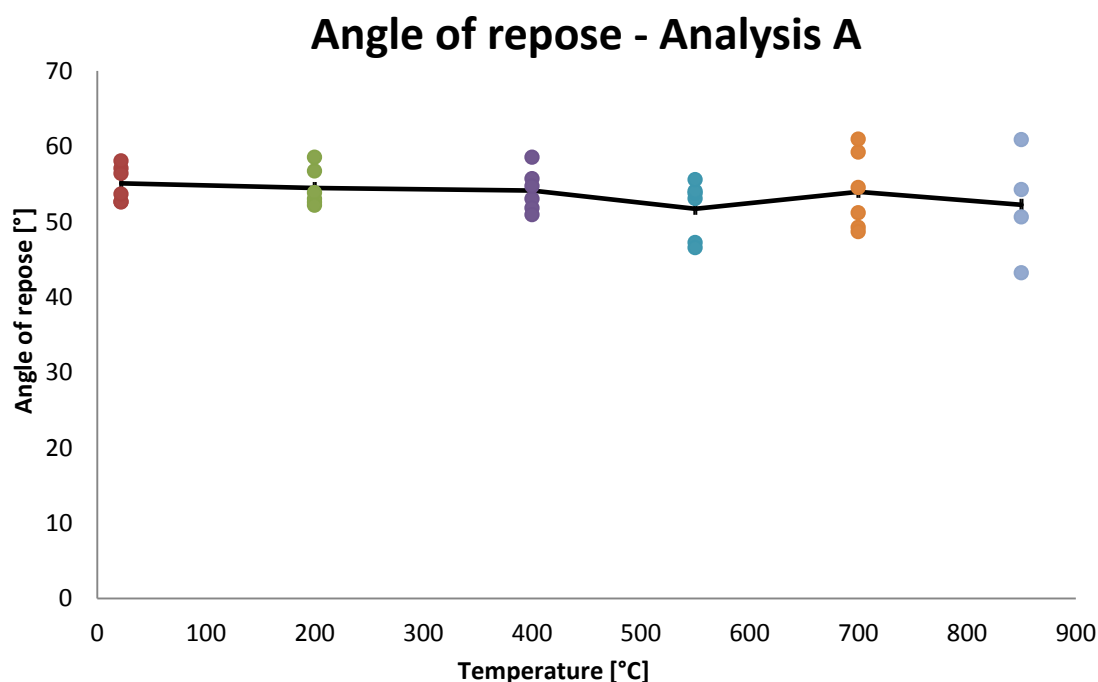


Figure 83. Angle of repose determined using the *Analysis method A* as a function of the temperature.

It should be noted that during the angle of repose measurement, due to the relatively big agglomerates formed at 850 °C, only 2 of the 3 performed repetitions could be used for the angle of repose determination obtaining 4 values instead of 6 at that temperature.

Using the *Analysis A* to determine the angle of repose does not appear any relevant dependence of the raw meal flow behavior with the temperature. Besides, although the deviation of the results is not so big (coefficient of variation between 4,35 % and 14,10 %), the differences between the different temperatures are extremely small. The biggest deviations occur at 850 °C and 700 °C due to the agglomerates formed at these temperatures (especially at 850 °C).



Figure 84. Performance of the angle of repose measurement at 850 °C discarded for the angle of repose measurement due to the amount of agglomerates formed.

### 5.3.2 Analysis B

The measured angles of repose obtained with the Analysis B, which corresponds to the determination of the angle of repose on the base of the conical heap of raw meal, in all the repetitions at the different temperatures of interest are shown in the next graph:

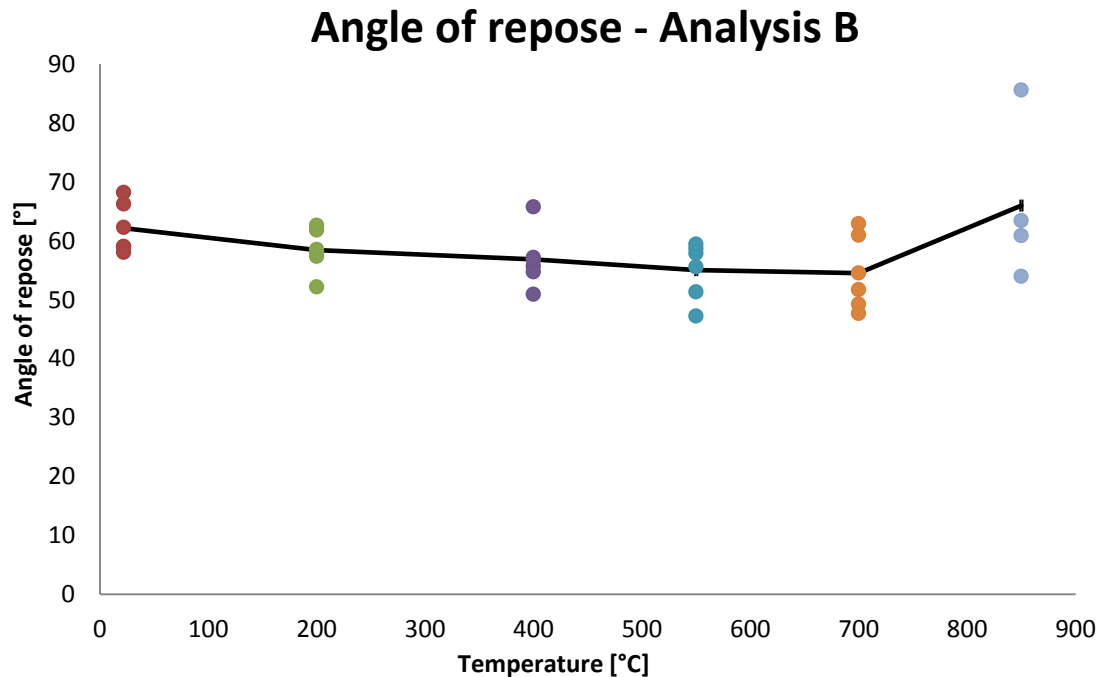


Figure 85. Angle of repose determined using the *Analysis method B* as a function of the temperature.

Determining the angle of repose with the *Analysis B*, similarly to the other analysis method, no clear relationship between the angle of repose and the operational temperature can be observed. In this case the coefficient of variation is slightly higher than the Analysis A (between 6,39 % and 20,74 %) occurring the highest deviations at 850 °C and 700 °C, respectively.



## 6. Statistical analysis

Calculated confidence intervals with a 95 % confidence level are computed and shown in this section in order to determine if statistical significant differences exist in the previously explained results obtained using the three performed testing methods: uniaxial shear test, rheological shear test and angle of repose measurement. Note that the complete data can be found in the Appendix A.

### 6.1 Uniaxial shear test

#### 6.1.1 System behavior

The confidence intervals with a 95% confidence level for the forces required to start moving the pushing wall at different temperatures in the uniaxial shear test in the empty system are plotted in Figure 86:

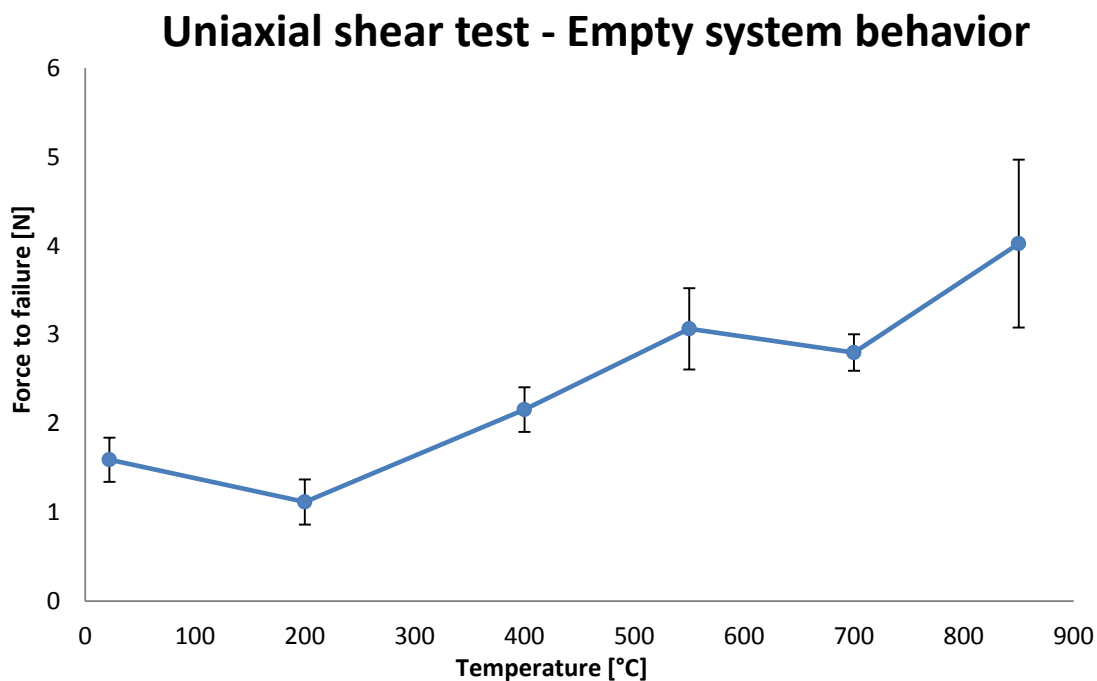


Figure 86. Confidence intervals for the force needed to move the pushing wall as a function of the temperature in the empty uniaxial shear test.

In this case, the confidence intervals are nearly the same as the standard deviation. Between 22 °C and 200 °C there is no statistical significant difference. The 400 °C data is statistically different than the other temperatures. The 550 °C and the 700 °C data are statistically different and even though there is no statistical difference between 550 °C and 850 °C, between 700 °C and 850 °C the statistical difference exists. This analysis confirms that although the profile is not linear, the force needed to start moving the pushing wall increases with the temperature.

### 6.1.2 Raw meal flow functions

Confidence intervals with a 95% confidence level for the unconfined yield strengths as a function of the consolidation stress (flow functions) at the different temperatures are illustrated as follows, so that it can be determined if statistical significant differences exist between the different consolidation stresses:

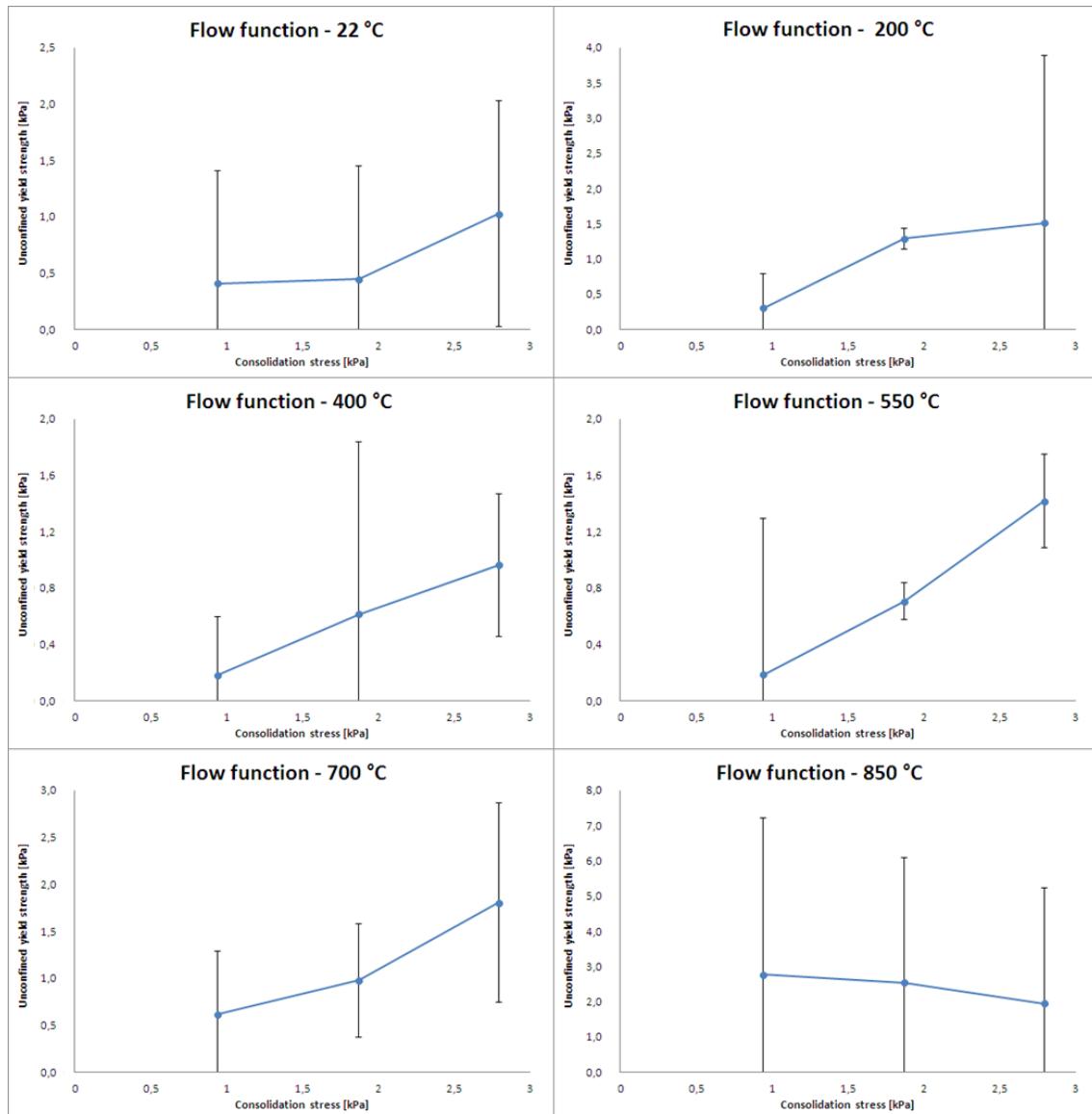


Figure 87. Confidence intervals for the raw meal flow functions obtained at the different studied temperatures.

Concerning the raw meal flow functions (i.e. the dependence of the unconfined yield strength with the consolidation stress), only two pair of values which are statistically different exist:

- At 200 °C: Unconfined yield strengths obtained at 0,94 kPa and 1,87 kPa.
- At 550 °C: Unconfined yield strengths obtained at 1,87 kPa and 2,79 kPa.

In the next figures the confidence intervals with a 95 % confidence level for the unconfined yield strengths are plotted on the unconfined yield strength – temperature diagrams so that it can be analyzed if statistical significant differences exist between the different temperatures:

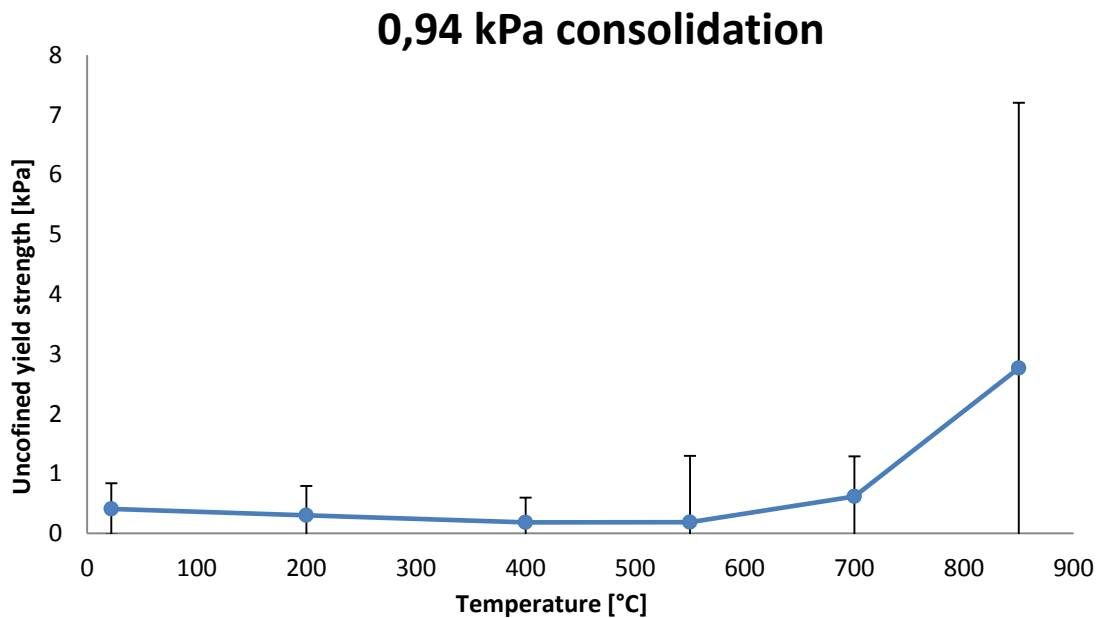


Figure 88. Confidence intervals for the raw meal unconfined yield strength as a function of the temperature when exerting the **0,94 kPa** consolidation stress.

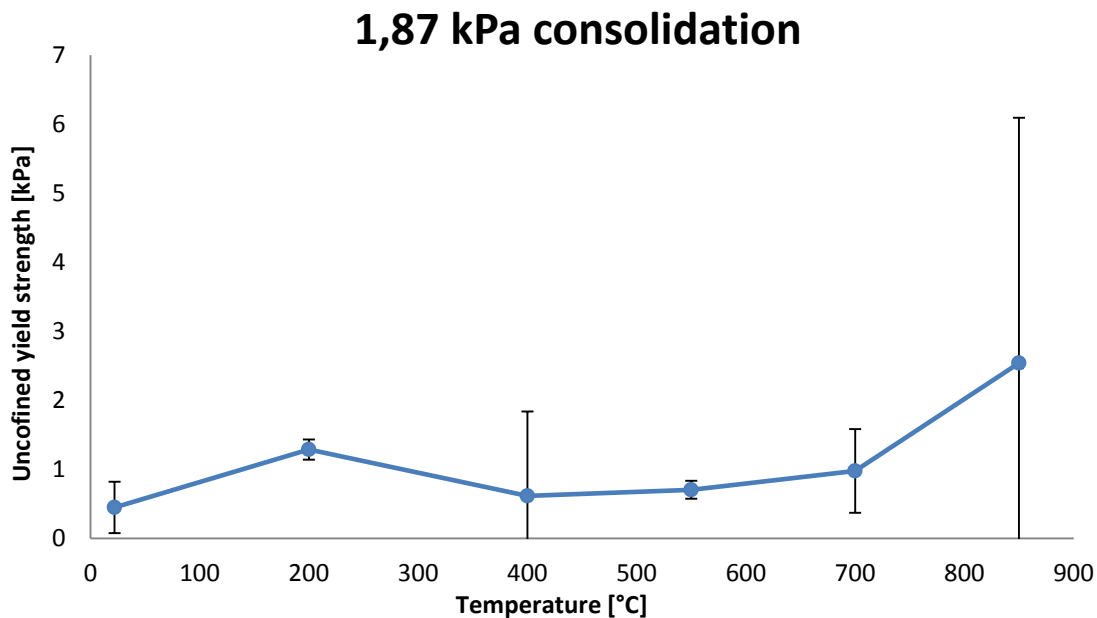


Figure 89. Confidence intervals for the raw meal unconfined yield strength as a function of the temperature when exerting the **1,87 kPa** consolidation stress.

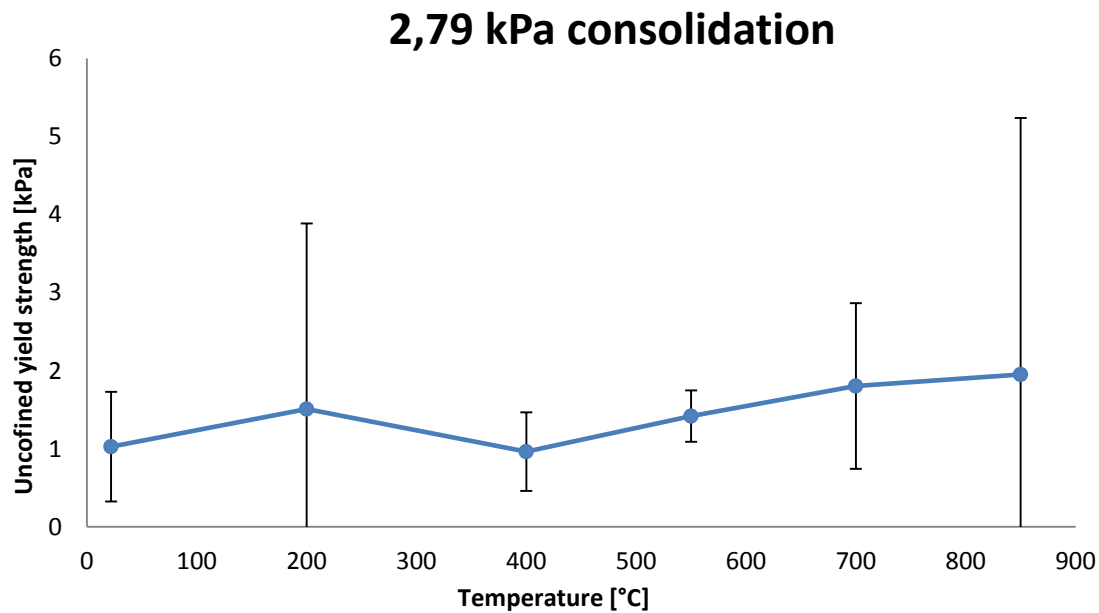


Figure 90. Confidence intervals for the raw meal unconfined yield strength as a function of the temperature when exerting the **2,79 kPa** consolidation stress.

The last figures (Figure 88, Figure 89 and Figure 90) show that even though the results seem to show a trend in which the cohesion of the raw meal samples increases exponentially from 700 °C onwards, there are practically no significant statistical differences on the unconfined yield strength values due to the extremely high confidence intervals. Only in the 1,87 kPa consolidation, a statistical difference appears between 200 °C and the values at 22 °C and 550 °C, which do not correspond to the observed trend of the results and could be caused to a possible errors on the measurements or uncertainties of the uniaxial shear test.

The reason of these extremely high confidence intervals is that on one hand the uniaxial shear test used for the measurements has a big standard deviation on its values. On the other hand, when subtracting the mean value of the force needed to shift the pushing wall from the cell to the different obtained values when determining the force needed to break the raw meal specimen, the standard deviation increases notably while the mean value is reduced, leading to a drastic increase on the resultant standard deviation.



## 6.2 Rheological shear test

First of all, must be commented that in the determination of the confidence intervals for the torque to failure, the fact that the experiments at 300 °C and 500 °C with a 2 kPa consolidation stress were performed only two times instead of three must be taken into account for the statistical analysis. Hence, the student's  $t$  with  $n = 2$  and  $\alpha = 0,05$  equals to 12,71.

Analogously than performed with the data from the uniaxial shear test, confidence intervals with a 95% confidence level were calculated for the torques required to reach the specimen failure in the rheological shear test:

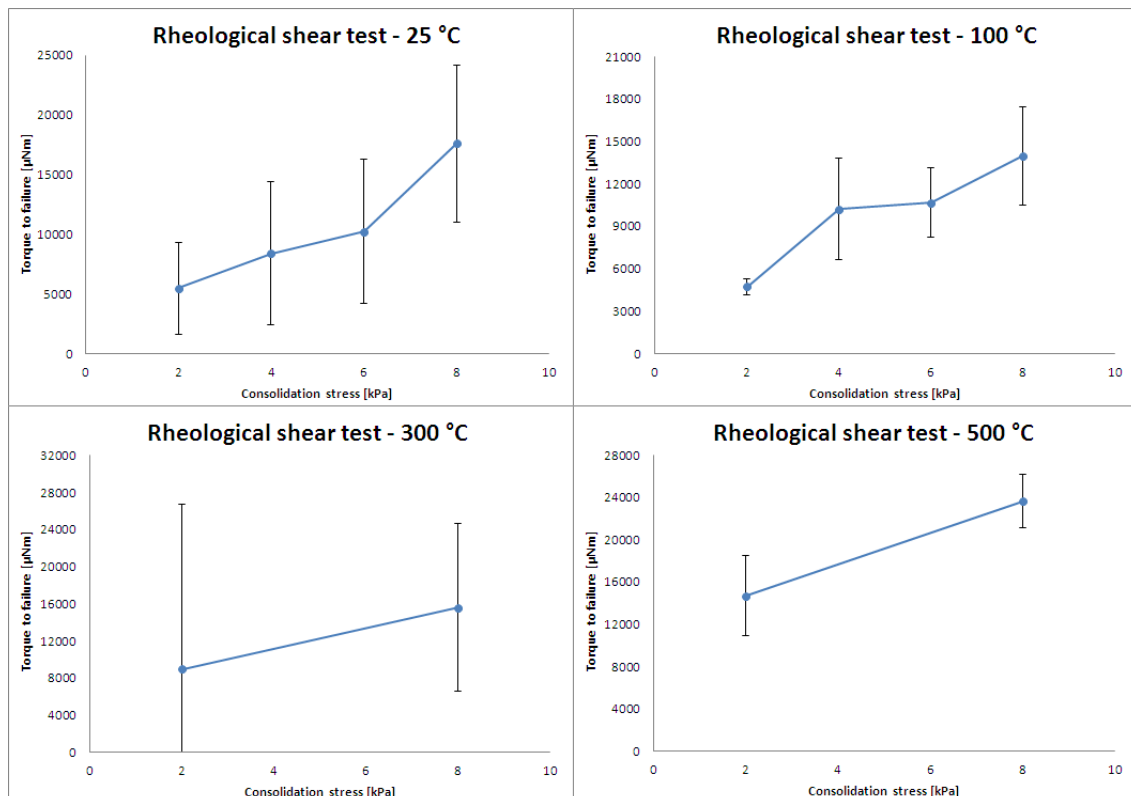


Figure 91. Confidence intervals for the torque needed to obtain the raw meal specimen failure as a function of the consolidation stress in the rheological shear test at the different studied temperatures.

At 25 °C the confidence intervals are very large due to a huge standard deviation. In this case only a significant statistical significant difference can be affirmed between the 2 kPa and 8 kPa consolidation data. Between all the other values no statistical difference exists.

At 100 °C the confidence intervals are quite big except for the 2 kPa consolidation stress. It is just the data obtained at this consolidation stress which shows a significant statistical difference with the data obtained from all the other previous consolidation stresses.

At 300 °C none statistical significant difference exists between the two different applied consolidation stresses measured data. Nevertheless, at 500 °C a statistical difference between the 2 kPa and 8 kPa values can be observed.

In the figures showed in the following, the confidence intervals with a 95 % confidence level for the torque needed to attain the failure of the raw meal specimens are plotted on torque to failure – temperature diagrams in order to corroborate if statistical significant differences exist between the different studied temperatures:

## 2 kPa consolidation

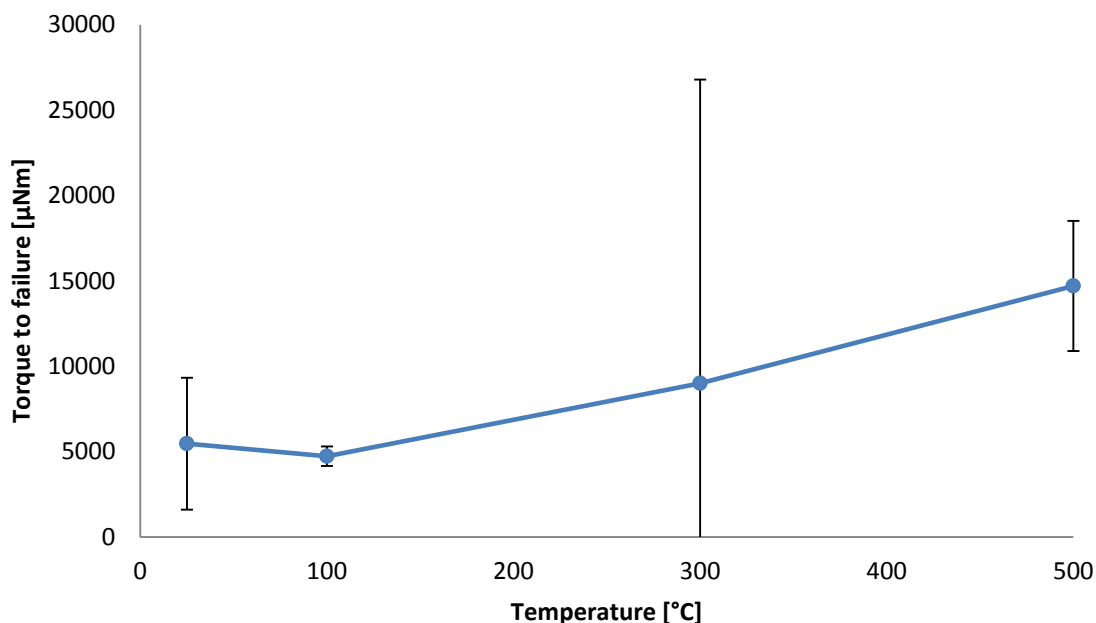
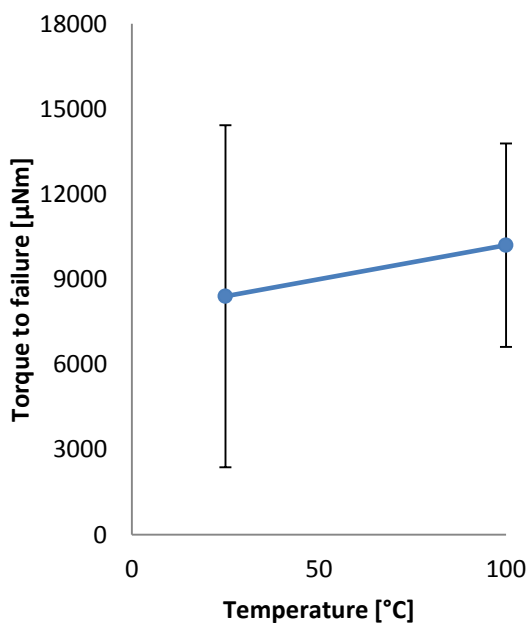


Figure 92. Confidence intervals for the torque needed to obtain the specimen failure as a function of the consolidation stress when exerting the **2 kPa** consolidation stress in the rheological shear test.

## 4 kPa consolidation



## 6 kPa consolidation

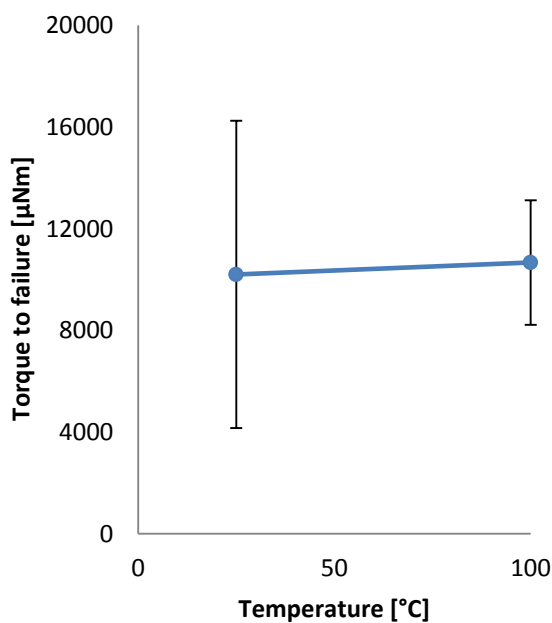


Figure 93. Confidence intervals for the torque needed to obtain the specimen failure as a function of the consolidation stress when exerting the **4 kPa** and **6 kPa** consolidation stresses in the rheological shear test.

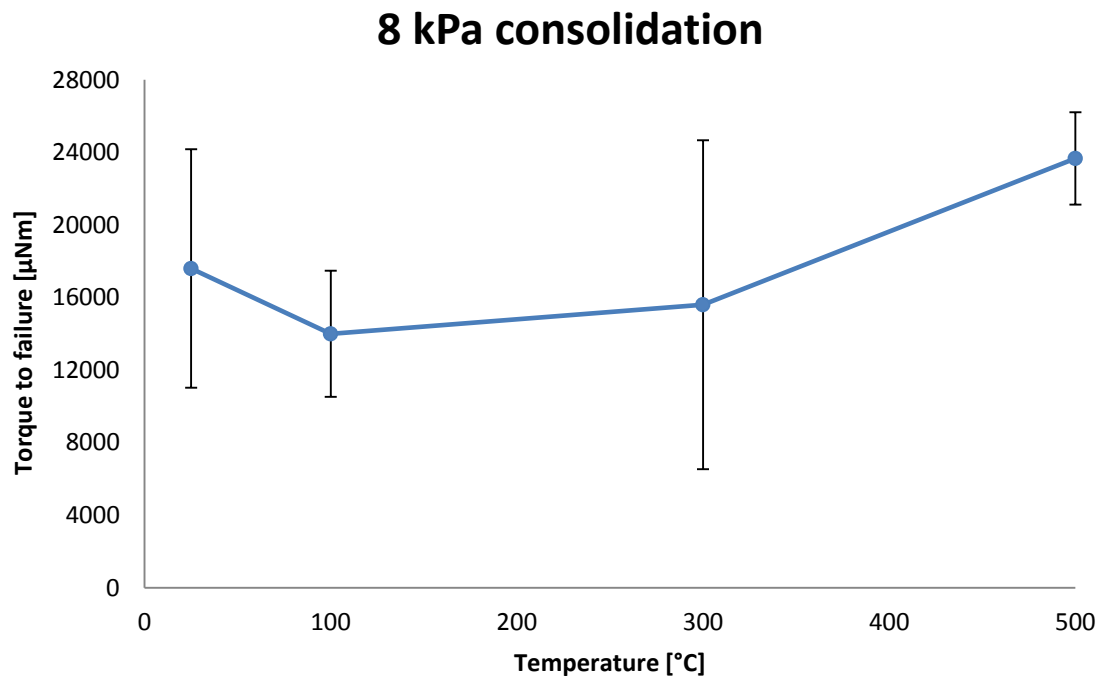


Figure 94. Confidence intervals for the torque needed to attain the specimen failure as a function of the consolidation stress when exerting the **8 kPa** consolidation stress in the rheological shear test.

Concerning the temperature effect on the raw meal cohesion with the rheological shear test, only two statistical significant differences have been found.

On one hand, when exerting the 2 kPa consolidation stress on the bulk solid specimens, a statistical significant difference appear between the 500 °C and the values obtained at 22 °C and 100 °C. However, between the 300 °C data and the 500 °C data a statistical difference does not exist due to the extremely big confidence interval at 300 °C even though the experimentally determined values are considerably different. This large confidence interval at 300 °C is mainly caused by the fact that only 2 measurements were performed at these conditions. Therefore the student's *t* changed from 4,30 to 12,71 obtaining a confidence interval between 3 and 4 times larger.

On the other hand, during the 8 kPa consolidation stress, the data obtained at 100 °C is statistically different from the data obtained at 500 °C.

### 6.3 Angle of repose measurement

As for the two other tests, the confidence intervals with a 95% confidence level for the angles of repose determined at the different temperatures of study using the two different ways to calculate it (Analysis A and Analysis B), are provided:

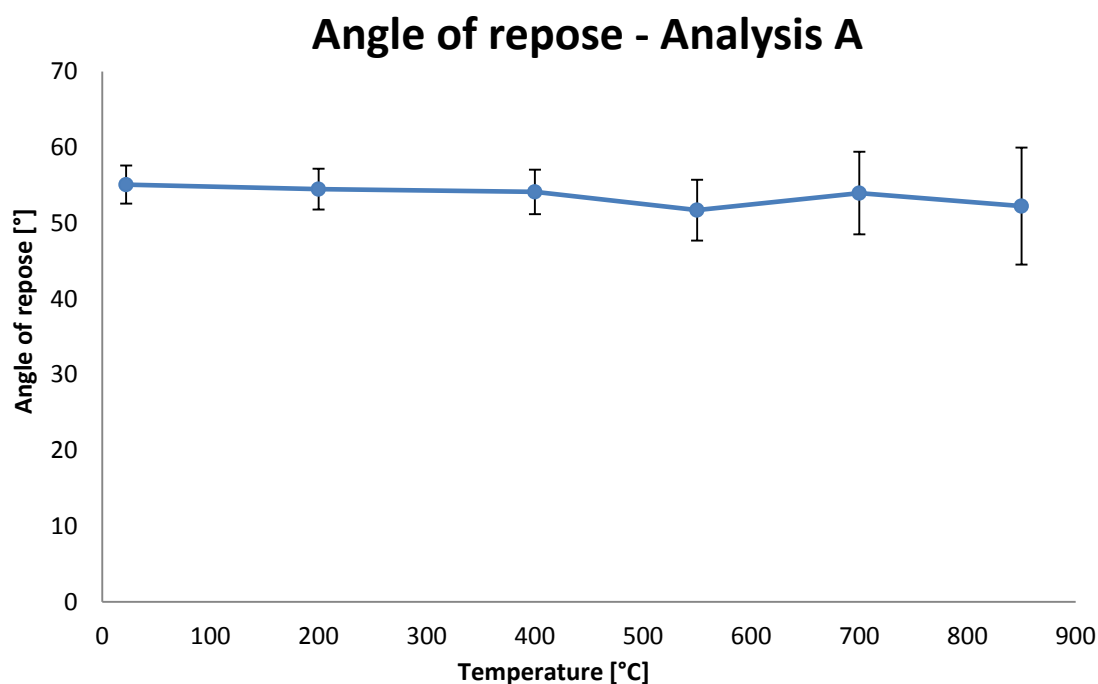


Figure 95. Confidence intervals for the angle of repose determined using the **Analysis A** as a function of the temperature.

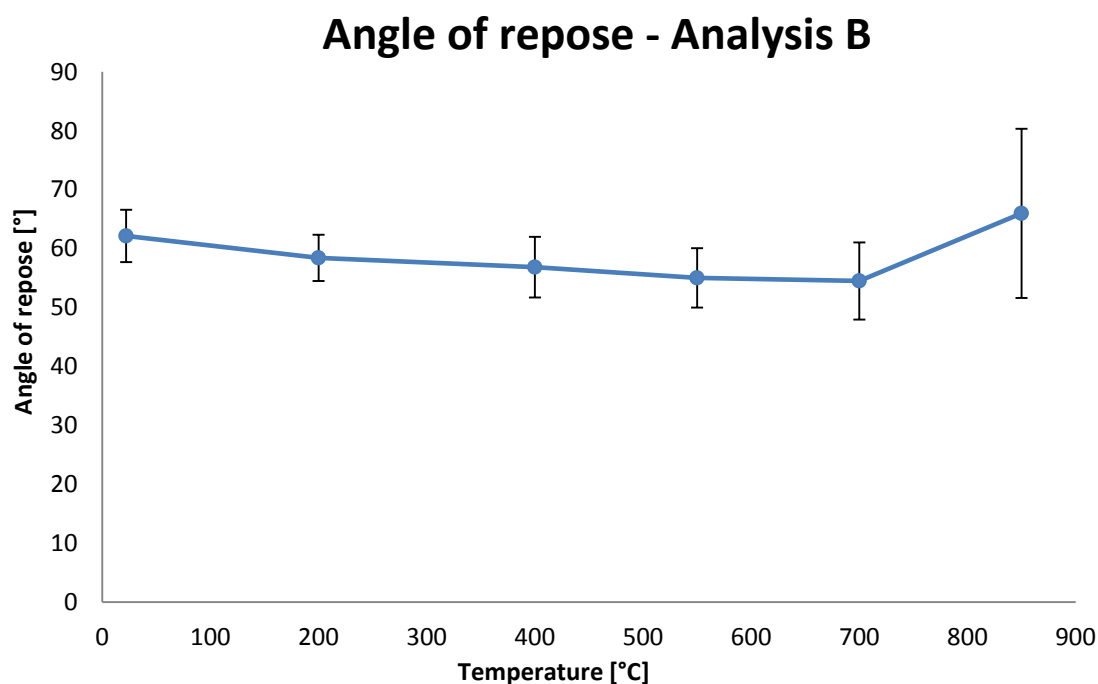


Figure 96. Confidence intervals for the angle of repose determined using the **Analysis B** as a function of the temperature.

As it can be clearly observed, there is no statistical significant difference between any of the angles of repose at the different operational temperatures when the angle of repose is determined using the Analysis A. Neither when the Analysis B is used.

## 7. Discussion

Even though the results presented in section 5 show that the raw meal flowability has an exponential trend which is kept nearly constant until 700 °C and after that temperature the cohesion drastically increases (the flowability decreases), the statistical analysis could not affirm that statement due to the large confidence intervals.

The mainly reason for these large confidence intervals was that the measurements of the experiments were performed only 3 times. Hence, the determination of the confidence intervals from only 3 measured data points yielded to confidence intervals even more high than the standard deviation boundaries. This is caused by the high student's  $t$  (4,30). Increasing the number of measured points from 3 to 5 a notably change on the confidence intervals would have been attained due to a halve of the student's  $t$  (2,78) which multiplies the standard deviation, and also due to an increase of the denominator (from  $\bar{3}$  to  $\bar{5}$ ) of the confidence interval addend term.

Moreover, the raw meal flow behavior observed in the results is also found in coal fly ash where a significant increase of the adhesive forces (increase of factor  $\kappa$ ) occurs after 600 °C meanwhile at lower temperatures its cohesion remains constant [32]:

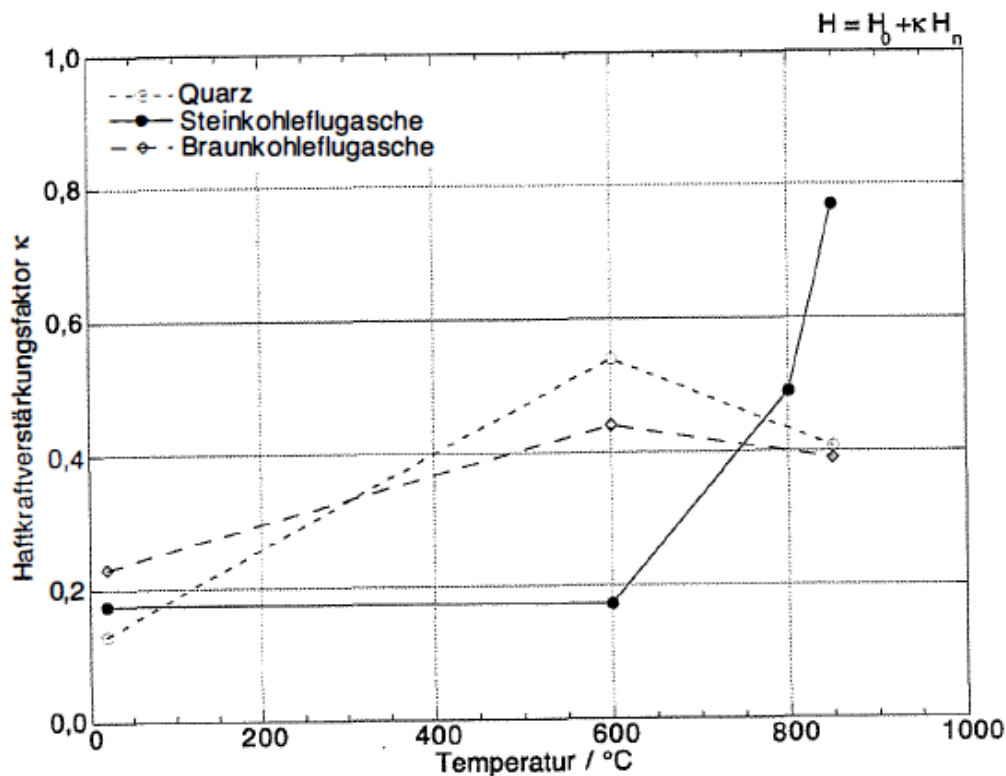


Figure 97. Temperature influence on the dimensionless factor  $\kappa$ . Note that the coal fly ash profile corresponds to Steinkohleflugasche [32].

Concerning the uniaxial shear test used to test the raw meal flowability in this thesis it has been seen that useful information can be provided even though it is not highly accurate.

With the purpose to improve this testing method and get more reliable and less dispersed results, a new test cell which could avoid sideways movements of the pushing wall in order to reduce the side friction should be built. Furthermore the new device should allow a perfectly straight movement of the piston despite of the temperature changes (the piston slightly bended at high temperatures) so that it could hit the pushing wall always in its center.

Finally, another matter to improve should be the reduction of the internal friction of the cell using any of the thoughts explained below:

- Use high temperature resistant lubricants so that the subtraction of the force needed to move the pushing wall in the empty system to the raw meal determinations would affect less in the final result, especially in the deviation.
- Use a new design of the test cell which test cell would not have internal friction. In order to do that, the pushing wall of the test cell used in this thesis should be fixed to the static part of the cell so that its only function would be to confine the powder. Thus, a thin metal sheet pushed by the piston from a hole in the pushing wall should be the one exerting the stress to the powder specimen. A sketch of this idea is provided as follows:

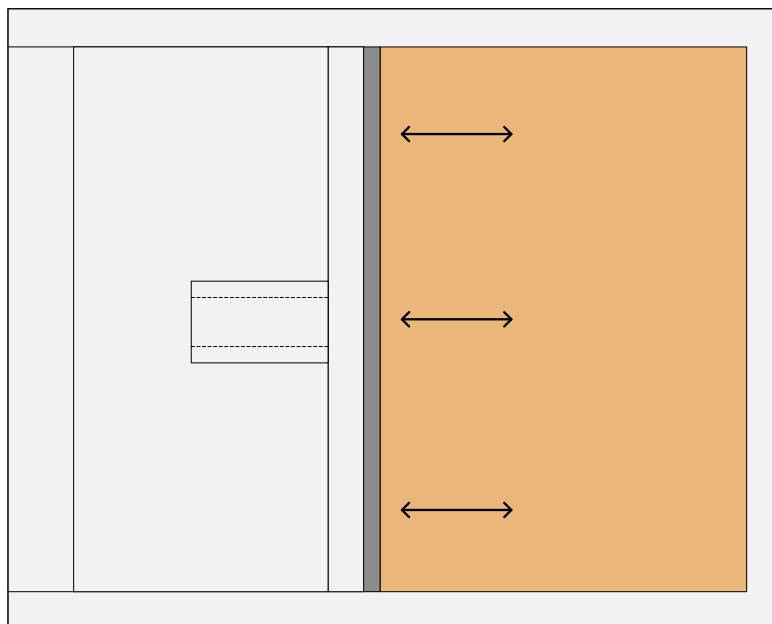


Figure 98. New uniaxial shear test cell idea. The new pushing wall is marked in a darker grey tonality.

Concerning the rheological shear test, considering that the device used for the test is not precisely designed for the flowability determination of bulk solids, it provides relatively good results. However, there are several issues when using the rheometer used in this thesis as a particle characterization:

- It is an extremely slow method when testing high temperatures.
- Only temperatures up to 500 °C can be reached without taking risks.
- The position of the vaned lid cannot be raised (and so the normal force cannot be decreased) when the heater hatches are closed. Therefore the yield locus cannot be determined and the test can only be used as a comparison between the cohesion at different conditions.
- The consolidation normal force to exert on the bulk solid specimen is difficult to control accurately, since it is achieved by lowering manually the vaned lid.
- The torque increase cannot be progressively done and has to be performed step by step.

Concerning the angle of repose measurement, as it was performed in this thesis, the results does not show valuable conclusions concerning the raw meal flow behavior. The principal issues found with the equipment used to perform the test are listed as follows:

- The inside volume of the oven was too small to set a testing device inside which could allow the pouring of the powder always in the same place (in the center of the ceramic crucible placed face down).
- Not all the raw meal agglomerates formed at high temperature could be broken shaking manually the pouring ceramic crucible where the raw meal was heated up, leading to erroneous angle of repose values.





## 8. Conclusions

As it has been observed in the results, the uniaxial shear test is slightly influenced by the temperature since the internal friction of the test cell increases with the temperature. For this reason a study of the empty system behavior needs to be done before and after the experiments with raw meal are performed. Besides, this internal friction between the mobile and fixed parts is one of the principal reasons for the high deviation on the results obtained with this method. Therefore, the main improvement which can be done to a new design of the uniaxial shear test cell would be with the aim to decrease, as much as possible, the internal friction of the system.

However, it has been seen that the uniaxial shear test provides valuable information about the dependence of the raw meal flowability with the temperature. The trend of a nearly constant raw meal flowability until around 700 °C, which decreases as the temperature reaches 850 °C has been stated and discussed by means of the determined unconfined yield strengths, bulk densities, force – time diagrams directly obtained from the procedure of the test, and physical changes occurring to the raw meal powder when heated up. An increase of the cohesion with the previously exerted consolidation stress has also been shown at all the temperatures with the exception of the 850 °C data (which belong to the data with the highest deviation).

Concerning the rheological shear test, which has been developed from a rheometer used for the study of the viscoelasticity on polymers, it has been observed that the method provides results more accurate than the uniaxial shear test. Nevertheless, this method has several limitations on its performance of the test (at least with the device used in this thesis). The principal limitations are the slowness of the procedure (especially the cooling down of the device), that the results can only be used as a comparison between different conditions (the yield locus cannot be determined) and the last and more important is that only measurements up to 500 °C can be done without taking risks of damaging the rheometer.

Even so, the results obtained with the rheological shear test have shown that a decrease of the raw meal flowability occurs from 300 °C to 500 °C, meanwhile at lower temperatures the flowability seems to remain rather similar. Moreover, increases of the raw meal cohesion with the previous consolidations stresses have been clearly observed at all the temperatures.

Finally, the poured angle of repose measurement, as it was performed in this thesis, the results does not provide any valuable information concerning the temperature trend of the raw meal flowability, but several issues showed up when trying to perform the angle of repose measurement in an oven with such a small interior volume. These troubles were the impossibility of placing a testing device inside the oven and of breaking the agglomerates formed at temperatures above 700 °C (especially at 850 °C).



## 9. References

- [1] J. I. Bhatti: *Innovations in Portland Cement Manufacturing*. Portland Cement Association. 2004.
- [2] The European Cement Association (CEMBUREAU): *"Best available techniques" for the cement industry*. 1999.
- [3] C. M. Rasmussen: *Energy Flows and Cogeneration of Power in Cement Plants*. 2009.
- [4] D. C. MacLaren; M. A. White: *Cement: Its Chemistry and Properties*. Journal of Chemical Education 623-635. 2003.
- [5] F. L. Smidth: *Dry process kiln systems*.
- [6] D. Schulze: *Powders and Bulk Solids: Behavior, Characterization, Storage and Flow*. 2008.
- [7] D. Turki; N. Fatah: *Behavior and fluidization of the cohesive powders: Agglomerates size approach*. Brazilian Journal of Chemical Engineering 697-711. 2008.
- [8] D. Schulze: *Flow Properties of Powders and Bulk Solids*. 2011.
- [9] J. Schwedes: *Consolidation and flow of cohesive bulk solids*. Chemical Engineering Science 287-294. 2002.
- [10] Q. Li; V. Rudolph; B. Weigl; A. Earl: *Interparticle van der Waals force in powder flowability and compactibility*. International Journal of Pharmaceutics 77-93. 2004.
- [11] S. A. Mohammed; E. C. Abdullah; D. Geldart; A. A. A. Raman: *Measuring powder flowability with a modified Warren Spring cohesion tester*. Particuology 148-154. 2011.
- [12] P. Juliano; G. V. Barbosa-Cánovas: *Food Powders Flowability Characterization: Theory, Methods and Applications*. Food Science Technology 211-239. 2010.
- [13] E. Teunou; J. J. Fitzpatrick; E. C. Synnott: *Characterisation of food powder flowability*. Journal of Food Engineering 31-37. 1999.
- [14] D. Hann; J. Strazisar: *Influence of Particle Size Distribution, Moisture Content, and Particle Shape on the Flow Properties of Bulk Solids*. Instrumentation Science and Technology 571-584. 2007.
- [15] D. Geldart; E. C. Abdullah; A. Hassanpour; L. C. Nwoke; I. Wouters: *Characterization of powder flowability using measurement of angle of repose*. China Particuology 104-107. 2006.
- [16] W. Wang; J. Zhang; S. Yang; H. Zhang; H. Yang; G. Yue: *Experimental study on the angle of repose of pulverized coal*. Particuology 482-485. 2010.

- [17] I. M. F. Wouters; D. Geldart: *Characterising Semi-Cohesive Powders Using Angle of Repose*. Part. Syst. Charact. 254-259. 1996.
- [18] D. Geldart; E. C. Abdullah; A. Verlinden: *Characterisation of dry powders*. Powder Technology 70-74. 2009.
- [19] W. Schräml: *On the Measurement of the Flow Properties of Cement*. Powder Technology 221-227. 1967.
- [20] M. Harini; G. Shaalini; G. Dhinakaran: *Effect of Size and Type of Fine Aggregates on Flowability of Mortar*. KSCE Journal of Civil Engineering 163-168. 2012.
- [21] D. Geldart: *Types of gas fluidization*. Powder Technology 285-292. 1973.
- [22] J. P. K. Seville; C. D. Willett; P. C. Knight: *Interparticle forces in fluidization: a review*. Powder Technology 261-268. 2000.
- [23] F. Podczek; Y. Miah: *The influence of particle size and shape on the angle of internal friction and the flow factor of unlubricated and lubricated powders*. International Journal of Pharmaceutics 187-194. 1996.
- [24] E. Teunou; J. J. Fitzpatrick: *Effect of storage time and consolidation on food powder flowability*. Journal of Food Engineering 97-101. 2000.
- [25] A. Santomaso; P. Lazzaro; P. Canu: *Powder flowability and density ratios: the impact of granules packing*. Chemical Engineering Science 2857-2874. 2003.
- [26] M. Krantz; H. Zhang; J. Zhu: *Characterization of powder flow: Static and dynamic testing*. Powder Technology 239-245. 2009.
- [27] Y. Jiang; S. Matsusaka; H. Masuda; Y. Qian: *Development of measurement system for powder flowability based on vibrating capillary method*. Powder Technology 242-247. 2009.
- [28] C. Wang; A. Hassanpour; M. Ghadiri: *Characterisation of flowability of cohesive powders by testing small quantities of weak compacts*. Particuology 282-285. 2008.
- [29] J. Schwedes: *Review on testers for measuring flow properties of bulk solids*. 2003.
- [30] F. L. Smid: *Laboratory report*. 2011.
- [31] F. Carmona; A. Sánchez: *Estadística Matemàtica II - Apunts*. Departament d'Estadística de la Universitat de Barcelona. 2005.
- [32] T. Pilz: *Zu den Wechselwirkungen bei der Oberflächenfiltration unter besonderer Berücksichtigung der Heißgasreinigung mit keramischen Filtern*. 1996.

## Appendix A. Tables with the data

All the measured and calculated data for the three experimental methods used in this thesis are shown in this appendix. The data used for the statistical analysis is also shown here.

### Uniaxial shear test

Table 6. Mean values of the **height [mm]** of the raw meal specimens used in the uniaxial shear test with the different consolidation stresses at all the studied temperatures.

Consolidation stress	0,94 kPa	1,87 kPa	2,79 kPa
Mean value (22 °C)	<b>18,90</b>	<b>17,37</b>	<b>16,96</b>
Mean value (200 °C)	<b>19,01</b>	<b>17,78</b>	<b>17,05</b>
Mean value (400 °C)	<b>19,20</b>	<b>18,39</b>	<b>17,81</b>
Mean value (550 °C)	<b>20,01</b>	<b>18,62</b>	<b>18,09</b>
Mean value (700 °C)	<b>20,36</b>	<b>18,83</b>	<b>18,81</b>
Mean value (850 °C)	<b>20,41</b>	<b>19,72</b>	<b>19,47</b>

Table 7. Mean values of the **bulk density [g/cm<sup>3</sup>]** of the raw meal specimens used in the uniaxial shear test with the different consolidation stresses at all the studied temperatures.

Consolidation stress	0,94 kPa	1,87 kPa	2,79 kPa
Mean value (22 °C)	<b>1,134</b>	<b>1,234</b>	<b>1,263</b>
Mean value (200 °C)	<b>1,127</b>	<b>1,205</b>	<b>1,257</b>
Mean value (400 °C)	<b>1,116</b>	<b>1,165</b>	<b>1,203</b>
Mean value (550 °C)	<b>1,071</b>	<b>1,151</b>	<b>1,185</b>
Mean value (700 °C)	<b>1,052</b>	<b>1,138</b>	<b>1,139</b>
Mean value (850 °C)	<b>1,050</b>	<b>1,087</b>	<b>1,101</b>

Table 8. **Force [N]** needed to start moving the pushing wall with the empty system in the uniaxial shear test at the different temperatures. The 6 measured values, the mean value, the standard deviation and the coefficient of variation are shown.

Temperature	22 °C	200 °C	400 °C	550 °C	700 °C	850 °C
Test 1	1,869	1,385	2,320	3,288	2,553	5,591
Test 2	1,585	1,185	2,420	3,171	2,837	3,722
Test 3	1,736	1,068	2,170	3,755	2,854	3,555
Test 4	1,352	0,818	1,802	2,620	2,820	4,606
Test 5	1,268	0,868	2,286	2,620	3,104	3,421
Test 6	1,736	1,368	1,936	2,937	2,620	3,254
Mean value	<b>1,591</b>	<b>1,115</b>	<b>2,156</b>	<b>3,065</b>	<b>2,798</b>	<b>4,025</b>
Standard deviation	<b>0,2369</b>	<b>0,3434</b>	<b>0,2396</b>	<b>0,4357</b>	<b>0,1951</b>	<b>0,9012</b>
Coefficient of variation [%]	<b>14,89</b>	<b>21,73</b>	<b>11,12</b>	<b>14,21</b>	<b>6,97</b>	<b>22,39</b>

Table 9. **Force [N]** needed to attain the failure of the raw meal specimens (including the force required to move the pushing wall) in the uniaxial shear test at **22 °C** with the different consolidation stresses, together with the mean value, the standard deviation and the coefficient of variation.

Consolidation stress	0,94 kPa	1,87 kPa	2,79 kPa
Test 1	2,403	2,220	2,787
Test 2	2,670	2,670	3,521
Test 3	2,019	2,220	3,688
Mean value	<b>2,364</b>	<b>2,370</b>	<b>3,332</b>
Standard deviation	<b>0,3272</b>	<b>0,2602</b>	<b>0,4794</b>
Coefficient of variation [%]	<b>13,84</b>	<b>10,98</b>	<b>14,39</b>

Table 10. **Force [N]** needed to attain the failure of the raw meal specimens (including the force required to move the pushing wall) in the uniaxial shear test at **200 °C** with the different consolidation stresses, together with the mean value, the standard deviation and the coefficient of variation.

Consolidation stress	0,94 kPa	1,87 kPa	2,79 kPa
Test 1	1,318	3,521	1,953
Test 2	1,686	3,371	3,922
Test 3	2,069	3,321	5,190
Mean value	<b>1,691</b>	<b>3,404</b>	<b>3,688</b>
Standard deviation	<b>0,3755</b>	<b>0,1042</b>	<b>1,6314</b>
Coefficient of variation [%]	<b>22,21</b>	<b>3,06</b>	<b>44,23</b>

Table 11. **Force [N]** needed to attain the failure of the raw meal specimens (including the force required to move the pushing wall) in the uniaxial shear test at **400 °C** with the different consolidation stresses, together with the mean value, the standard deviation and the coefficient of variation.

Consolidation stress	0,94 kPa	1,87 kPa	2,79 kPa
Test 1	2,854	4,005	3,922
Test 2	2,453	3,588	3,488
Test 3	2,220	2,270	4,206
Mean value	<b>2,509</b>	<b>3,288</b>	<b>3,872</b>
Standard deviation	<b>0,3207</b>	<b>0,9060</b>	<b>0,3614</b>
Coefficient of variation [%]	<b>12,78</b>	<b>27,56</b>	<b>9,33</b>

Table 12. **Force [N]** needed to attain the failure of the raw meal specimens (including the force required to move the pushing wall) in the uniaxial shear test at **550 °C** with the different consolidation stresses, together with the mean value, the standard deviation and the coefficient of variation.

Consolidation stress	0,94 kPa	1,87 kPa	2,79 kPa
Test 1	4,439	4,489	5,357
Test 2	2,720	4,339	5,724
Test 3	3,154	4,306	5,808
Mean value	<b>3,438</b>	<b>4,378</b>	<b>5,630</b>
Standard deviation	<b>0,8939</b>	<b>0,0978</b>	<b>0,2397</b>
Coefficient of variation [%]	<b>26,00</b>	<b>2,23</b>	<b>4,26</b>

Table 13. **Force [N]** needed to attain the failure of the raw meal specimens (including the force required to move the pushing wall) in the uniaxial shear test at **700 °C** with the different consolidation stresses, together with the mean value, the standard deviation and the coefficient of variation.

Consolidation stress	0,94 kPa	1,87 kPa	2,79 kPa
Test 1	4,606	4,539	6,258
Test 2	4,055	5,140	6,959
Test 3	3,505	4,239	5,357
Mean value	<b>4,055</b>	<b>4,639</b>	<b>6,191</b>
Standard deviation	<b>0,5507</b>	<b>0,4589</b>	<b>0,8031</b>
Coefficient of variation [%]	<b>13,58</b>	<b>9,89</b>	<b>12,97</b>

Table 14. **Force [N]** needed to attain the failure of the raw meal specimens (including the force required to move the pushing wall) in the uniaxial shear test at **850 °C** with the different consolidation stresses, together with the mean value, the standard deviation and the coefficient of variation.

Consolidation stress	0,94 kPa	1,87 kPa	2,79 kPa
Test 1	13,868	6,208	6,091
Test 2	7,827	9,045	6,592
Test 3	7,310	11,849	10,781
Mean value	<b>9,668</b>	<b>9,034</b>	<b>7,821</b>
Standard deviation	<b>3,6465</b>	<b>2,8204</b>	<b>2,5752</b>
Coefficient of variation [%]	<b>37,72</b>	<b>31,22</b>	<b>32,92</b>

Table 15. **Unconfined yield strength [kPa]** of the raw meal specimens tested in the uniaxial shear test at 22 °C with the different consolidation stresses, together with the mean value, the standard deviation and the coefficient of variation.

Consolidation stress	0,94 kPa	1,87 kPa	2,79 kPa
Test 1	0,430	0,362	0,705
Test 2	0,571	0,621	1,138
Test 3	0,227	0,362	1,237
Mean value	<b>0,409</b>	<b>0,448</b>	<b>1,027</b>
Standard deviation	<b>0,173</b>	<b>0,150</b>	<b>0,283</b>
Coefficient of variation [%]	<b>42,31</b>	<b>33,40</b>	<b>27,54</b>

Table 16. **Unconfined yield strength [kPa]** of the raw meal specimens tested in the uniaxial shear test at 200 °C with the different consolidation stresses, together with the mean value, the standard deviation and the coefficient of variation..

Consolidation stress	0,94 kPa	1,87 kPa	2,79 kPa
Test 1	0,107	1,353	0,491
Test 2	0,300	1,269	1,646
Test 3	0,502	1,241	2,390
Mean value	<b>0,303</b>	<b>1,288</b>	<b>1,509</b>
Standard deviation	<b>0,198</b>	<b>0,059</b>	<b>0,957</b>
Coefficient of variation [%]	<b>65,22</b>	<b>4,55</b>	<b>63,41</b>

Table 17. **Unconfined yield strength [kPa]** of the raw meal specimens tested in the uniaxial shear test at 400 °C with the different consolidation stresses, together with the mean value, the standard deviation and the coefficient of variation..

Consolidation stress	0,94 kPa	1,87 kPa	2,79 kPa
Test 1	0,364	1,006	0,992
Test 2	0,155	0,779	0,748
Test 3	0,033	0,062	1,151
Mean value	<b>0,184</b>	<b>0,615</b>	<b>0,963</b>
Standard deviation	<b>0,167</b>	<b>0,493</b>	<b>0,203</b>
Coefficient of variation [%]	<b>90,79</b>	<b>80,03</b>	<b>21,06</b>



**Table 18. Unconfined yield strength [kPa] of the raw meal specimens tested in the uniaxial shear test at 550 °C with the different consolidation stresses, together with the mean value, the standard deviation and the coefficient of variation..**

Consolidation stress	0,94 kPa	1,87 kPa	2,79 kPa
Test 1	0,687	0,765	1,267
Test 2	-0,172	0,684	1,470
Test 3	0,044	0,666	1,516
Mean value	<b>0,186</b>	<b>0,705</b>	<b>1,418</b>
Standard deviation	<b>0,447</b>	<b>0,053</b>	<b>0,133</b>
Coefficient of variation [%]	<b>239,83</b>	<b>7,45</b>	<b>9,35</b>

**Table 19. Unconfined yield strength [kPa] of the raw meal specimens tested in the uniaxial shear test at 700 °C with the different consolidation stresses, together with the mean value, the standard deviation and the coefficient of variation..**

Consolidation stress	0,94 kPa	1,87 kPa	2,79 kPa
Test 1	0,888	0,925	1,840
Test 2	0,617	1,244	2,213
Test 3	0,347	0,765	1,361
Mean value	<b>0,617</b>	<b>0,978</b>	<b>1,804</b>
Standard deviation	<b>0,270</b>	<b>0,244</b>	<b>0,427</b>
Coefficient of variation [%]	<b>43,81</b>	<b>24,92</b>	<b>23,67</b>

**Table 20. Unconfined yield strength [kPa] of the raw meal specimens tested in the uniaxial shear test at 850 °C with the different consolidation stresses, together with the mean value, the standard deviation and the coefficient of variation..**

Consolidation stress	0,94 kPa	1,87 kPa	2,79 kPa
Test 1	4,823	1,107	1,062
Test 2	1,863	2,546	1,319
Test 3	1,609	3,967	3,471
Mean value	<b>2,765</b>	<b>2,540</b>	<b>1,950</b>
Standard deviation	<b>1,787</b>	<b>1,430</b>	<b>1,323</b>
Coefficient of variation [%]	<b>64,61</b>	<b>56,30</b>	<b>67,83</b>

## Rheological shear test

Table 21. **Torque [ $\mu\text{N}\cdot\text{m}$ ]** needed for the failure of the raw meal specimens in the rheological shear test at **25 °C** with the different consolidation stresses, together with the mean value, the standard deviation and the coefficient of variation.

Consolidation stress	2 kPa	4 kPa	6 kPa	8 kPa
Test 1	5000	5600	11800	19600
Test 2	7200	9800	11400	14600
Test 3	4200	9800	7400	18600
Mean value	<b>5476</b>	<b>8400</b>	<b>10200</b>	<b>17600</b>
Standard deviation	<b>1553</b>	<b>2425</b>	<b>2433</b>	<b>2646</b>
Coefficient of variation [%]	<b>28,42</b>	<b>28,87</b>	<b>23,85</b>	<b>15,03</b>

Table 22. **Torque [ $\mu\text{N}\cdot\text{m}$ ]** needed for the failure of the raw meal specimens in the rheological shear test at **100 °C** with the different consolidation stresses, together with the mean value, the standard deviation and the coefficient of variation.

Consolidation stress	2 kPa	4 kPa	6 kPa	8 kPa
Test 1	5000	9000	10200	15000
Test 2	4600	9800	11800	12400
Test 3	4600	11800	10000	14600
Mean value	<b>4733</b>	<b>10200</b>	<b>10667</b>	<b>14000</b>
Standard deviation	<b>231</b>	<b>1442</b>	<b>987</b>	<b>1400</b>
Coefficient of variation [%]	<b>4,88</b>	<b>14,14</b>	<b>9,25</b>	<b>10,00</b>

Table 23. **Torque [ $\mu\text{N}\cdot\text{m}$ ]** needed for the failure of the raw meal specimens in the rheological shear test at **300 °C** with the different consolidation stresses, together with the mean value, the standard deviation and the coefficient of variation.

Consolidation stress	2 kPa	8 kPa
Test 1	10400	17400
Test 2	7600	18000
Test 3	-	11400
Mean value	<b>9000</b>	<b>15600</b>
Standard deviation	<b>1980</b>	<b>3650</b>
Coefficient of variation [%]	<b>22,00</b>	<b>23,40</b>

Table 24. **Torque [ $\mu\text{N}\cdot\text{m}$ ]** needed for the failure of the raw meal specimens in the rheological shear test at **500 °C** with the different consolidation stresses, together with the mean value, the standard deviation and the coefficient of variation.

Consolidation stress	2 kPa	8 kPa
Test 1	14400	24800
Test 2	15000	23400
Test 3	-	22800
Mean value	<b>14700</b>	<b>23667</b>
Standard deviation	<b>424</b>	<b>1026</b>
Coefficient of variation [%]	<b>2,89</b>	<b>4,34</b>

## Angle of repose measurement

Table 25. **Angle of repose [°]** determined with the angle of repose measurement at the different temperatures using the **Analysis A**. The 6 measured values, the mean value, the standard deviation and the coefficient of variation are shown.

Temperature	22 °C	200 °C	400 °C	550 °C	700 °C	850 °C
Test 1.1	52,59	52,57	53,02	47,24	49,25	43,22
Test 1.2	57,09	56,73	55,71	53,07	54,53	50,63
Test 2.1	52,67	53,03	51,81	53,78	51,18	-
Test 2.2	56,41	53,86	58,54	54,06	59,23	-
Test 3.1	53,66	52,17	50,93	46,56	48,67	54,26
Test 3.2	58,06	58,54	54,73	55,57	60,95	60,88
Mean value	<b>55,08</b>	<b>54,48</b>	<b>54,13</b>	<b>51,71</b>	<b>53,97</b>	<b>52,25</b>
Standard deviation	<b>2,39</b>	<b>2,57</b>	<b>2,80</b>	<b>3,82</b>	<b>5,19</b>	<b>7,37</b>
Coefficient of variation [%]	<b>4,35</b>	<b>4,72</b>	<b>5,17</b>	<b>7,39</b>	<b>9,62</b>	<b>14,10</b>

Table 26. **Angle of repose [°]** determined with the angle of repose measurement at the different temperatures using the **Analysis B**. The 6 measured values, the mean value, the standard deviation and the coefficient of variation are shown.

Temperature	22 °C	200 °C	400 °C	550 °C	700 °C	850 °C
Test 1.1	68,20	57,38	57,17	47,24	49,25	63,43
Test 1.2	59,04	61,82	55,71	57,88	54,53	53,97
Test 2.1	59,04	57,99	56,77	58,67	47,66	-
Test 2.2	66,25	62,65	65,77	59,42	62,92	-
Test 3.1	62,29	52,17	50,93	51,34	51,71	85,60
Test 3.2	58,06	58,54	54,73	55,57	60,95	60,88
Mean value	<b>62,14</b>	<b>58,43</b>	<b>56,85</b>	<b>55,02</b>	<b>54,50</b>	<b>65,97</b>
Standard deviation	<b>4,23</b>	<b>3,74</b>	<b>4,91</b>	<b>4,80</b>	<b>6,24</b>	<b>13,68</b>
Coefficient of variation [%]	<b>6,81</b>	<b>6,39</b>	<b>8,64</b>	<b>8,73</b>	<b>11,44</b>	<b>20,74</b>

## Statistical analysis

### Uniaxial shear test

Table 27. Mean value, standard deviation and confidence intervals with a 95% confidence level for the force [N] needed to start moving the pushing wall with the empty system in the uniaxial shear test at the different temperatures.

Temperature	22 °C	200 °C	400 °C	550 °C	700 °C	850 °C
Mean value	1,591	1,115	2,156	3,065	2,798	4,025
Standard deviation	0,237	0,242	0,240	0,436	0,195	0,901
$t \cdot s \over \bar{n}$	0,249	0,254	0,251	0,457	0,205	0,946
Confidence interval lower limit	<b>1,342</b>	<b>0,861</b>	<b>1,904</b>	<b>2,608</b>	<b>2,593</b>	<b>3,079</b>
Confidence interval upper limit	<b>1,840</b>	<b>1,370</b>	<b>2,407</b>	<b>3,522</b>	<b>3,003</b>	<b>4,971</b>

Table 28. Mean value, standard deviation and confidence intervals with a 95 % confidence level for the **unconfined yield strength [kPa]** from the raw meal specimens tested in the uniaxial shear test at 22 °C with the different consolidation stresses.

Consolidation stress	0,94 kPa	1,87 kPa	2,79 kPa
Mean value	0,409	0,448	1,027
Standard deviation	0,173	0,150	0,283
$t \cdot s \over \bar{n}$	0,430	0,372	0,702
Confidence interval lower limit	<b>0,000</b>	<b>0,076</b>	<b>0,324</b>
Confidence interval upper limit	<b>0,839</b>	<b>0,820</b>	<b>1,729</b>

Table 29. Mean value, standard deviation and confidence intervals with a 95 % confidence level for the **unconfined yield strength [kPa]** from the raw meal specimens tested in the uniaxial shear test at 200 °C with the different consolidation stresses.

Consolidation stress	0,94 kPa	1,87 kPa	2,79 kPa
Mean value	0,303	1,288	1,509
Standard deviation	0,198	0,059	0,957
$t \cdot s \over \bar{n}$	0,491	0,146	2,377
Confidence interval lower limit	<b>0,000</b>	<b>1,142</b>	<b>0,000</b>
Confidence interval upper limit	<b>0,793</b>	<b>1,433</b>	<b>3,887</b>

Table 30. Mean value, standard deviation and confidence intervals with a 95 % confidence level for the **unconfined yield strength [kPa]** from the raw meal specimens tested in the uniaxial shear test at **400 °C** with the different consolidation stresses.

Consolidation stress	0,94 kPa	1,87 kPa	2,79 kPa
Mean value	0,184	0,615	0,963
Standard deviation	0,167	0,493	0,203
$t \cdot s \quad \bar{n}$	0,415	1,224	0,504
Confidence interval lower limit	<b>0,000</b>	<b>0,000</b>	<b>0,459</b>
Confidence interval upper limit	<b>0,599</b>	<b>1,839</b>	<b>1,467</b>

Table 31. Mean value, standard deviation and confidence intervals with a 95 % confidence level for the **unconfined yield strength [kPa]** from the raw meal specimens tested in the uniaxial shear test at **550 °C** with the different consolidation stresses.

Consolidation stress	0,94 kPa	1,87 kPa	2,79 kPa
Mean value	0,186	0,705	1,418
Standard deviation	0,447	0,053	0,133
$t \cdot s \quad \bar{n}$	1,110	0,130	0,329
Confidence interval lower limit	<b>0,000</b>	<b>0,575</b>	<b>1,089</b>
Confidence interval upper limit	<b>1,296</b>	<b>0,836</b>	<b>1,747</b>

Table 32. Mean value, standard deviation and confidence intervals with a 95 % confidence level for the **unconfined yield strength [kPa]** from the raw meal specimens tested in the uniaxial shear test at **700 °C** with the different consolidation stresses.

Consolidation stress	0,94 kPa	1,87 kPa	2,79 kPa
Mean value	0,617	0,978	1,804
Standard deviation	0,270	0,244	0,427
$t \cdot s \quad \bar{n}$	0,672	0,605	1,061
Confidence interval lower limit	<b>0,000</b>	<b>0,372</b>	<b>0,743</b>
Confidence interval upper limit	<b>1,289</b>	<b>1,583</b>	<b>2,865</b>

Table 33. Mean value, standard deviation and confidence intervals with a 95 % confidence level for the **unconfined yield strength [kPa]** from the raw meal specimens tested in the uniaxial shear test at **850 °C** with the different consolidation stresses.

Consolidation stress	0,94 kPa	1,87 kPa	2,79 kPa
Mean value	2,765	2,540	1,950
Standard deviation	1,787	1,430	1,323
$t \cdot s \quad \bar{n}$	4,438	3,553	3,286
Confidence interval lower limit	<b>0,000</b>	<b>0,000</b>	<b>0,000</b>
Confidence interval upper limit	<b>7,203</b>	<b>6,093</b>	<b>5,237</b>

### Rheological shear test

Table 34. Mean value, standard deviation and confidence intervals with a 95% confidence level for the torque [ $\mu\text{N}\cdot\text{m}$ ] needed to achieve the failure of the raw meal specimens in the rheological shear test at 25 °C at the different consolidation stresses.

Consolidation stress	2 kPa	4 kPa	6 kPa	8 kPa
Mean value	5467	8400	10200	17600
Standard deviation	1553	2425	2433	2646
$t \cdot s \quad \bar{n}$	3859	6024	6044	6572
Confidence interval lower limit	<b>1608</b>	<b>2376</b>	<b>4156</b>	<b>11028</b>
Confidence interval upper limit	<b>9326</b>	<b>14424</b>	<b>16244</b>	<b>24172</b>

Table 35. Mean value, standard deviation and confidence intervals with a 95% confidence level for the torque [ $\mu\text{N}\cdot\text{m}$ ] needed to achieve the failure of the raw meal specimens in the rheological shear test at 100 °C at the different consolidation stresses.

Consolidation stress	2 kPa	4 kPa	6 kPa	8 kPa
Mean value	4733	10200	10667	14000
Standard deviation	231	1442	987	1400
$t \cdot s \quad \bar{n}$	574	3583	2451	3478
Confidence interval lower limit	<b>4160</b>	<b>6617</b>	<b>8216</b>	<b>10522</b>
Confidence interval upper limit	<b>5307</b>	<b>13783</b>	<b>13117</b>	<b>17478</b>

Table 36. Mean value, standard deviation and confidence intervals with a 95% confidence level for the torque [ $\mu\text{N}\cdot\text{m}$ ] needed to achieve the failure of the raw meal specimens in the rheological shear test at 300 °C at the different consolidation stresses.

Consolidation stress	2 kPa	8 kPa
Mean value	9000	15600
Standard deviation	1980	3650
$t \cdot s \quad \bar{n}$	17789	9066
Confidence interval lower limit	<b>0</b>	<b>6534</b>
Confidence interval upper limit	<b>26789</b>	<b>24666</b>

Table 37. Mean value, standard deviation and confidence intervals with a 95% confidence level for the torque [ $\mu\text{N}\cdot\text{m}$ ] needed to achieve the failure of the raw meal specimens in the rheological shear test at 500 °C at the different consolidation stresses.

Consolidation stress	2 kPa	8 kPa
Mean value	14700	23667
Standard deviation	424	1026
$t \cdot s \quad \bar{n}$	3812	2550
Confidence interval lower limit	<b>10888</b>	<b>21117</b>
Confidence interval upper limit	<b>18512</b>	<b>26216</b>

### Angle of repose measurement

Table 38. Mean value, standard deviation and confidence intervals with a 95% confidence level for the angle of repose [ $^{\circ}$ ] determined in the at the different temperatures with the angle of repose measurement using the Analysis A.

Temperature	22 °C	200 °C	400 °C	550 °C	700 °C	850 °C
Mean value	55,08	54,48	54,13	51,71	53,97	52,25
Standard deviation	2,39	2,57	2,80	3,82	5,19	7,37
$t \cdot s \quad \bar{n}$	2,51	2,70	2,94	4,01	5,45	7,73
Confidence interval lower limit	<b>52,57</b>	<b>51,79</b>	<b>51,19</b>	<b>47,70</b>	<b>48,52</b>	<b>44,52</b>
Confidence interval upper limit	<b>57,59</b>	<b>57,18</b>	<b>57,06</b>	<b>55,72</b>	<b>59,42</b>	<b>59,98</b>

Table 39. Mean value, standard deviation and confidence intervals with a 95% confidence level for the angle of repose [ $^{\circ}$ ] determined in the at the different temperatures with the angle of repose measurement using the Analysis B.

Temperature	22 °C	200 °C	400 °C	550 °C	700 °C	850 °C
Mean value	62,14	58,43	56,85	55,02	54,50	65,97
Standard deviation	4,23	3,73	4,91	4,80	6,24	13,68
$t \cdot s \quad \bar{n}$	4,44	3,92	5,15	5,04	6,54	14,36
Confidence interval lower limit	<b>57,70</b>	<b>54,51</b>	<b>51,69</b>	<b>49,98</b>	<b>47,96</b>	<b>51,61</b>
Confidence interval upper limit	<b>66,59</b>	<b>62,35</b>	<b>62,00</b>	<b>60,06</b>	<b>61,05</b>	<b>80,33</b>








## Appendix B. Chemical Risk Assessment (APV) for the uniaxial shear test

### Chemical Risk Assessment /APV

Fill in this Form when using for New Application or of New Users

<b>Name of Chemicals/Materials/Products</b>	
<b>Product content /- description (evt.)</b>	Calcium carbonate (CaCO <sub>3</sub> ) Clay Calcium oxide (CaO) Sand
<b>CAS no.</b>	Calcium carbonate: 471-34-1 1317-65-3 (limestone) Clay: No CAS number Calcium oxide: 1305-78-8 Sand: No CAS number
<b>Supplement to KBA (Kemibrug)/ MSDS, etc. (name source of MSDS and enclose)</b>	<a href="http://www.kemibrug.dk/">http://www.kemibrug.dk/</a>
<b>Research Group</b>	CHEC
<b>Name of the set ups / Workplace (e.g. room)</b>	Building 229, Room 037, Black muffle oven with particle strength setup
<b>Description of the usage covered by the Risk Assessment</b> <i>E.g. Name of the practice course, No. of exercise, name of the process/ project etc.</i>	
Uniaxial shear test at high temperatures for the flow behavior characterization of bulk solids. Project name: Characterization and parametric study of the flow properties of cohesive powders at temperatures up to 850 °C.	
<b>Limits of the usage (KBA pt. A)</b> <i>Age, pregnancy, education, referring to the announcement of cancer, etc.</i>	
No limitations in this work process.	
<b>Classification, R- and S- Phrases</b> <i>Both no. and Phrases have to be written</i>	
<p><b>Classification symbol:</b> Calcium carbonate:   Clay: None</p> <p>Calcium oxide:  Sand: None</p> <p><b>R-Phrases:</b> Calcium carbonate: R 37/38: Irritating to respiratory system and skin R 41: Risk of serious damage to the eyes Clay: None</p>	

Name of Chemicals/Materials/Products	
<p>Calcium oxide: R 35: Causes severe burns  R 36/38: Irritating to eyes and skin  R 41: Risk of serious damage to the eyes</p> <p>Sand: None</p> <p><b><u>S-Phrases:</u></b></p> <p>Calcium carbonate: S 26: In case of contact with eyes, rinse immediately with plenty of water and seek medical advice.  S 39: Wear eye/face protection</p> <p>Clay: None</p> <p>Calcium oxide: S 26: In case of contact with eyes, rinse immediately with plenty of water and seek medical advice.  S 37/39: Wear suitable gloves and eye/face protection</p> <p>Sand: None</p>	
Description of the chemicals/material/product: (KBA pt. D)	
<p>Calcium carbonate: Fine-grained white powder. Moisture may affect product quality. Contact with strong oxidizing agents, acids, fluorine (violently flammable if contact exists), magnesium and aluminium salts must be avoided. At temperatures above 700 - 850 °C, the calcination of calcium carbonate takes place, yielding to calcium oxide and releasing carbon dioxide (CO<sub>2</sub>).</p> <p>Clay: Fine-grained soil with a particle size smaller than 2 µm.</p> <p>Calcium oxide: Fine-grained white powder. Contact with acids, moisture (it vigorously reacts with water) must be avoided. Reacts with CO<sub>2</sub> from the air forming calcium carbonate.</p> <p>Sand: Coarse-grained soil with a particle size between 0,0625 and 2 mm. The most usual component in sand is silicon dioxide (SiO<sub>2</sub>), usually found in quartz form.</p>	
Description of the work process <i>Including weighing, solvents used, concentration, amounts used, .etc.</i>	
<p>The raw meal (mixture of 75 % calcium carbonate and 25 % clay) is loaded into the metal cell and introduced inside the oven.</p> <p>When the desired temperature is achieved, the specimen is consolidated with a compressive force and after that, it is shifted horizontally by the pushing wall of the cell, moved by the action of a monitored piston.</p> <p>The horizontal force necessary for the failure of the specimen is measured by a sensor and the results are shown in the computer.</p> <p>The same procedure is performed with sand.</p>	
Essentials hazards/health risk of the chemicals/work process <i>E.g. laser, vacuum, weighing, decanting, mixing, high pressure, etc.. Only the most hazardous compounds should be included. The fact that chemicals are harmful by inhalation does not necessarily means that there is a risk for inhalation in this work process.</i>	
<p>No health risk of the chemicals in this work process, only in case of contact with skin and eyes or inhalation of the dust particles, damaging seriously the respiratory system.</p> <p>There is a risk of get burnt when handling improperly the hot metal cell during the procedure.</p>	

<b>Name of Chemicals/Materials/Products</b>			
<b>Exposure frequency:</b> (E.g. daily, 1 day/week, 1 hr/month)	Daily		
<b>Precautions during usage / Necessary security precaution (KBA pt C)</b> <i>E.g. ventilation, gloves, others personal protective measures to take, special equipment for emergency aid</i>			
<p>During the handling of the chemical substances (raw meal) it is necessary to use safety goggles and nitrile gloves to avoid direct contact with them.</p> <p>It is not possible to find suitable disposable gloves for calcium oxide. Using nitrile gloves the penetration time is expected to be short, so that in case of spillage it is recommended to renew the gloves and wash the hands with soap before using new gloves.</p> <p>Emergency showers, eye wash bottles and sink with soap must be easily accessible.</p> <p>Effective process ventilation is necessary during the procedure (fume hood) due to the fact that heating increases the risk of inhalation of vapours besides the risk of inhalation of dust particles. It is advisable to use a particle filter. Filtering respiratory protective device must be only used 3 hours a day.</p> <p>When the metal cell is handled either introducing or removing it from the oven, it is necessary to wear thermal gloves and to move the cell using a metal fork. The metal lid of the cell used to compress the specimen must be handled with a metal rod.</p> <p>The hot metal cell should be allowed to cool to approximately 500 °C before attempted to be removed from the oven. Once the cell is outside the oven, it must be placed above bricks due to its high temperature.</p> <p>It is advisable to cover the floor next to the oven with a protection metal sheet.</p>			
<b>Hazardous Waste disposal consideration.</b> <i>E.g. Action by accident, spill clean up and waste disposal, procedure for information by accident.</i>			
<p>It is important to limit the generation of dust particles, keep unauthorized people away and announce any risk of adverse effects.</p> <p>The contact with the substances must be avoided using (if appropriate) gloves and breathing equipment with a combination filter (Type ABEK-P).</p> <p>The spillage must be cleared up with a damp cloth and both must be discarded in a tightly sealed container. The area where the spillage took place must be cleaned afterwards.</p> <p>After waiting for approximately one day to allow calcium oxide react with CO<sub>2</sub> from the air to form calcium carbonate, the materials can be immobilized by addition of water so they can be regarded as construction waste and should be handled like that. BBH has agreement of disposal of this kind of waste. Waste from this setup will be placed with the waste of BBH in 228 from the FGD-plant.</p>			
<b>Waste Groups, Kommunekemi:</b>		<b>UN nr.:</b>	Non-hazardous for road transport
<b>Safety regulations for storage (KBA pt. H)</b> <i>E.g. Signposting, ventilated, cool</i>			
The different samples must be signposted and stored in tightly sealed plastic containers, placed in a well-ventilated chemical cabinet. They must be kept up to a height of 160 cm.			
<b>Substitution Analysis (KBA pt. I)</b> <i>Write here your considerations for decreasing the risks by changing chemicals or process steps. Remember that choosing to use smaller amount is also a substitution.</i>			
This device is mainly destined to the flow characterization of raw meal, so that changing chemical substances may affect both risk and precaution considerations to apply in the work process.			

Name of Chemicals/Materials/Products			
	Name (full)	Date	Signature
APV executed by	Arnau Mestres Rosàs	17/04/2012	
Other users	Claus Maarup Rasmussen		
Projekt-/ responsible instructor	Claus Maarup Rasmussen		
Chemical-APV responsible	Claus Maarup Rasmussen		
Safety Representative	Anders Tiedje		
Leader Representative	Peter Arendt		
Dept. Safety committee			
Registration in personal file:	YES	NO	
<p>If the Chemical is carcinogen (R40, R45, R49), or a very toxic compound (TX) then the safety committee must approve usage before work commences. The electronically completed APV is given to the Chemical - APV responsible, who will ensure the signature before a version of paper is send to the day-to-day head of the Safety Group</p>			